KOMEX II

KURILE OKHOTSK SEA MARINE EXPERIMENT

CRUISE REPORT

RV AKADEMIK M.A. LAVRENTYEV CRUISE 29 LEG 1 AND LEG 2

VLADIVOSTOK – PUSAN – OKHOTSK SEA – PUSAN – OKHOTSK SEA – PUSAN - VLADIVOSTOK

MAY 25 - AUGUST 05, 2002

110

GEOMAR REPORT

KOMEX II

KURILE OKHOTSK SEA MARINE EXPERIMENT

CRUISE REPORT

RV AKADEMIK M.A. LAVRENTYEV CRUISE 29 LEG 1 AND LEG 2

VLADIVOSTOK – PUSAN – OKHOTSK SEA – PUSAN – OKHOTSK SEA – PUSAN - VLADIVOSTOK

MAY 25 - AUGUST 05, 2002

Edited by
Nicole Biebow, Ruslan Kulinich and Boris Baranov
with contributions of cruise participants

The KOMEX marine expeditions were initialized on responsibility of
the P. P. Shirshov Institute of Oceanology, Moscow,
the Pacific Oceanological Institute (POI), Vladivostok,
and the GEOMAR Research Center for Marine Geosciences, Kiel

GEOMAR
Forschungszentrum
für marine Geowissenschaften
der Christian-Albrechts-Universität
zu Kiel

KIEL 2003

GEOMAR REPORT 110

GEOMAR
Research Center
for Marine Geosciences
Christian Albrechts University
in Kiel

Redaktion dieses Reports:
Nicole Biebow und Katharina Georgeleit

GEOMAR REPORT
ISSN 0936 - 5788

GEOMAR
Forschungszentrum
für marine Geowissenschaften
Wischhofstr. 1-3
D - 24148 Kiel
Tel. (0431) 600-2555, 600-2505

Editors of this issue:
Nicole Biebow and Katharina Georgeleit

GEOMAR REPORT
ISSN 0936 - 5788

GEOMAR
Research Center
for Marine Geosciences
Wischhofstr. 1-3
D - 24148 Kiel
Tel. (49) 431 / 600-2555, 600-2505

PART I:

RV AKADEMIK LAVRENTYEV CRUISE 29

LEG 1

VLADIVOSTOK - PUSAN - SEA OF OKHOTSK - PUSAN

MAY 25 - JUNE 27, 2002

Table of contents

INTRODUCTION

Ruslan Kulinich and Nicole Biebow

The 29th cruise of RV *Akademik Lavrentyev* was organized within the scope of the joint Russian - German KOMEX II project (2001 - 2004) which is a continuation of the first phase of joint research in the Okhotsk Sea (KOMEX I, 1998-2000). The expeditions carried out in KOMEX I made essential contributions to understand the geology, geochemistry, geophysics, paleoceanology and hydrology of this unique region, and their results have formed the basis for KOMEX II. As in KOMEX I, the main purpose of the KOMEX II project is to understand the mechanisms of the complex climate-controlling system 'Okhotsk Sea' and to study its influence on chemical distribution, chemical cycles, water mass formation, circulation and climate.
The main research topics of the joint project KOMEX II concentrate on the following problems:

- development of a plate tectonic model of the evolution of the Okhotsk Sea;
- characterization of the seismic facies and estimation of the influence of regional tectonics on sedimentation processes, distribution of the BSR and vent phenomena;
- record of material and temporal changes in magmatism and quantification of chemical and fluid cycles in the Kurile Kamchatka Subduction System;
- quantification of the trace element input into the atmosphere depending on seasonally changing hydrography and ice cover;
- quantification of gas and fluid expulsion rates and of the biogeochemical material and energy turnovers in vent areas;
- geochemical, mineralogical and isotopic characterization of the barite precipitates in the Derugin Basin to reconstruct the history, intensity and geochemical composition of the emanating fluids;
- quantification of the amount and type of gas hydrates, of their paleo-stability, temperature history and their influence on the recent as well as the paleo-environment;
- influence of Amur River on sea-ice formation, productivity and sedimentation processes during the last 50,000 years;
- paleoceanological significance of the Okhotsk Sea for water mass formation and climatic evolution in the Pacific Ocean.

On this basis and according to the results of previous expeditions, the research tasks and investigation areas for the LV29 cruise to the Okhotsk Sea were determined.
The first leg of the LV29 cruise focused on hydrochemical and geochemical investigations, video-controlled seafloor observations, sampling of vent sites and detailed mapping of the bottom relief by a swath bathymetry system. The main investigation areas comprise the shelf and slope of northeast Sakhalin and the "Barite Mounds" in the Derugin Basin.
In the second leg of the cruise, a coring program for paleoceanological purposes, plankton and water sampling, mapping of the seafloor with the sediment echosounder system SES-2000DS, dredging of volcanic rocks and reflexion seismics were the main targets. The investigation areas of the second leg covered the shelf and slope of Sakhalin and Kamchatka, the Sakhalin Gulf (Amur River mouth), the Derugin and Kurile Basins and La Perusa Strait.

The scientific objectives of cruise LV29 comprise and contribute to the following research topics of KOMEX:

1) One of the central scientific targets is to balance the geogenic and biogenic methane input into the atmosphere, as well as to find and to geochemically and geologically characterize the gas and fluid venting sites at the seafloor. The main component of these gas emanations off Sakhalin is methane which, alongside with CO_2, contributes to the so-called "greenhouse" effect causing global warming and as a consequence effecting the evolution of the planet`s climate. The following processes are responsible for the release of methane from the Okhotsk Sea into the atmosphere: degassing of methane from near-surface hydrocarbon deposits, degradation of gas hydrates in the sediments, and biologically derived methane. These processes are especially pronounced along the continental margin off Sakhalin and in the Derugin Basin, whereas along the Kurile Island Arc, tectonic and volcanic sources dominate.
Several expeditions within KOMEX I focused on these phenomena. A lot of earlier unknown gas emanation sources were discovered and sampled at the Sakhalin shelf and slope and in the Derugin Basin. The vent sites at the continental margin off NE Sakhalin are characterized by near-surface gas hydrate occurences, sulfide- and methane-rich pore waters, typical vent organisms, carbonate precipitates, methane bubbles forming flares and an enrichment of methane in the bottom waters. The investigations conducted within KOMEX I give the following scenario for methane venting off NE-Sakhalin: methane bubbles rise along faults from the sediment to the sediment surface. In the surface sediments, these bubbles are fixed as gas hydrates and - after microbiological oxidation- as carbonate precipitates. The remaining methane is converted at the sediment/water interface by vent organisms. Only a relatively small portion of the gas reaches the bottom water and the atmosphere.
During cruise LV29 these investigations were continued as follows: the stability of the gas venting sites, their venting intensity, and the hydrochemical characteristics of the surrounding waters were investigated, and a quantitative estimation of the gas bubbles` rising velocity was made. The hydrochemical work included the study of carbonate systems (pH, alkalinity, dissolved calcium), of dissolved oxygen and nutrients in the water columns above methane sources. The influence of methane venting on the carbonate system was the main target of these works. Apart from that, the geochemisty of pore waters was analyzed in order to study the formation processes of authigenic mineral precipitates.
The detection of new methane sources, the study of their spatial distribution and their connection with tectonics are other questions which were investigated in Leg 1 of RV *Akademik Lavrentyev* cruise LV29. For this purpose, mainly the 12 kHz hydroacoustic system ELAC was used. More than 100 flares were recorded, among which more than the half were earlier unknown. A generalization of all available data allowed us to suppose that the spatial extension of methane vents is controlled by a system of tectonic structures, mapped by geophysical methods during previous expeditions and verified on the present cruise by detailed mapping with the swath bathymetry system LOLA II.

2) A second main topic of previous expeditions within the framework of the KOMEX I project was the barite mineralization area in the Derugin Basin. This area is characterized by huge fields of barite precipitates, which cover the seafloor as massive rocks or chimneys. They even built a barite ridge with an elevation of ca. 50-100 m above the seafloor. These barites are associated with chemosynthetic organisms, which indicate a recent activity of fluid venting. Pore water analyzes show that extremly barium-rich fluids rise from the earth interior (>2 km sediment depth) to the sediment surface, react with the sulfate of sea water and form barite precipitates. Due to the high barium content of the very old bottom water of the Derugin Basin (ca. 1,600 years; Tiedemann, pers. com.) these precipitates are not dissolved.
Huge methane concentrations in the pore and bottom water of the barite mineralization area along with isotope studies on carbonate precipitates indicate that a large amount of methane is injected in the water column by the rising fluids. Sulfur and oxygen isotopes of the carbonate precipitates correspond to formation temperatures, which are certainly below 5°C (Greinert et

al., 2002), so that former theories of an hydrothermal origin could be revised within KOMEX I.
During the LV29 cruise, the investigations in the Derugin Basin concentrated on detailed mineralogical-petrographical investigations of carbonate and barite precipitates, determination of their distribution in the sediments and at the seafloor, and of their relationship with tectonic processes. Gas-geochemical and hydrochemical investigations were carried out at the "Barite Mounds" and in the surrounding areas, detailed mapping of the bottom relief by LOLA II, OFOS observations of the barite edifices and their environment and mapping of the barite mineralization area by the 12 kHz hydroacoustic system and OFOS accomplished these investigations. Additionally, the sediment and the precipitates were sampled by gravity corers and dredges.

3) The paleoceanological investigations carried out on previous expeditions to the Okhotsk Sea reveal the paleoceanographic potential of this NW-Pacific marginal basin. The carbonate-containing sediments allow to establish a continuous high-resolution oxygen isotope stratigraphy for the last approximately 350,000 years, which is outstanding in the Subarctic-Pacific area. The deposits facilitate insights into the closely coupled interplay between surface productivity, terrigenous supply and sea-ice coverage. This is of specific interest, since the interglacial high productivity in the N-Pacific and its marginal seas act as a sink of CO_2 that may counteract to the naturally induced atmospheric CO_2-increase during deglaciations and subsequent interglacials. The depositional environment of the Okhotsk Sea is dominated by terrigenous-siliciclastic material including high portions of ice-rafted material (IRD). The monotonous sequences are interrupted by short events of extremely high productivity, which characterize the end of glacial terminations and the subsequent interglacials. During glacials, surface productivity is reduced by a factor of 5 to 10. The productivity events exhibit a cyclicity of ca. 100 kyrs, and last typically for about 20 kyrs. Productivity maxima relate to changes in fluvial nutrient supply, sea-ice coverage and water mass stratification.
The cold deep-water masses of the Pacific Ocean originate from high-latitudinal marginal seas, among them the Okhotsk Sea. Insights into the scale of the influence on the global climate have not been reached yet. High-resolution studies of the sediments, especially in deep-water passages and in the influx area of the Kamchatka Current, were therefore one central question of Leg 2 of the LV29 cruise in order to paleoceanographically reconstruct the water masses. Another important objective is to study the influence of Amur River on sea-ice formation, circulation, productivity and sedimentation of the Okhotsk Sea. Amur River is the largest source for fresh water and sediment of the Okhotsk Sea and the 4th largest Siberian river. Apart from that, Amur River is the only of the large Siberian rivers which does not flow into the Arctic Ocean. Furthermore, the analysis of Amur sediments yield evidence about the development of the environment of the Siberian hinterland, for example by analyzing plant remains like spores and pollens which are transported by Amur waters into the Okhotsk Sea.

In order so solve the above-mentioned questions on cruise LV29, we took long gravity cores in the key areas of the Okhotsk Sea, e.g. the estuary of Amur River and along the straits into the Pacific Ocean. For the first time, we also deployed the sediment echosounder SES-2000DS from Rostock University with which we were able to survey and sample sediments which deposited without disturbance and continuously. This work was completed by multicorer, CTD and multinet deployments for plankton sampling. The plankton sampling on the LV29 cruise focused especially on the Kamchatka slope area, transects from the inner Kurile Basin towards the North Pacific and the Soya inflow area. The scientific goal of these investigations is to define the boundary conditions of the biological system between the

Okhotsk Sea and the North Pacific and the import of taxa via the Kamchatka Current (from the North Pacific) and the Soya Current (from the Japan Sea) into the Okhotsk Sea.

4) The main scientific objectives of the volcanological/petrological work within KOMEX I was to study interaction and dependencies between crustal and mantle sources, petrogenetic processes as well as the type and amount of volatiles in the eruptive products in different plate tectonic environments (e.g., rear arc/back-arc vs. volcanic front). Petrological work on previous cruises therefore aimed mainly to sample northern, central (Bussol Strait) and southern transects across the Kurile Island Arc as far as possible into the Kurile Basin. Extensive sampling of the Geophysicist seamount in the northeastern part of the Kurile Basin on the KOMEX I cruises and subsequent lab analyses of the dredged rocks also provided new informations on the structure and geodynamic evolution of the Kurile Basin (Baranov et al., 2002a; Werner et al., subm.).
The major goal of the volcanological, petrological, and geochemical studies of seamounts on the LV29 cruise was to make further contributions to a model for the geodynamic evolution of marginal basins by reconstruction of volcanic, magmatic and tectonic processes in the Kurile Basin. These objectives should be achieved by the reconstruction of the paleo-environment of the volcanoes at the time of their activity, age dating of the volcanoes, and characterization of tectonic setting of the volcanoes.
Accordingly, the planned dredge sites on RV *Akademik Lavrentyev* cruise did not primarily focus on submarine arc volcanoes but on volcanic structures in the Kurile Basin being probably not directly related to the Kurile Island Arc as, for example, the western foothills of Browton Ridge in the central Kurile Basin, Hydrographer Ridge west of Iturup Island, and Loskutov seamount in the southern Kurile Basin. These structures had been discovered on former Russian cruises but had not been mapped in detail, and the sampling of basement rocks failed since the volcanoes seem to be largely covered by marine sediment, ice-rafted debris (dropstones) and/or encrustations. Despite these difficulties we decided to focus on these volcanoes on cruise LV29 since we expected very interesting new results in case of successful sampling. To achieve the best possible results, approximately half of the time designated for petrological sampling was spent for detailed bathymetric and, at some places, additional seismic surveys. The hydroacoustic and seismic data gained on these surveys did not only enable us to select the most promising sites for dredge hauls, but also provided additional new informations on these volcanoes.
Apart from the Kurile Basin volcanoes, the dredging schedule included several structures in the Derugin Basin. The objectives of these dredging operations were sampling of basement rocks at the northern slope of the Derugin Basin (southern part of Kashevarov Bank) in order to get information on the basement structure of this area and sampling of tabular calcite and barite-calcite precipitates at the Barite Mounds in the northeastern part of the Derugin Basin.

5) The seismic survey on cruise LV29 in the central part of the Kurile Basin was carried out to study the nature of a specific basement rise, which separates two subbasins with a depth to the basement of up to 7 km. This basement rise in the central part of the basin was discovered during the Pacific expedition Souzmorgeo in 1976. The expedition showed that the rise has a complicated structure and consists of isometric basement highs. The depressions between them form fan-like, undulating systems that resemble river valleys. Over the top of the swell, the basement lies at a depth of about 5 km; in the depressions to the southwest and the northeast, it was found at depths of 8 and 7 km, respectively (Zhuravlev, 1982). The origin of the rise remained unknown. Much later they were supposed to represent shear/lateral fault

zones that defined an opening direction orthogonally to the general strike of the Kurile Basin (Gnibidenko et al., 1995).

For the second time, the rise was investigated during the SAKURA expedition in 1999 (Biebow et al., 2000). The data obtained showed that this rise (named Sakura Ridge) has a clear rift imprint. The morphology of its axial high suggests that it corresponds to a spreading axis. This axis (a spreading ridge) strikes N-S, i.e. in correspondence to the general strike of the Kurile Basin. Although this data is insufficient for a reliable identification of the spreading axis, it provides clear evidence for a SW-NE spreading direction, implying that the Kurile Basin opened along its general strike as a pull-apart basin (Baranov et al., 2002b). During the SAKURA expedition we mapped only one segment of it and the question how far the ridge continues to the north and south remained open. Obvious is only that it becomes wider to the north, and it was suggested that the ridge is apparently bounded near the northern slope of the Kurile Basin by a strike-slip or transform fault. On cruise LV29 the mapping of the ridge was therefore continued to the north.

1. CRUISE NARRATIVE

Nicole Biebow and Ruslan Kulinich

The research vessel *Akademik Lavrentyev* departed from Vladivostok on May 27th, 2002 with 17 Russian scientists and 35 crew members aboard. Modifications on the deck of the ship had been performed to accommodate a German self-contained mobile deep-sea winch system (MobiWinch) with a 20 mm conducting cable for work at sea. The MobiWinch was planned to be used for OFOS deployments, TV-grab sampling and coring. CTD castings and water sampling were planned to be carried out with the Russian hydrographical winch.
The vessel arrived in Pusan harbor on May 29th, 2002 in the morning. On the same day, 8 German, 2 Russian, 1 Italian and 1 Belgian scientist as well as their scientific equipment arrived and were transferred on board. At noon of May 30th RV *Akademik Lavrentyev* left Pusan harbor and made its way to the Sea of Okhotsk. The complete cruise track is shown in *Figure 1.1*; the working areas and stations are given in *Figure 1.2*.

Transit to the first area of investigations lasted about 4 days. This period was used for preparing and testing the equipment and laboratories for the upcoming work. At noon of June 1st we stopped for several hours in the Japan Sea to test the two winches. The Russian hydrographical winch had been equipped with a new cable and this had to be tested at 4,000 m water depth. The test of the cable was successful, but the test of the MobiWinch showed a malfunction of the spooling device, which seemed to be only a small problem at this time. During the stop, a Japanese reconnaissance plane several times overflew the vessel.

RV *Akademik Lavrentyev* reached the first area of investigations (Terpeniya Bay) in the afternoon of June 3rd, and the sampling program including CTD casts and hydrocorer deployment begun. We started with a CTD at a water depth of 80 m at one of the methane monitoring stations of the KOMEX I project. Again, we were able to detect very high methane concentrations, which were 200 times higher than the normal background values. The planned hydrocorer deployment had to be canceled due to a malfunction of the MobiWinch. Suddenly, we were not able to start the winch anymore, and both German technicians started to do whatever possible to repair the winch with the shipboard equipment. We finished this station with the calibration and a test of the swath bathymetry system called Lola II, which was successful. Then, RV *Akademik Lavrentyev* continued its way into the Derugin Basin.

We reached the Derugin Basin on June 5th at 4:00 p.m. local time and started our work in the area of the "Barite Mounds" known from the LV28 and GE99 cruises. Unfortunately, even with the help of specialists at home by e-mail and telephone we were up to then not able to repair the MobiWinch. Therefore, the period from June 7th to 11th was mainly devoted to CTD investigations along several profiles across the "Barite Mounds" area. For the first time, we were able to extensively map the methane plume and its extension in the barite area. Amazingly, our Russian colleagues were able to reproduce the concentration of methane in these plumes with the same values measured on cruises LV28 and GE99. This shows on the one hand that their method is very reliable and on the other hand that here methane venting is a continuous process over longer periods of time. The nights were used to map this area with the swath bathymetry system which worked very successful.
On June 10th, we thought for a short moment that we succeeded in repairing the MobiWinch, because we found and replaced a broken cable. But then, during trying to core sediments at 1,500 m water depth, it was found out that the winch had further defects which strongly hindered our work and because of which the deployment of cores and video equipment was impossible at water depths of more than 400 m. Nevertheless, the communication and

cooperation between the German and Russian teams and the vessels crew was excellent during this difficult time.

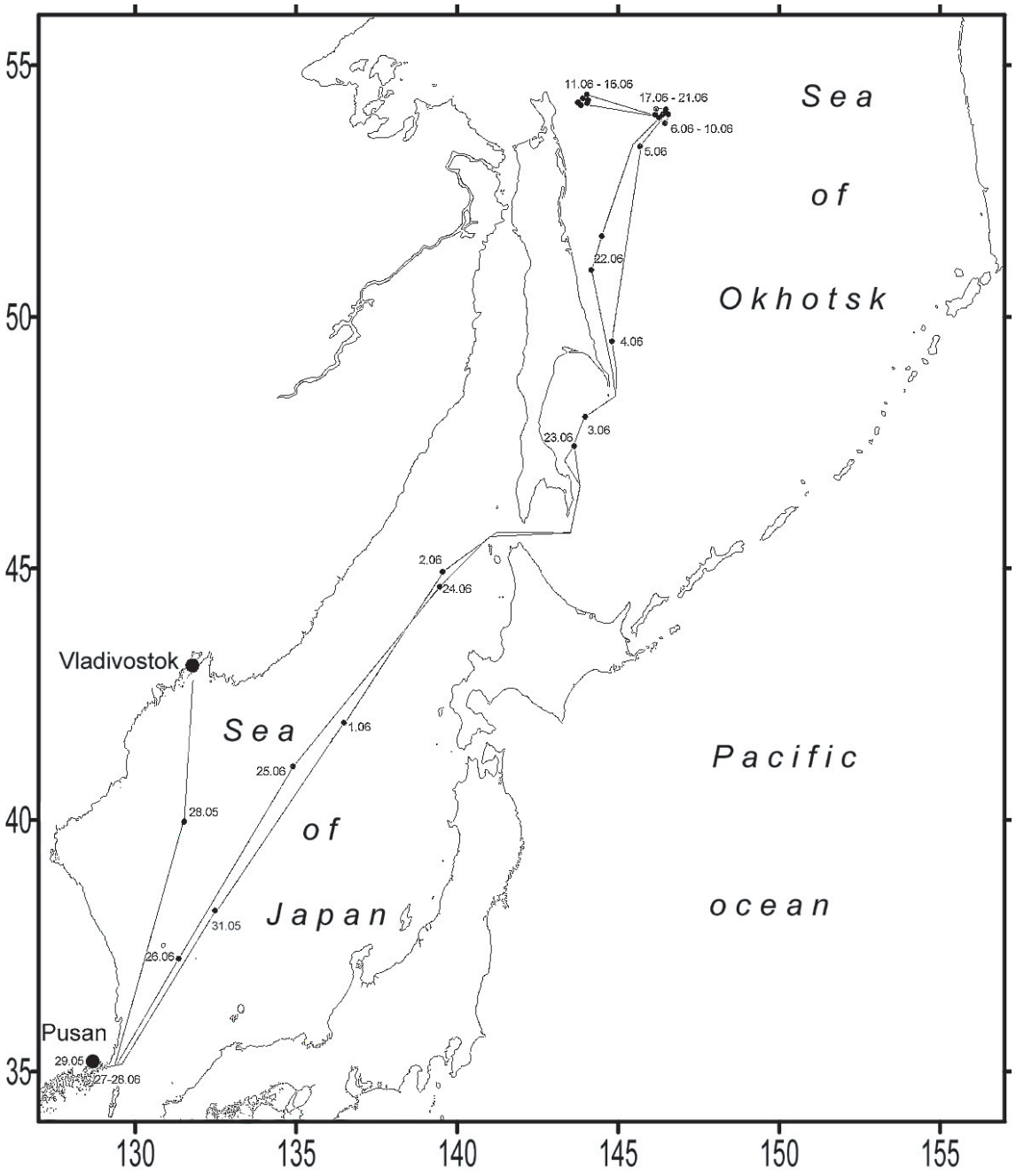

Fig.1.1: *Ships track of RV Akademik Lavrentyev 29th cruise, Leg 1, May - June 2002.*

In the evening of June 11th, we had to leave the Derugin Basin in direction of Sakhalin due to bad weather and bad performance of the MobiWinch. From the morning of June 12th on, we mapped and sampled the methane flares on the shelf and continental slope of Sakhalin. Apart from the flares already known from previous cruises, we discovered several so far unknown methane flares. We could record them now in more detail and also reconstruct the speed of the bubble rise by the improved echosounding system of our Russian colleagues. Methane flares from a water depth of 400 m ("Giselle flare") were visible up to the sea surface. This shows that methane produced here at the seafloor reaches the atmosphere.

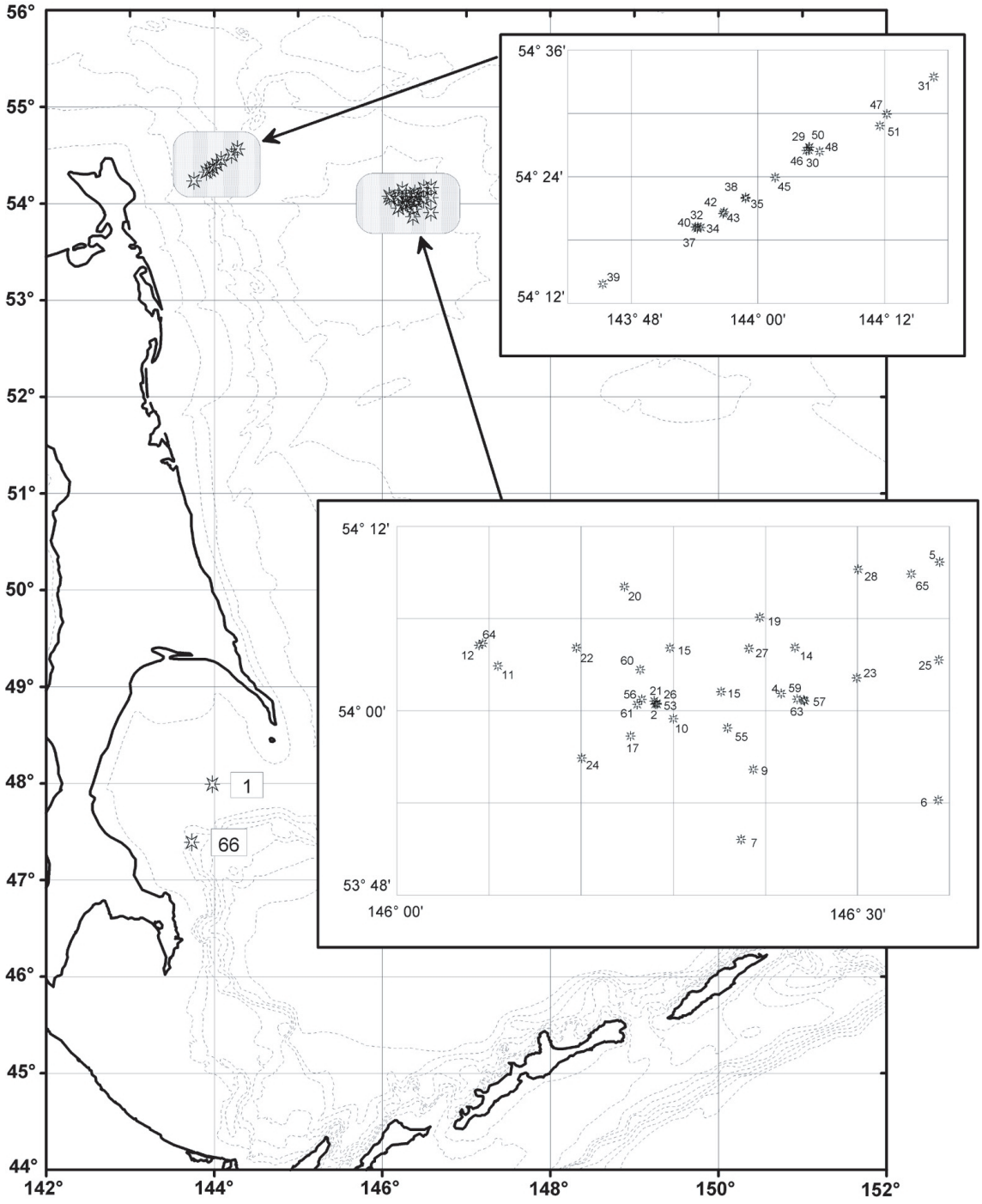

Fig. 1.2: *Map of the working areas (shaded rounded rectangles) and stations (asterisks) during 29th cruise, Leg 1 of RV Akademik Lavrentyev, May - June 2002.*

On June 12th, we were for the first time able to successfully deploy the gravity corer and twice the OFOS equipment on the shelf off Sakhalin at a water depth of 200 m in an area that is characterized by numerous methane flares. Apart from huge edible crabs, we also saw vent precipitates on the OFOS records. The attempt to sample the precipitates with the TV-grab on morning of June 13th failed due to problems with the MobiWinch: shortly after lowering the TV-grab into the water, we had to stop and were not able to get it out of the water again. Within several hours we picked it up meter by meter with the shipboard crane, and all of us were very glad that we did not loose the TV-grab and decided not to use it again.

On June 14th, our outstanding technicians succeeded in repairing the winch with only board devices to such an extent that most of our work could be carried out even in greater water

depths. Nevertheless, the winch had to be run by two persons during OFOS deployments, one person driving the winch and one person steering the spooling device. The whole group of Russian and German scientists we very enthusiastic to share the work with our technicians so that we could establish a dayround coring and OFOS program.

On June 15th, our patience was rewarded for the first time by a great success: we recovered gas hydrates in a sediment core from the Sakhalin slope (Obzhirov flare) at 4 m core depth. The core also contained large amounts of carbonate concretions and had a strong odor of hydrogen sulfide.
On June 16th we sampled a formerly unknown flare area at 800 m water depth by gravity corer and CTD.

On June 17th, we returned to the Derugin Basin in order to continue the work which we had to cancel on June 10th due to the defect winch and bad weather. From June 17th to June 21st, investigations were carried out mainly in the carbonate-barite mineralization area. Unfortunately, a lot of the cruise time had been wasted due to the malfunction of the MobiWinch, and our initial working plan had to be changed significantly. We therefore decided to shift additional coring and dredging program to the second leg of this cruise and started to extensively map the barite mineralization area by OFOS and swath bathymetry, which was very successful.
We observed huge vent sites with barite chimneys up to 10 m height and living *Calyptogena* clams. Thereby, it was found out that the Russian hydroacoustic system is able to detect the barite chimneys as individual reflectors. By comparing the hydroacoustic records with our OFOS profiles we were able to map these barite sites extensively. Apart from that, we discovered numerous smaller vent sites in the Derugin Basin which do not show such large barites, but are characterized by dense clusters of living *Calyptogena* clams.
We also recovered 4 sediment cores from the barite mineralization area which contain many barite and carbonate precipitates as well as shells of *Calyptogena* clams. The cores show typical degassing structures at their bases. This indicates that we sampled here the barite-forming fluids.

In the night of June 21st the works had to be finished and the vessel started to proceed towards Pusan. We shortly stopped on June 22nd in Terpeniya Bay to carry out one final CTD station in an area where we had observed a new methane flare at the beginning of the cruise. We passed La Perusa Strait in the evening of June 23rd and arrived in Pusan in the evening of June 26th. The next morning, a pilot was taken aboard and we proceeded into the port of Pusan and tied up at pier at 7:00 a.m. local time.

2. TECHNICAL SUPPORT OF THE HYDROACOUSTIC OBSERVATIONS

Alexander Salomatin

Acoustic observations were carried out using a hydroacoustic system created on the basis of the modernized shipboard echosounders Sargan-AM, ELAC, two sonars Sargan-GM and two multichannel systems of digital sonar signal registration.
The modernization of the shipboard echosounders included:

- making the operation of the echosounder Sargan-AM at two frequencies simultaneously possible;
- ping synchronization of all acoustic devices being in use;
- an exchange of a part of the receiver of the echosounder and the Sargan sonars;
- a change of the analog acoustic signal registration systems (by pen recorders on special paper) into multichannel systems of digital registration at personal computers with visualization in form of color echograms.

The hydroacoustic system provided the opportunity to simultaneously registrate acoustic signals by five independent channels at frequencies of 12, 19.7 and 135 kHz.

Tab. 2.1: *General properties of the different sonars*

Device	**ELAC**	**Sargan-AM**		**Sargan-GM**	
Operating frequency, kHz	12	19.7	135	19.7	135
Beam width, °	12	10	10	14	4
Impulse power, W	2000	-	-	-	-
Duration of sounding impulses, ms	0.8; 3; 10	0.5; 1; 3; 10	0.16; 0.3;1; 3	1; 3; 10; 30	0.16; 0.3;1; 3

2.1 Multichannel system of digital registration

The multichannel system of digital registration (SDR) is designed for acquisition, preprocessing, accumulation and visualization of hydroacoustic information by four channels simultaneously and comprises:

- an analog unit;
- two sound cards Creative Labs;
- a personal computer (Pentium-200 or better);
- an operating system Windows 2000;
- software for input, processing and visualization of echo signals – “Sonic”.

The acoustic signals are converted into digital form by using the four 16-bit analog-digital converters of the sound cards. The parameters of the acoustic signal registration (depth range, depth resolution, average sound speed and others) are determined by software. The digitized acoustic signals are written into data files on the computer’s harddisk, 700 acoustic signal samples in each file (the quantity of samples in the file is determined by the software).
The acoustic signals were visualized on a monitor screen in form of color echograms, in which each channel was plotted in two echograms with respective depth scales and color palettes. The software provided synchronous detection, filtration, registration and visualization of the acoustic signals throughout all depth ranges.

2.2 Scope of the acoustic survey

The main purpose of the work was to detect and investigate acoustic indications of underwater gas emission sources. For this purpose, the level of acoustic backscattering was collected simultaneously at frequencies of 12, 19.7 and 135 kHz in the water column and from the seafloor.
Calibration measurements were carried out to provide a valuable calibration for all sonars by the method of multiple reflections. This enables us to determine the absolute values of acoustic backscattering at different frequencies.
The received data can also be used for:

- evaluation of the magnitude of underwater gas emission sources;
- evaluation of the reflection coefficient and other seafloor characteristics;
- registration of frontal zones, internal waves and other oceanological processes;
- registration of the spatial distribution of fish, large and middle zooplankton and acoustic evaluation of their biomass.

Acoustic backscattering was recorded in all stations and, allowing for weather conditions (sea roughness and wind-force less than 4-5), on the tracks between them. The total time of acoustic observations amounted to 480 hours.

2.3 Preliminary results

In the first leg of cruise LV29, 114 hydroacoustic anomalies (HA) were registered, the coordinates of which are shown in Appendix 2. The map of HA (gas flares) of the eastern Sakhalin slope is shown in *Figure 6.3*, Chapter 6. HA were registered at best at frequencies 12 and 19.7 kHz with an elevation of the signal above the noise of minimum 20 dB. We divided the HA into deep-water (water depth >300 m) and shallow (water depth <300 m) ones. While the vessel is moving, the appearance of deep-sea HA is totally different from that of sound-scattering layers so that the HA are easy to detect. Another fact confirming that these HA are caused by emissions from the seafloor is the absolute constancy of the HA occurrence over an extended period of time. Some examples of HA recorded while the vessel was moving are shown in *Figure 2.1*.
HA 54 rises from the bottom to 200 m depth and ascents with a constant slope from the seafloor to a depth of 360 m, determined by the relation of the speed of the rising scatterers, causing the HA, and the current speed at the seafloor. In this case, these speeds are approximately the same and the real angle of slope is slightly less than 45°. Above 360 m, the current speed decreases and the HA runs nearly vertically. The acoustic signals reach maximum values at depths of 350-500 m. This shows that the vessel slightly passed the center of the HA source. The width of the HA source is, obviously, less than 100 m. The diameter of the area sounded by the ELAC echosounder is 150 m and 80 m for 700 m and 400 m depths, correspondingly, which hinders a more exact determination of the diameter of this HA.
HA 57 consists of two separate sources located in a distance of about 100 m from each other. The peculiarity of this HA is that its forming scatterers are observed up to a depth of 50 m below the sea surface. HA 41 (“Giselle flare”), composed of minimum three sources, has an even more complicated form. In *Figure 2.2*, several tracks in “Giselle flare” with different speeds and courses are shown. The records made at slow speed and while the vessel was drifting are of particular interest. They show that the scatterers causing the HA rise from the seafloor to the sea surface. Moreover, the individual scatterers are distinctly visible in the last record, which allows to evaluate their rising velocity. The evaluation of a group of scatterers running from 100 m to 75 m depth yields a rising velocity of 15 cm/s.

In many cases, deep-water HA are associated with particular forms of seafloor morphology. In *Figure 2.3*, an enlarged echogram fragment of the near-bottom part of HA 54 is shown. It is well visible that the HA source is a small elevation with a height of about 6 m and a width of about 300 m. Such elevations were observed near the bases of HA 72, 73 and 83, too.
This allows us to draw the conclusion that deep-water HA are very likely caused by emission of gas bubbles from the seafloor.
It is more difficult to make such well defined conclusions about the shallow HA, especially when recorded at maximum vessel speed, because of an increased density of fish schools in the shelf area, which can have various forms. Several somewhat doubtful HA are given at the end of Appendix 2 by letters a, b, c and d. Very interesting records of shallow HA were made at slow vessel speed. An example of such a record during drift is shown in *Figure 2.4*. Due to a higher spatial resolution it is obvious that HA 35 consists of scatterers rising with practically equal and constant speed. Here, the rising velocity is a little bit higher and amounts to 20 cm/s. But there were also several scatterers rising with a noticeably higher speed.
An interesting result was the discovery of deep-water HA 94 separately situated at a water depth of 1,200 m (*Fig. 2.5*).
Additionally, a survey of barite build-ups was carried out in the Derugin Basin. This became possible due to the fact that the initial parts of acoustic signals from a bottom area covered with barite build-ups and a bottom area without them significantly differ from each other (*Fig. 2.6*). The occurrence of barites results in the appearance of an additional signal directly at the bottom, the so-called “upper barite reflector”, the duration of which depends on the height of the build-ups and their amplitude. With correctly chosen registration parameters, bottom areas with barite build-ups are well defined on echograms. An example of such an echogram is given in *Figure 2.7*.

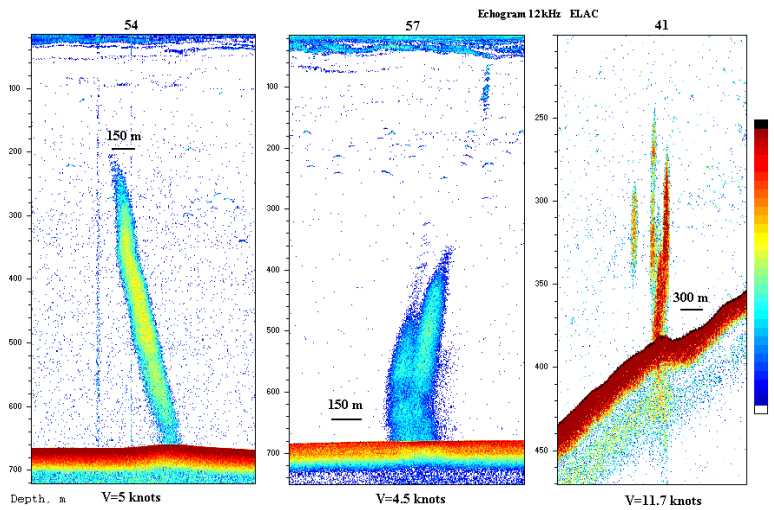

Fig. 2.1: *Echograms of deep-water HA made while vessel was moving.*

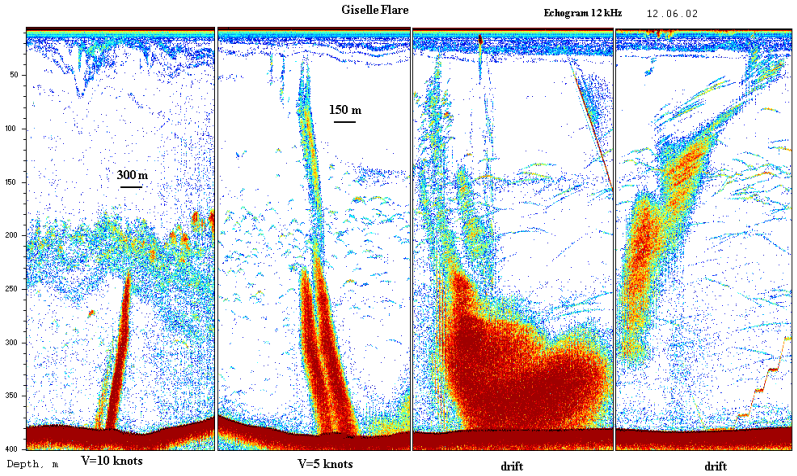

Fig. 2.2: *Echograms of deep-water HA made while vessel was slowly moving or drifting.*

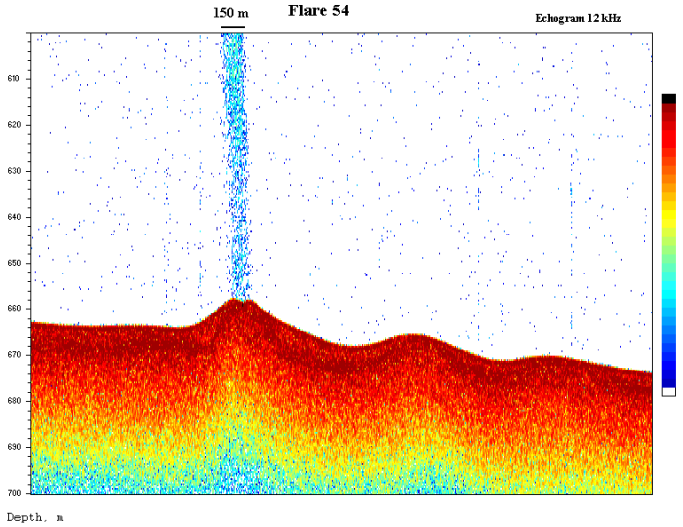

Fig. 2.3: *Echogram of the near-bottom part of HA 54.*

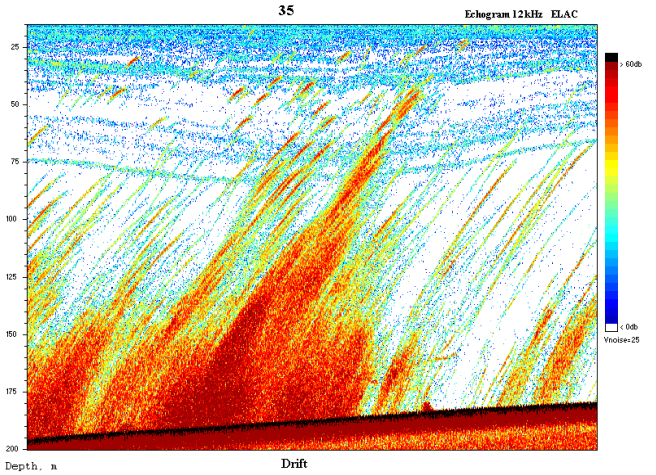

Fig. 2.4: *Echogram of the shallow HA 35 made while vessel was drifting.*

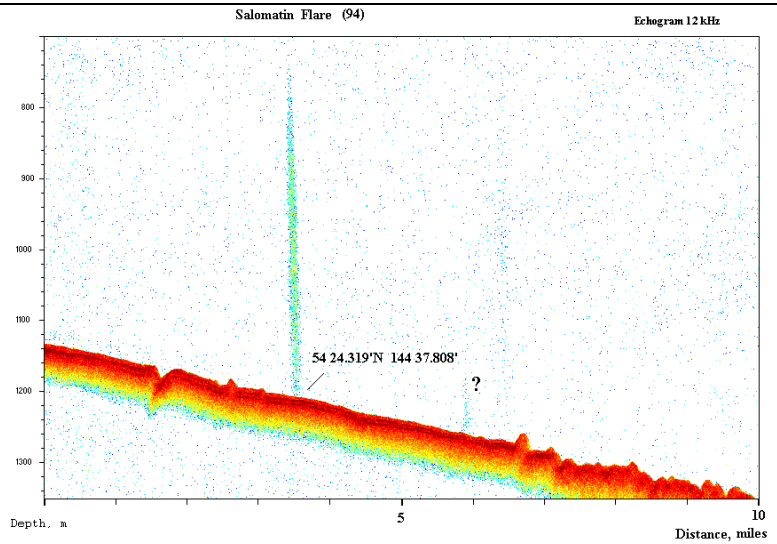

Fig. 2.5: *Echogram of the new deep-water HA 94 made while vessel was moving.*

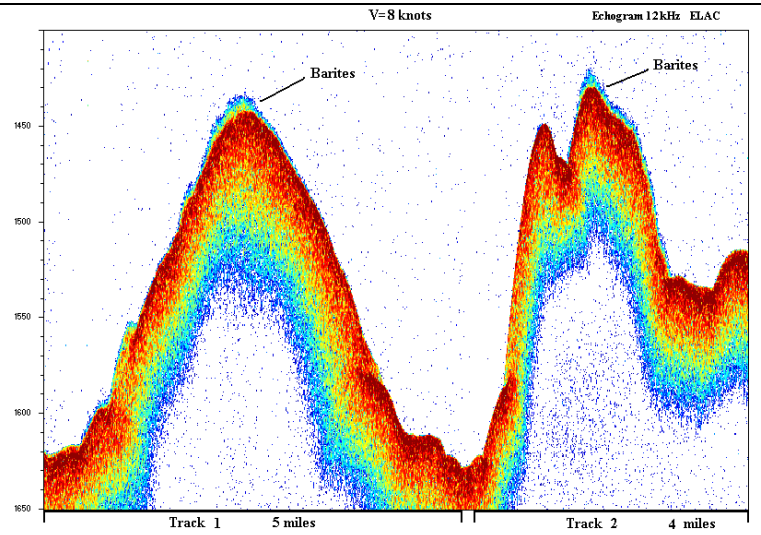

Fig. 2.7: *Echogram of barite build-ups in the Derugin Basin.*

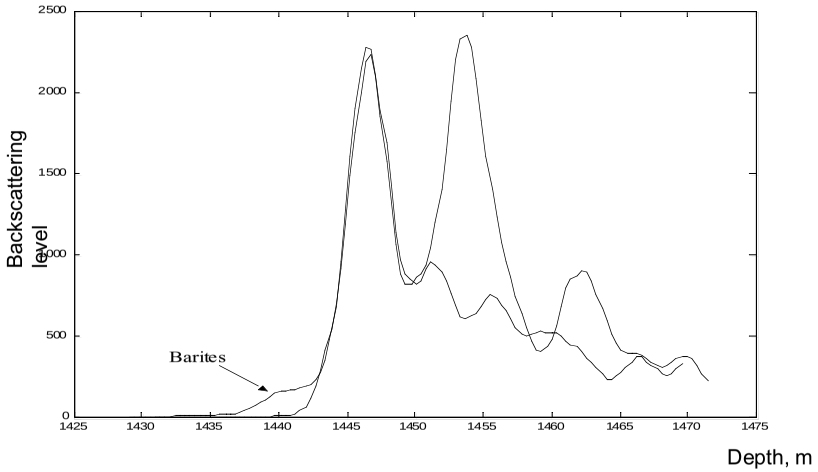

Fig. 2.6: *Initial parts of the reflected signals from a bottom covered with barite build-ups (solid line) and a bottom without them (dashed line).*

3. SWATH BATHYMETRY MAPPING

Hartmut Hein

A multibeam echosounder is a useful tool to get good bathymetric models and maps. Only with such a system it is possible to achieve full bottom coverage. These bathymetric models allow to map the real morphology of the seafloor for geodynamic interpretations and for planning detailed observations (coring, video-controlled records).
For the transducers/receiver arrays of the multibeam system, a special frame (called LOLA II) with 6 bouncy bodies was built at GEOMAR in Kiel. This construction was towed by a steel rope in a distance of 5 - 6 m to the ship's starboard side.
To get information about the heading and motion (hieve, rollangle, pitchangle) of LOLA II, a Gyrocompass (Octans3000 from iXSEA) with an integrated Motion Sensor was fixed in the middle of the frame. The used multibeam sytem was BOTTOM CHART MKII from ELAC-L3-Communications. *Hydrostar* software controlled the system and saved all rawdata with the position. The ship's GPS was used to get the positions in NMEA format. For postprocessing, we had to use *HPedit* and *HPpost* (ELAC).

Tab. 3.1: *Coordinates of swath bathymetry stations*

Station	*Investigation Area*		*Water Depths*	*Remarks*
	SW Edge	*NE Edge*	[m]	
Derugin Basin				
3-1	53°57.3' 146°10.0'	53°58.9' 146°45.4'	1410-1580	
8-1	53°56.5' 146°12.0'	53°58.0' 146°45.5'	1420-1590	sometimes no GPS
13-1	53°55.5° 146°10.1'	53°56.6' 146°45.2'	1480-1600	no positions
18-1	53°52.1' 146°32.2'	54°10.4' 146°35.8'	1480-1600	
54-1	54°02.0' 146°10.6'	54°03.5' 146°31.7'	1480-1680	problems to detect bottom
58-1	53°58.8' 146°28.8'	54°10.1' 146°33.0'	1520-1620	
62-1	54°01.3' 146°04.2'	54°06.5' 146°09.7'	1450-1650	
Sakhalin Shelf				
33-1	54°19.2' 143°55.0'	54°28.0' 143°27.9'	650 - 790	
36-1	54°19.2' 143°58.2'	54°27.9' 144°03.1'	180 - 650	
41-1	54°19.2' 144°02.2'	54°28.0' 144°06.7'	160 - 230	
44-1	54°17.9' 143°54.0'	54°21.4' 143°56.2'	220 - 400	
49-1	54°27.9' 143°54.1'	54°21.2' 144°02.2'	390 - 670	
52-1	54°27.7' 144°02.4'	54°31.2 144°06.6'	650 - 720	

3.1 Testing and calibration

At the beginnig of the cruise the behavior of LOLA II in the water had to be tested (unfortunately, it was only possible to test in Kiel whether the construction floats). After testing LOLA II in Terpeniya Bay we decided to use only five bouncy bodies in order to get the frame a little bit deeper into the water.
Due to an offset between the real rollangle of each transducer and the rollangle measured by the Motion Sensor, the system has to be calibrated. This problem can be solved by an overlap of the adjacent tracks in shallow water. The sound velocity model from CTD measurements was used to calibrate the depth values.

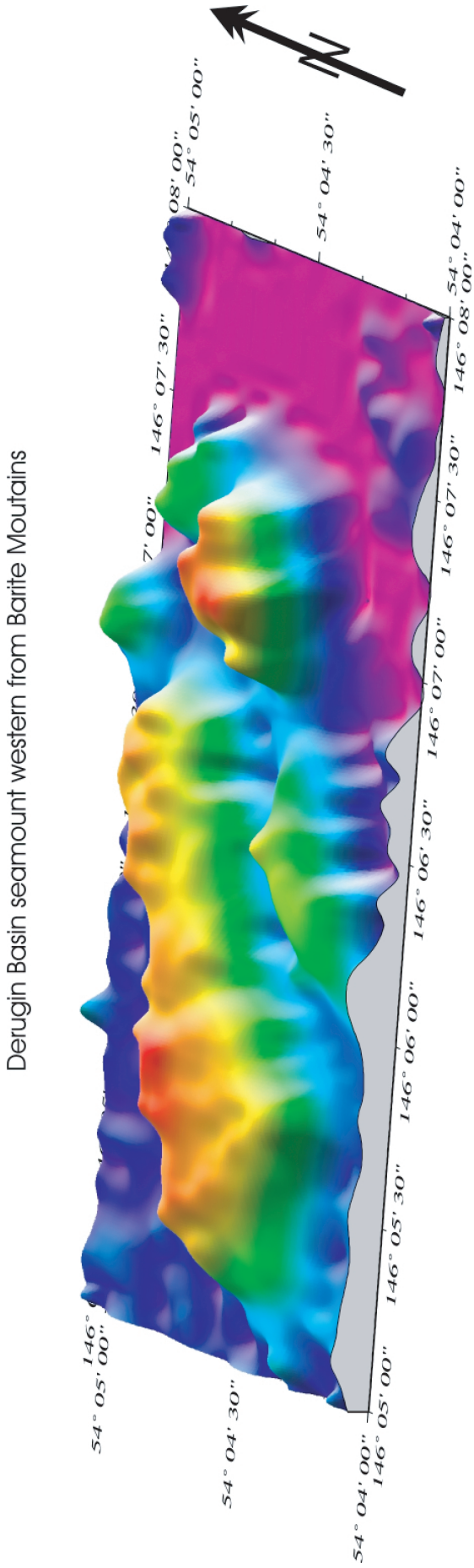

Fig. 3.1: *3D-image of the hills in the west of the "Barite Mounds" in the Derugin Basin.*

After the calculation of the offsets we were able to say that the accuracy of the depth error depending on a wrong calibration fits to the accuracy of the bathymetric model (min. 4 times better).

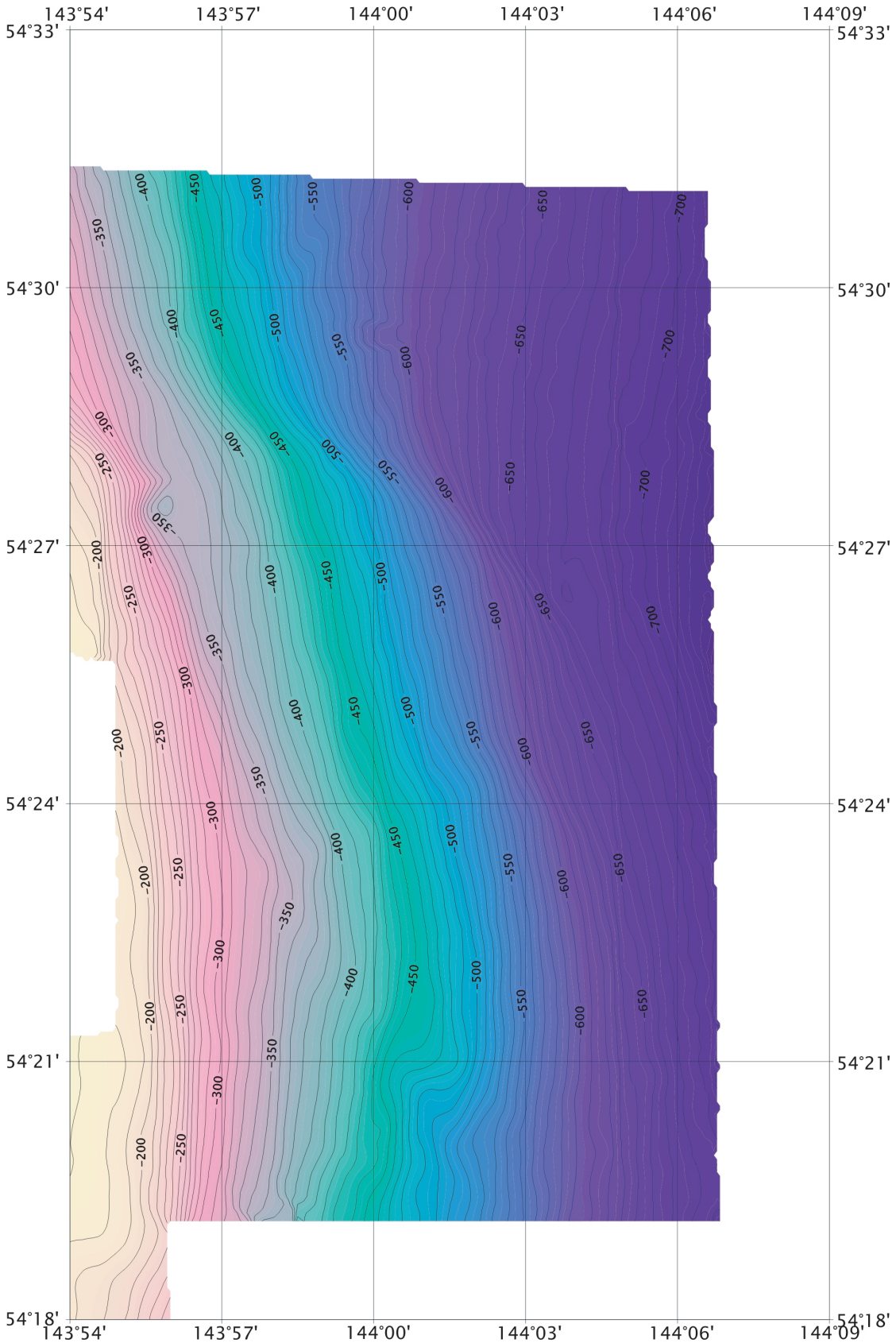

Fig. 3.2: *Bathymetric map of the northeastern Sakhalin shelf and slope.*

3.2 Investigation areas

The beam angle can be varied in discrete steps from 120° down to 18°. We decided to use beam angles from 60° up to 120° depending on the water depth: in shallow water, it is possible to use greater angles than in deeper water. The overlap of the tracks was defined as 20%. The ship's speed was 2 to 4 knots depending on water depth and weather conditions, which were quite well most of the time.

We were able to get a good coverage in the Derugin Basin and mapped areas in the south, in the north and in the east from the area mapped on cruise GE99 (see *Fig. 4.4*, Chapter 4). We also investigated hills west of this area (*Fig. 3.1)*, but we had not enough time to connect this with the bathymetric survey of cruise GE99.
On the Sakhalin shelf, the whole area between "Erwin flare" and "Obzhirov flare" (*Fig. 3.2*) was mapped as well.

3.3 Conclusions

The multibeam system worked quite well most of the time. A catamaran is not the optimal device for bathymetric mapping, because it is not easy to handle its movements. Probably, it would be a better solution to mount the transducers directly onto the ship`s body. For better measurement, it is important to get the transducers deeper into the water.
Sometimes, the positioning data of the ship`s GPS was not very well. An own GPS supported by the data from the Motion Sensor and the Gyrocompass would help to avoid such a problem. Additionally, the measurements from both systems could be connected with a Kalman filter to bridge the times with bad or no GPS data.

4. SEAFLOOR MORPHOLOGY OFF THE EASTERN OKHOTSK SEA COAST: RESULTS OF SINGLE- AND MULTIBEAM ECHOSOUNDER SURVEY

Boris Baranov, Hartmut Hein, Aleksander Salomatin, Aleksey Radyukin, and Gennady Nepomiluyev

4.1 Introduction

The bathymetric investigations conducted in the first leg of the 29th RV *Akademik Lavrentyev* cruise concentrate on two main targets:

1. Mapping of the seeping area along the eastern Sakhalin slope and the area of barite mineralization in the Derugin Basin in order to obtain an idea about specific bottom features connected with these phenomena;
2. Mapping of the major morphological features of these areas for tectonic purposes.

In addition to this, the obtained bathymetric maps served as a basis for sediment sampling, OFOS observations, dredging and hydrocasts. Two kinds of equipment were used for the bathymetric surveys: 1. single-beam echosounder ELAC (see Chapter 2 for technical details) and 2. multibeam echosounder LOLA II (see Chapter 3 for technical details).
The single-beam echosounder operated during the whole cruise, whereas the multibeam echosounder was used only in distinct areas which were chosen for detailed bathymetric investigations. There was no special track network for the single-beam survey except for the mapping of the "upper barite reflector" in the Derugin Basin (see Chapter 2). The space in between the multibeam tracks varied from 0.25 up to 1.1 nm depending on water depth and track direction. The total length of the LOLA II tracks was equal to 302 nm. In the first leg, one area was mapped on the eastern Sakhalin slope and two areas in the Derugin Basin (*Fig. 4.1*).

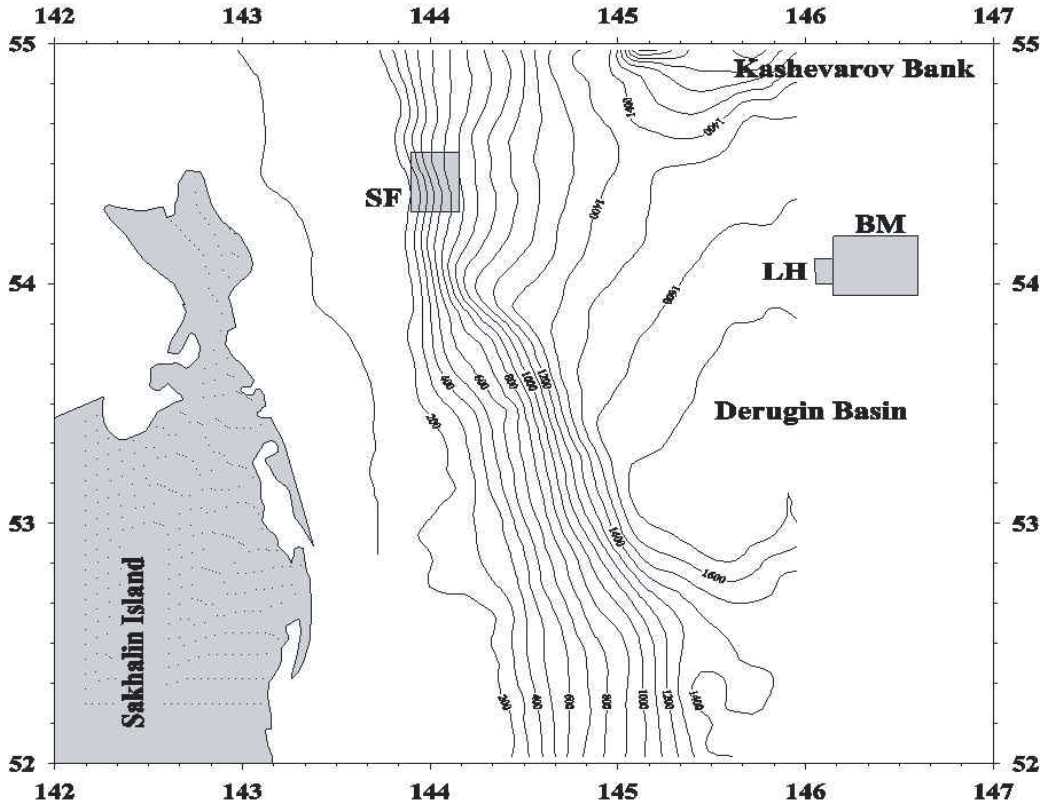

Fig. 4.1: *General location of the study areas (gray rectangular). SF = Sakhalin flares, BM = Barite Mounds, LH = Lola Hills. Contour interval is 100 m.*

4.2 Eastern Sakhalin slope

The morphology of the slope was investigated on the basis of a track network in a 180-700 m depth range. This network was regular and consisted of 30 N-S-striking tracks orientated along the general trend of the slope. The length of tracks varied from 3 up to 8 nm and the space between the tracks from 0.25 up to 0.8 nm. The total length of the survey was equal to 145 nm.

The bathymetric investigations along the Sakhalin slope show that the shelfbreak is very distinct and that it can be traced at depths between 180-190 m (*Figs. 4.2* and *4.3*, profile 1). Landwards of the shelfbreak lies the shelf which is represented by an eastward-sloping plain within a depth range of 50-180 m. The shelfbreak strikes generally in N-S direction except for the northernmost parts of the study area, where it slightly deflects to the west. Its contour is rather straight throughout the study area except for the southern part. Two small swells evident from the serpentine-shaped 190 m contour line and the shaded relief occur there. The larger one of them strikes in NW-SE direction and the smaller one trends to SW-NE. Another small swell is located at the northern shelfbreak (western margin of the study area) and has probably a SW-NE strike.

The slope has a slightly concave profile and can be divided into three parts: an upper (180-300 m), a middle (300-600 m) and a lower slope (600-650 m and below) which differ from each other in their forms and their angle of inclination (*Figs. 4.2* and *4.3*). The slope morphology is in general extremely simple and changes only slightly from south to north. The bathymetric maps (*Fig. 4.2*) of the study area show that the contour lines strike mainly in N-S direction with small deviations that occur in the northern part where the contour lines of the lower slope trend in NNE direction. Along the middle part of the slope the contour lines are clearly banded.
The upper slope has a maximal inclination angle of 2-3°. The shape of the upper slope is simple except for its northern part where a small asymmetric spur appears in depth interval 300-350 m. It has an asymmetric profile with its steep side trending to the northeast and facing to the southeast and is the most distinct feature of the whole slope (*Fig. 4.3*, profile 1). Two small spurs appear also on the southern boundary of the study area and strike in NW-SE direction.
The middle slope has the most remarkable structure. The contour lines in the northern part of the area show a sharp bend forming oblique steps, which are clearly visible as lineations of a NW-SE strike. Two more prominent lineations trending in NW-SE and NE-SW directions can be distinguished in the central part of area, as well (*Fig. 4.2*). These lineations restrict the small bulge that has a triangle shape and is slightly uplifted under the slope surface. In contrast to the general concave profile of the whole slope, its middle part has a convex form. Hummocks of a few meters height appear along both lineations and inside the bulge. Small hummocks occur also between the oblique steps and the northern edge of the bulge. They align in a more or less regular manner forming chains trending in SSW-NNE direction and are visible on the profile as a wavy surface (*Fig. 4.3*, profile 1). They occur also along the middle slope north of the oblique steps.
The lower slope is very shallow and has a simple morphology. Its characteristic feature is a divergence of the contour lines northward from the oblique step to the east, but not to the west. The seafloor of the lower slope is very smooth with occurrences of many small hummocks of a few meters height. These hummocks align in chains, which strike in two directions, namely SSW-NNE and NW-SE. The first direction corresponds to the strike of the lower slope contour in the northern part of the study area, and the second one coincides with the trend of the oblique step.

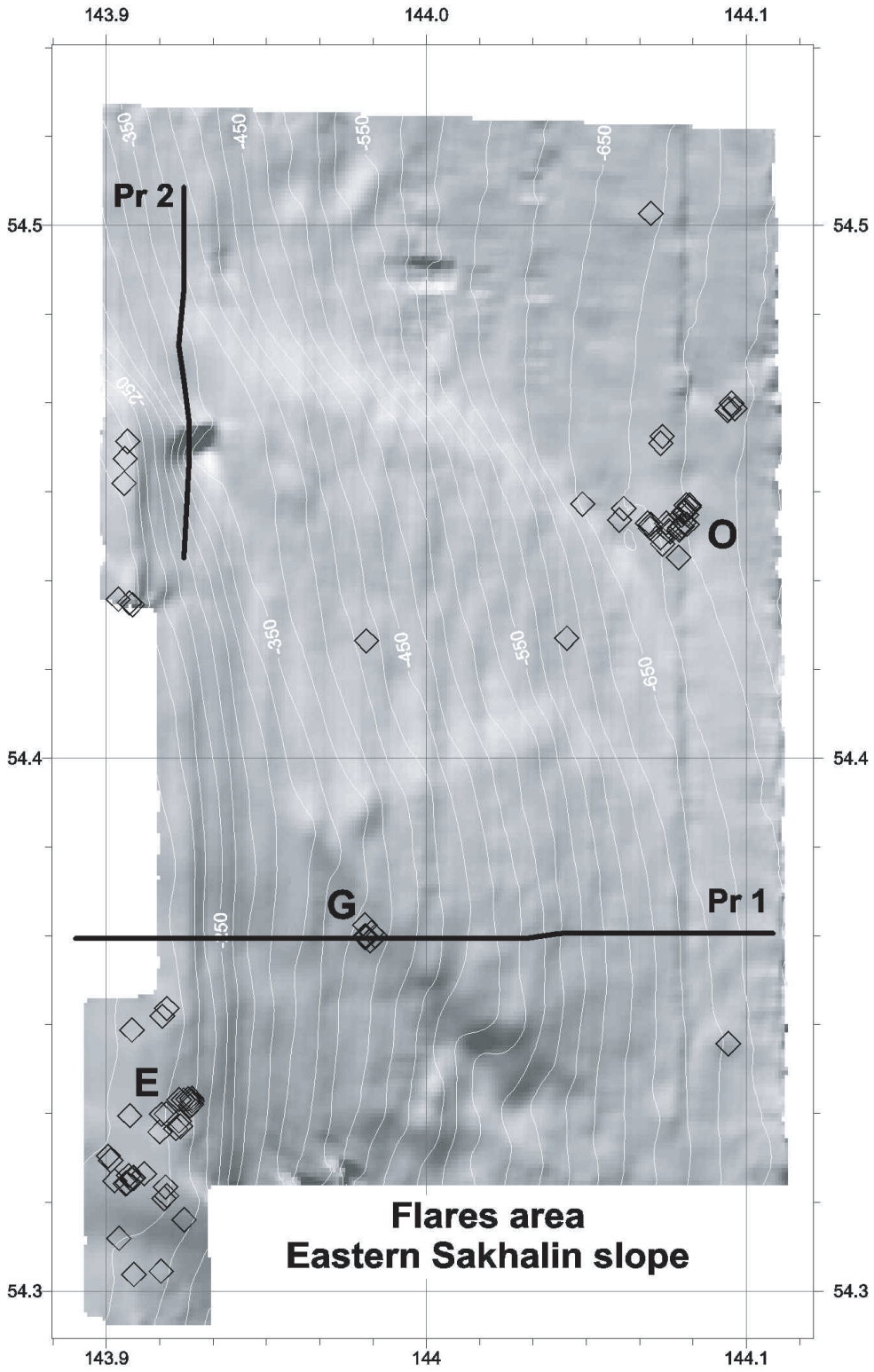

Fig. 4.2: *Shaded relief map of the Sakhalin flares area with overlapped contour lines. Contour interval is 20 m. Lines mark the location of the bathymetric profiles shown in Fig. 4.3. Diamonds indicate the positions of the hydroacoustic anomalies (gas flares). Flare fields: E = Erwin, G = Giselle, O = Obzhirov. Location of the map is shown in Fig. 4.1.*

The single-beam echosounder survey shows a good correlation between the observed hydroacoustic anomalies (flares) (see Chapter 2) and the morphological features. The detected flares concentrate in three locations: 1. near the shelfbreak, 2. in the middle part of the slope and 3. in the lower part of the slope.

Along the shelfbreak, the maximal concentration of flares was observed in the northern part of the area (the "Erwin flare" field) (*Fig. 4.2*). The flares line up in several zones, which have a NE and NW strike and are located in the small swells mentioned before or in flexures (sags) in between, which are trending in the same direction. The next two groups of flares are located in the northern part of the area and each one of them consists of three single flares. The flares of the first group concentrate more or less in single points and are located along the NE-striking swell. The flares of the second group trend in NS direction and occur at the beginning of the spur located in the middle slope.

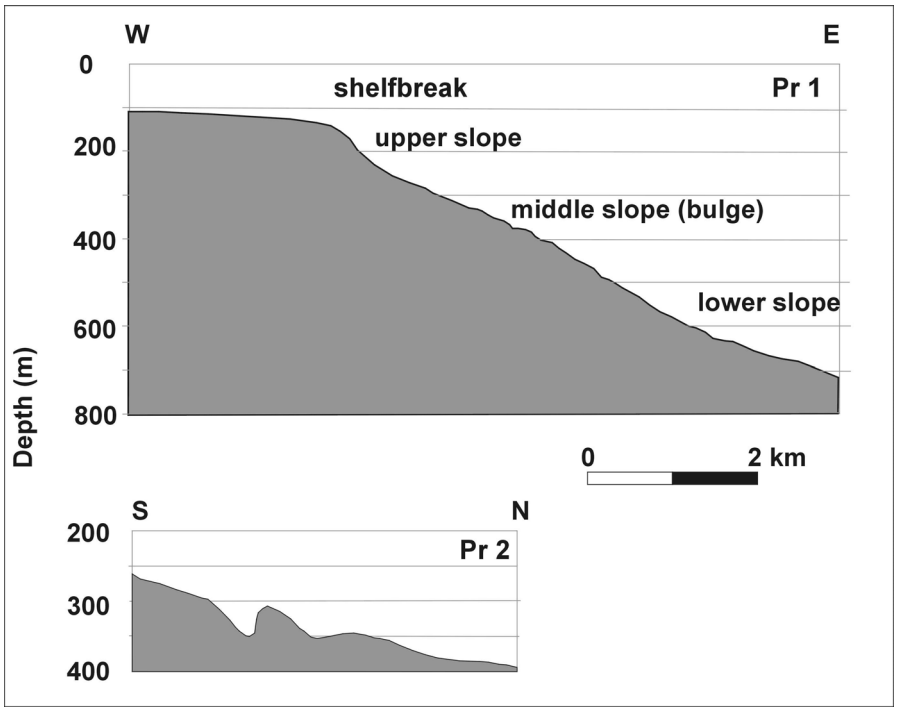

Fig. 4.3: *Bathymetric profiles showing the main morphological features of the eastern Sakhalin slope. Locations of profiles see in Fig. 4.2.*

Along the middle slope, maximum concentrations of flares were observed at the "Giselle flare" field (*Fig. 4.2*). This flare field is located on the slope of the hummock along the NW lineation, which limits the bulge from the south. The next two flares detected here appear on the slope of the hummocks.
Along the lower slope, maximum flare concentrations ("Obzhirov flare" field) occur at the southeastern end of the oblique step (*Fig. 4.2*). Similar to the shelfbreak, the flares concentrate here along two directions: SW-NE and NW-SE and occur on small swells consisting of separate hummocks.
Except for the "Obzhirov flare" field, several single flares or group of flares were detected on the lower slope as well. The deepest of them is located in a water depth of 800-900 m (outside the detailed bathymetric survey area). Most of these flares are concentrated on the slopes and less of them in the central parts of the hummocks. One of the deepest groups of them, consisting of five flares, trends in NW-SE direction.

4.3 Derugin Basin

Two areas were investigated in the Derugin Basin:
1. "Barite Mounds", and
2. "Lola Hills" (see *Fig. 4.1* for location).

The first area represents the extension of the map, which was prepared on the basis of a LOLA survey on the MV *Marshall Gelovany* cruise in 1999 (Biebow et al., 2000). This work intended to map the barite mineralization area.
On cruise LV29, the mapping area was extended to the south and to the east from the formerly mapped "Barite Mounds" (*Fig. 4.4*). The track lines for echosounding were carried out with a regular spacing. The lines strike in E-W direction for the southern part and in N-S direction for the eastern part of the study area. The maximum length of profiles was equal to 17.5 nm and the space between the tracks varied from 0.4 to 1.1 nm. The total length of the survey was 145 nm. The mapping of the second area was specially devoted to investigations of the small height, which was crossed on the GERDA cruise in 1995. This height looks like a diapir structure on the seismic profiles.

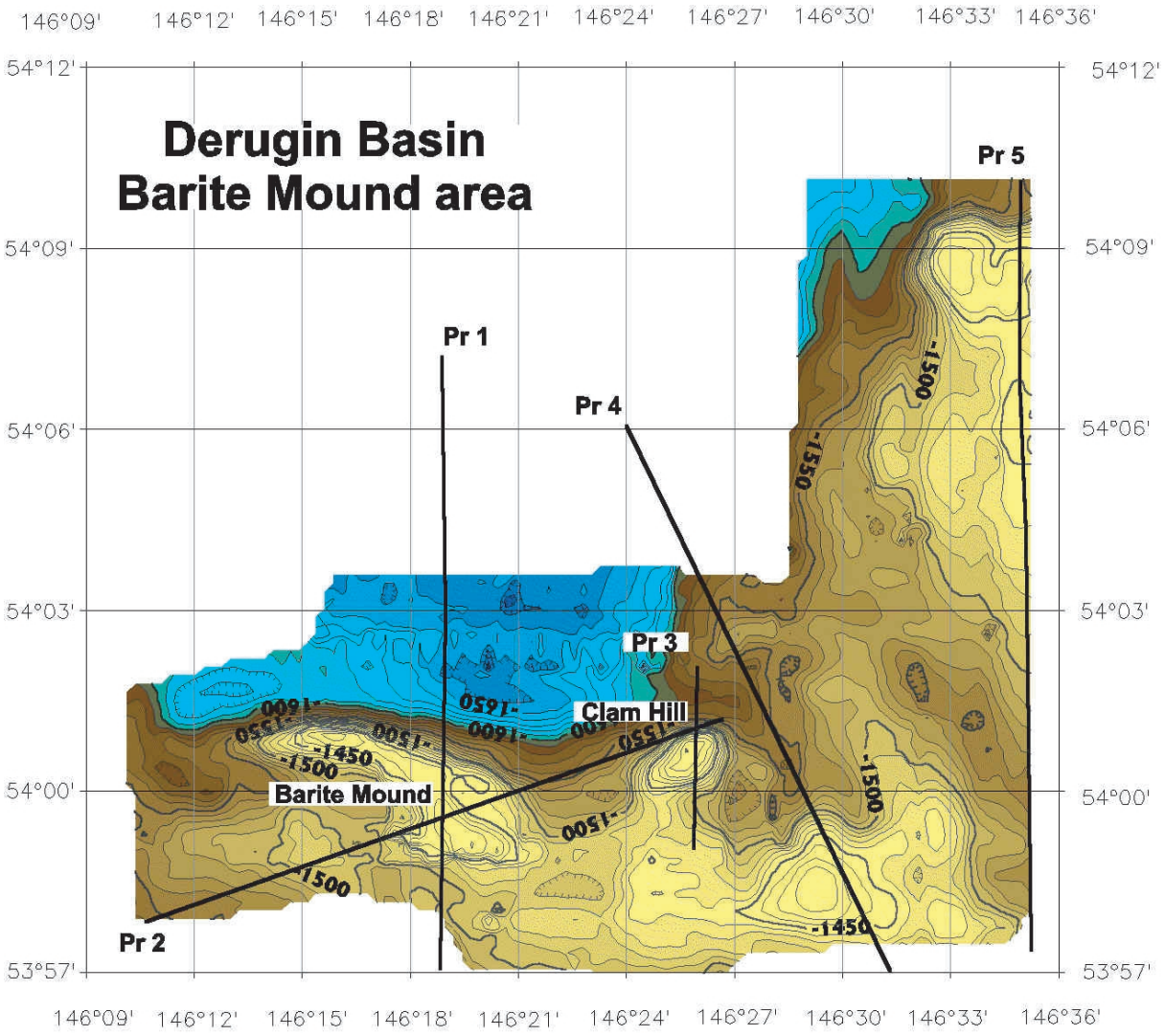

Fig. 4.4: *Bathymetric map of the "Barite Mounds" area. Contour interval is 10 m. Thick lines mark the location of the profiles shown in Fig. 4.5.*

4.3.1 "Barite Mounds" area

A basin with a water depth of up to 1,680 m occupies the central part of this area (*Fig. 4.4*). It is outlined along the south and east by a system of heights with a minimum depth of up to 1,420 m. As it was obtained before from seismic reflection investigations carried out in the framework of the KOMEX I project (Biebow et al., 2000), the basement of the Derugin Basin consists of tilted blocks. These tilted blocks have very characteristic forms. One side of the

block is steep and has a normal fault origin, and the second one is tilted. Sometimes, the tilted blocks are cut by normal faults from both sides forming a horst structure, but even in this case the surface of the horst is not plain, but tilted. Although the tilted blocks are covered by a blanket of sediments in the Derugin Basin, they appear in the seafloor morphology as small elongated ridges with one steep hillside and another slightly tilted hillside. Therefore, this structure can be determined even during the echosounder survey.

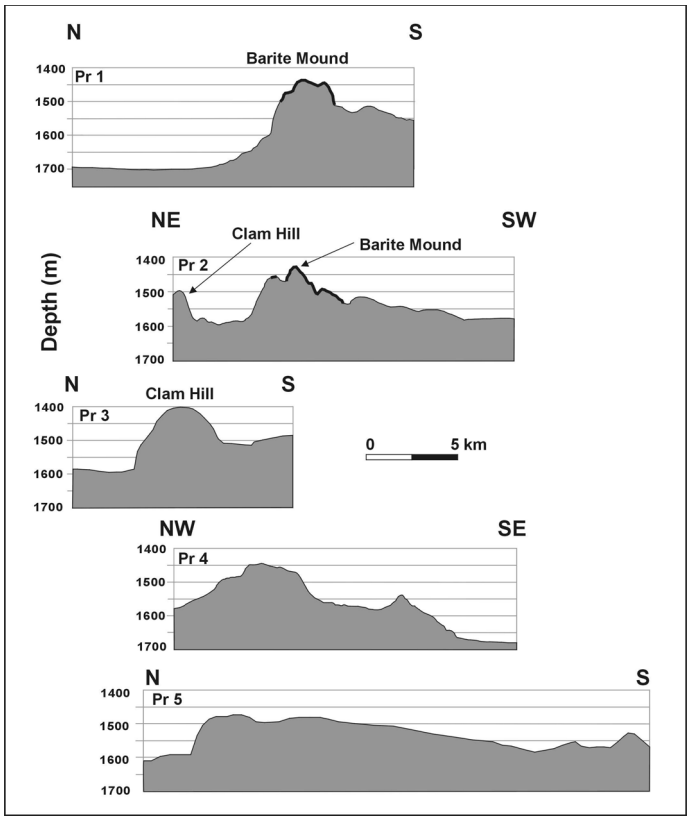

Fig. 4.5: *Bathymetric profiles showing different morphological features of the "Barite Mounds" area. Thick line indicates the area of barite mineralization. Location of the profiles is shown in Fig. 4.3. See text for discussion.*

Three tilted blocks with their tops outlined by contour line 1,450 m were distinguished in the investigation area. The eastern part of the area is occupied by a single block, which tilts to the south. The steep side of the block has a W-E strike and faces to the north (*Figs. 4.4* and *4.5*, profile 5). The top and southern slope of the block are smooth; its western side trends in NW-SE direction and has wandering outlines.

The second block is located in the southeastern corner of the map (*Fig. 4.4*) and separated from the previous one by a NW-SE-striking trough with a maximal depth of 1,550 m. This block has an E-W strike submerging from east to west. Its top tilts to the north and is cut from the north and the south by steep slopes forming a horst structure (see profile 4 in *Fig. 4.5*).

The third block yielding barite mineralization is located further to the west and strikes almost in W-E direction. Its northern slope is steep and faces to the basin. The top and the southern slope of the block are not plain like the blocks mentioned above, but are occupied by a mound. The mound can be subdivided into two parts: the western and eastern ones are arranged in an en-echelon pattern. Both parts strike in W-E direction. The northern and the southern sides of the mound are steep and probably have a fault origin. Exactly on this mound a giant field of barite chimneys was observed by OFOS on cruise LV28 in 1998 (Biebow & Hütten, 1999).

Due to the fact that the barite chimneys show a specific reflection on the echosounding profiles (see Chapter 2), a detailed single-beam echosounder survey was carried out on this mound in order to outline the area of barite mineralization (*Fig 9.3*, Chapter 9). This area roughly coincides with contour line 1,500 m (profiles 1 and 2 in *Fig. 4.5)* and strongly corresponds to the outlines of the mound.

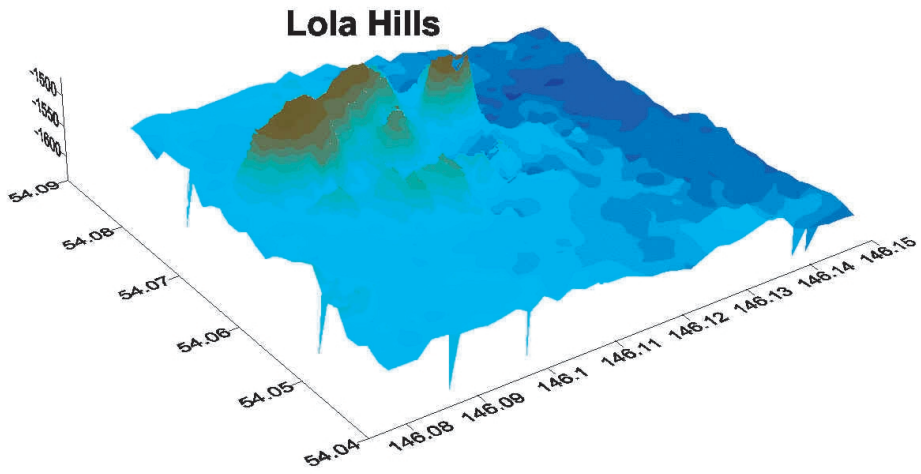

Fig. 4.6: *3D image of the "Lola Hills" area. This area consists of several hills and elongates in NE-ENE direction. See Fig. 4.1 for location.*

There are other morphological structures apart from the tilted blocks. The largest of them, called "Clam Hill" (due to the abundance of several *Calytogena* clams observed during OFOS survey), is located to the east from the "Barite Mounds". Its top is located in depths of a little more than 1,400 m (*Fig. 4.4*, profile 3), and the hill has rounded outlines slightly elongated in NNE direction. Another structure of such kind is located on the strike of the titled blocks and is orientated in WE or NW direction.

4.3.2 "Lola Hills" area

This area is connected to the "Barite Mounds" area in the west (*Fig. 4.1*) and was chosen for detailed investigations on the basis of seismic profiles carried out on the GERDA expedition (1995). The profile shows very amazing structures represented by a height which is elevated above the seafloor. It does represent neither an outcrop of bedrock's nor a volcanic edifice, but is more similar to an uplifted column of sedimentary cross-sections. A wipe-out structure was observed beneath this height that can be indicative of gas expulsions.
Because of the small size of the structure, only three tracks with a total length of 12 nm were run there. Our survey shows that several hills are located inside this area (we therefore named this place Lola Hills). They are situated on the shallow swell mentioned above, which limits the basin from the west. The hills have different sizes and altitudes. The minimal depth observed is a little less than 1,480 m, and the maximal dimension is about 1 nm. The sides of the hills are very steep (inclination is up to 30-40°); their altitudes reach 100 m. The total elevation of the highest hill above the flat basin floor is equal to approximately 150 m.

These hills are aligned in three groups from north to south. The northern group contains the largest hill striking in SW-NE (55°) direction (*Fig. 4.6*). This hill has a flat top outlined by the 1,480 m contour and seems to consist of four hills accreted each other. The middle group is represented by two large and one small hill of rounded outlines, which strike in the same direction. The southern group consists of five hills orientated in W-E direction.

4.4 Preliminary conclusions

1. Three directions of lineations were distinguished in the morphology of the eastern Sakhalin slope: NW-SE, NE-SW and NNE-SSW. The first two are the most pronounced. The hydroacoustic anomalies (flares) inside two flare fields ("Erwin flare" and "Obzhirov flare") concentrate along lines striking in NW-SE and NE-SW direction. This could be connected with the existence of fault systems.

2. Two directions are typical for the morphological features of the northeastern Derugin Basin: WE and NW-SE. The first of them is connected with fault scarps limiting the tilted blocks. The second direction is possibly connected with the existence of a second fault system.

3. The area of barite mineralization has a very good coincidence with the mound located on the top and the southern slope of the titled block. Due to the fact that it has very sharp northern and southern limits, we can suggest that its origin is connected with a fault system.

4. The origin of the "Lola Hills" remains unclear, and additional data is needed. However, the bathymetric survey shows that this structure consists of several hills, which align in NE-WE-striking lines, i.e. have more or less the same direction as the fault scarps of the "Barite Mounds" area. Therefore, we suggest that this structure can represent a diapir originating from compressional tectonics, which prevail recently in the Derugin Basin (Biebow et al., 2000).

5. WATER COLUMN STUDIES

Anatoly Salyuk, Valery Sosnin, Anatoly Obzhirov, Pavel Tishchenko, Galina Pavlova, Olga Vereshchagina, Natasha Khodorenko, Sergey Sagalayev, Nicole Biebow, Klaus Wallmann, and Bettina Domeyer

5.1 Introduction

The main objectives of the CTD observations in the first leg of cruise LV29 were water column investigations and water sampling in the methane venting area on the Northeast Sakhalin shelf and slope and in the barite mineralization area of the Derugin Basin. In the Derugin Basin, we concentrated our efforts on the mapping of a methane plume around the "Barite Mounds" in the central part of the basin. In the methane venting area we continued previous observations to compare methane concentrations in the well known vents like "Obzhirov flare", "Giselle flare", "Erwin flare" and searched for new ones.
Our observation demonstrated the importance of precise positioning of the ship during repeated observation of the same flare due to the high temporal and spatial variability of the flare orientation and its properties. For this purpose, we successfully used the shipboard echosounder.

5.2 CTD observations

Water column sampling was carried out using a rosette water sampling system consisting of a Sea-Bird-32 twelve position system with 10 liter Niskin-type bottles and a CTD probe Sea-Bird-911 with standard temperature, pressure, conductivity sensors and also sensors for oxygen light transmission, altimeter and bottom contact. The CTD was lowered up to 3 m above the seafloor at stations shallower than 100 m and to 8 m at deeper ones. Water sampling was started at maximum depths and the samples were taken during the upcasts. The interval of water sampling depended on the purpose of investigation, and the water depths varied during observations from 5 to 500 m.

5.2.1 Dissolved oxygen

The calibration of the CTD sensor for dissolved oxygen (DO) was done measuring DO in water samples by the modified Winkler method. DO concentrations in the water column at the moment of sampling were calculated from the DO sensor data taking into account the time deviation of the DO sensor for temperature.

5.2.2 CTD depth calibration

The depth of the seafloor was determined for each station by 3 different methods:

1) directly by CTD bottom contact. The depth at the moment of the bottom contact was calculated according to normal CTD formulas (UNESCO) using CTD pressure and station latitude;
2) calculated from the travel time of the acoustic signal measured by the ELAC echosounder and by the sound velocity, using the real temperature and salinity (TS) profile of the water column measured by CTD;
3) calculated from water compressibility, CTD pressure and TS data, using UNESCO formulas.

The calibrated ELAC echosounder depth data can be used also for depth calibration of historical depth data tracks crossed on this expedition, and for depth data obtained from other echosounding devices (LOLA II, SES-2000DS).
A total of 32 stations was carried out during the first leg of cruise LV29. Water samples were taken for pH and alkalinity, methane, oxygen concentration, oxygen isotopes, calcium, helium, and additionally 30 samples for investigations of the bacteria *Listeria monocytogena* were collected. All data is tabulated in Appendix 3.

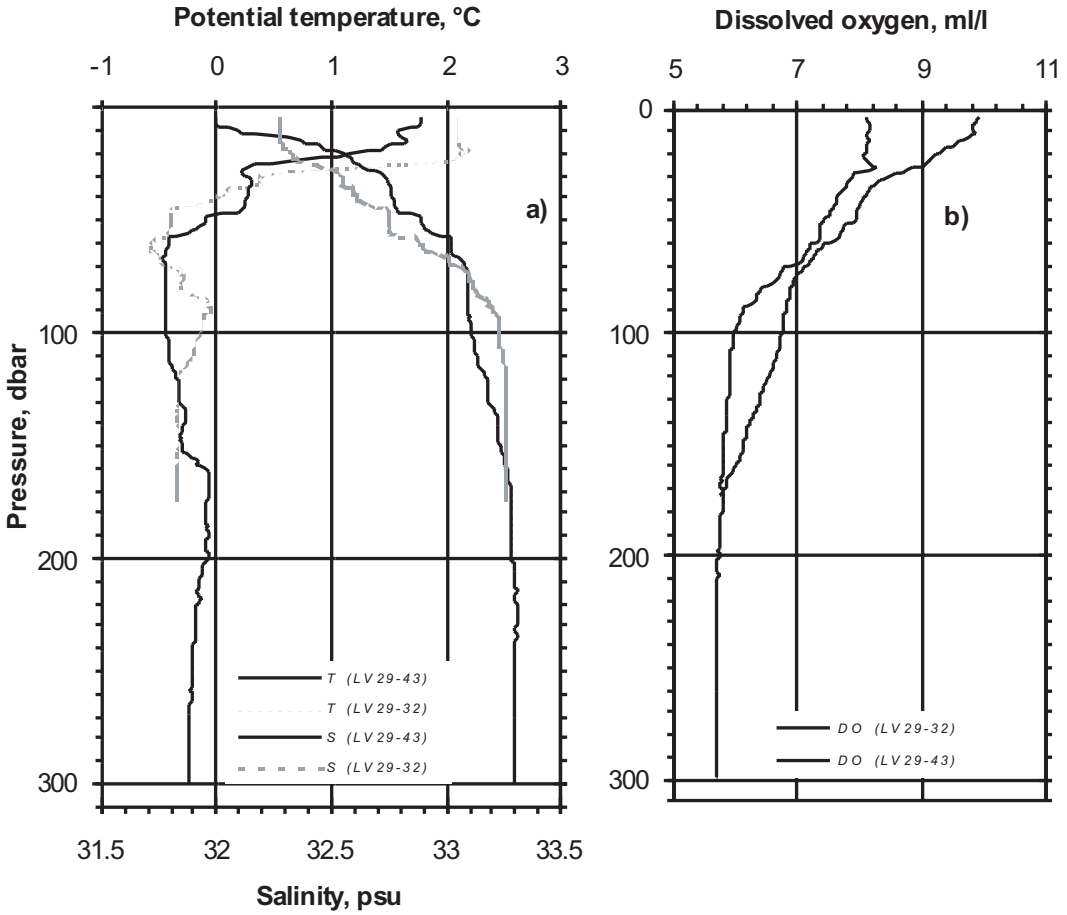

Fig. 5.1: *Vertical profiles of Potential temperature and Salinity (a) and Dissolved oxygen (b) at station LV29-43 and LV29-32.*

5.3 General hydrographic situation

The first leg of the LV29 cruise took place in spring subsequent to an anomalously warm winter season. In comparison with the analogous season of 1999, the properties of the sea water reflected warmer conditions indicated by higher water temperatures. The shelf waters had a temperature significantly above the freezing point. But winter conditions could still be observed in Terpeniya Bay. The hydrographic conditions of this area showed an anomalously intensive development of the dichothermal layer which is a product of winter cooling and of the specific circulation in this bay. The dichothermal layer was characterized by almost thermostad and halostad conditions at subsurface depths between 50-250 m.
Anticyclonic activity and meteorological conditions with calm weather dominating during Leg 1 were favorable for CTD and other observations. During the whole period of Leg 1 sea-ice fields were concentrated in the northern part of the sea as well as in the western part of the Tugur area and around northern Sakhalin. Sea-ice fields were observed on the eastern side of

Sakhalin towards 52°N. The average air temperature was 3-4°C. At the end of Leg 1, sea ice remained only in Tugur Bay.
All necessary information about the general water circulation in the Okhotsk Sea is given in the cruise reports of the KOMEX I expeditions (Biebow & Hütten, 1999; Biebow et al., 2000) and is therefore not repeated here.

5.4 Main hydrographic features

The CTD stations of Leg 1 were divided into two groups according to their purposes and geographical location: the Derugin Basin barite area and the gas hydrate and methane venting shelf and slope area. The total number of CTD stations was 32, 21 of which were carried out in the Derugin Basin and 9 in the slope area. The shipboard echosounder was used for more correct methane studies, for finding flares and for a precise positioning of the ship directly above the vent.

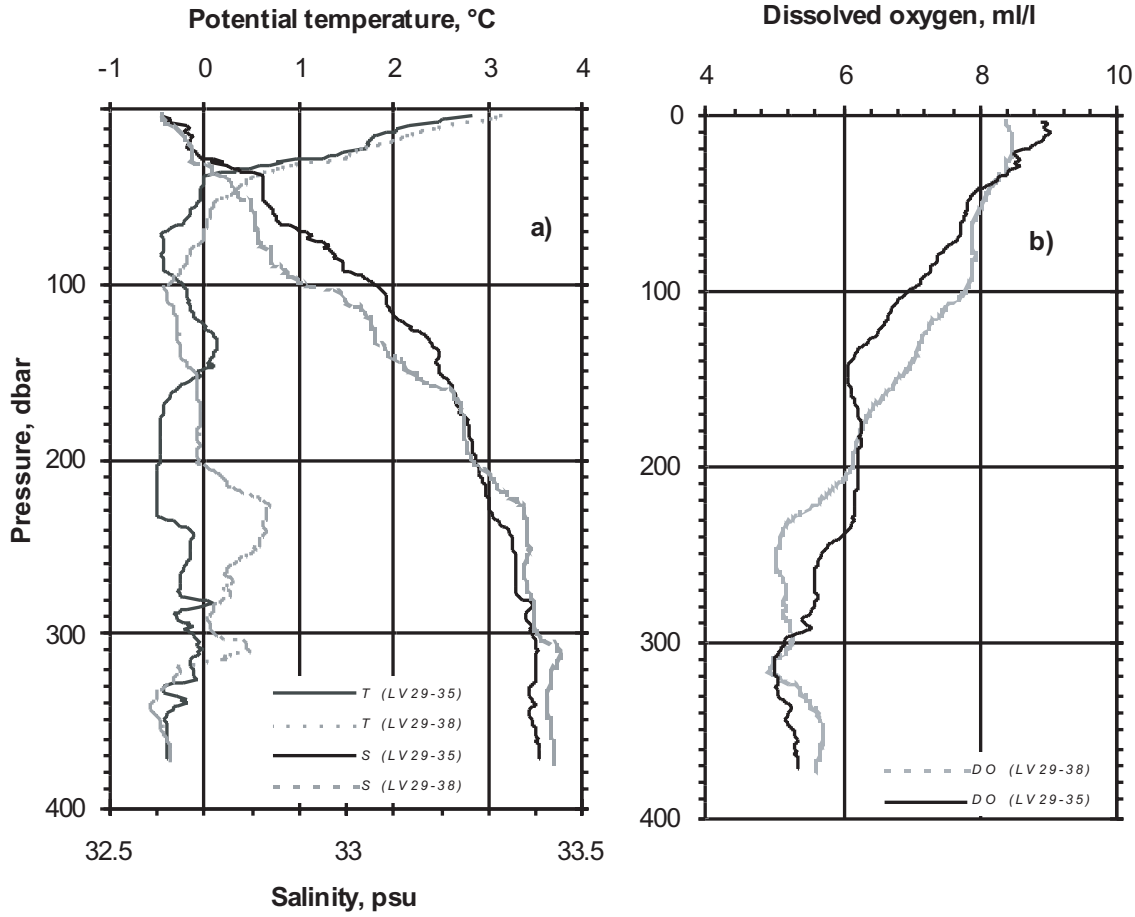

Fig. 5.2: *Vertical profiles of Potential temperature and Salinity (a) and Dissolved Oxygen (b) at stations LV29-35 and LV38.*

5.4.1 Shelf - slope area

The hydrological conditions on the shelf reflected the spring heating with positive (1.5°C) surface temperatures and negative temperatures in the homogeneous near-bottom layer (*Fig.* 5.1, station LV29-43).

Our new observations support previous conclusions from other KOMEX expeditions about an intensive mixing activity near the slope. Waters with different properties coming into this region from the northern and western shelf and from the deep sea mix and produce a lot of fine structural elements in the water column. The following comparison of two CTD stations serves as a good example for this:

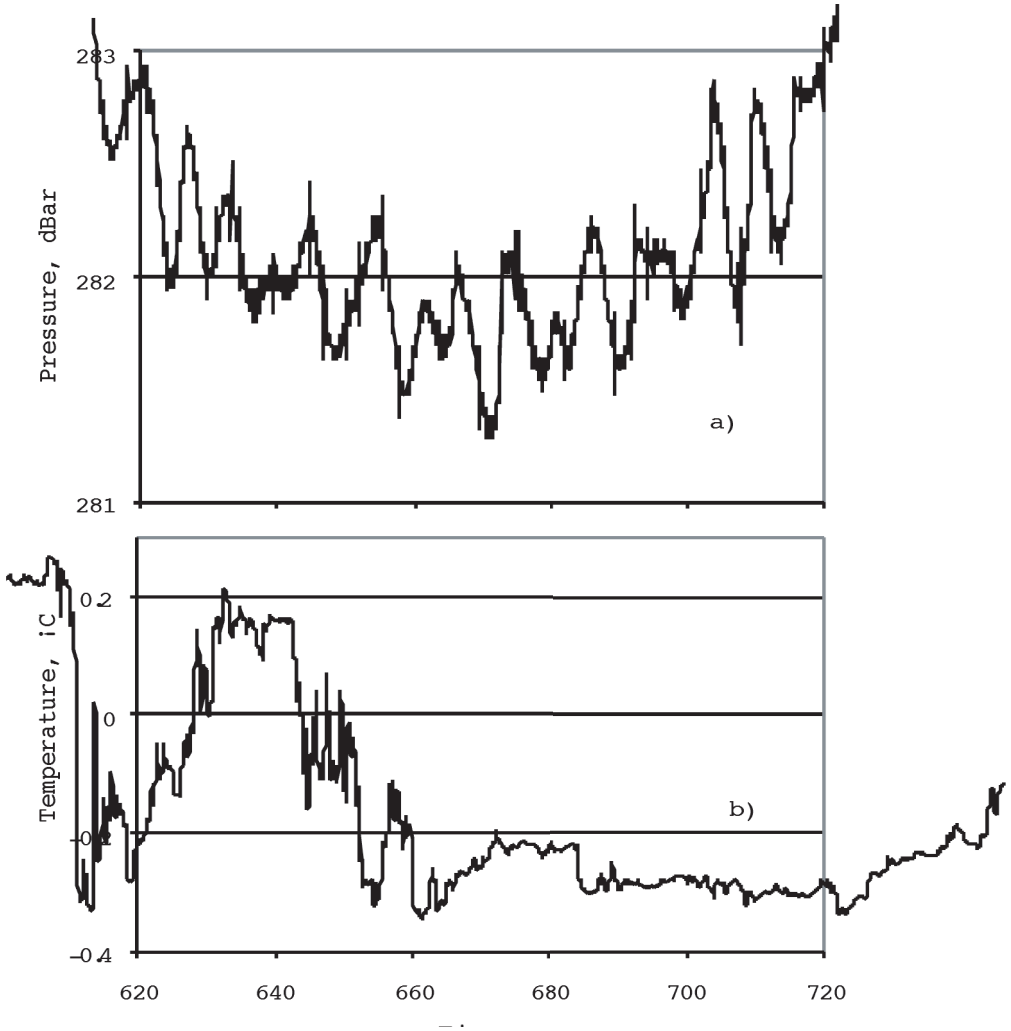

Fig. 5.3: *Temporal variability of pressure (a) and temperature (b) during a longer stop at station LV29-35, downcast.*

Two CTD deployments were carried out (station LV29-35 and -38) on the Sakhalin continental slope in the gas hydrate area ("Giselle flare"). Both stations were sampled nearly in the same location directly in the flare, but the observational results surprisingly differ from each other. Firstly, the echosounder showed different images of "Giselle flare" during the CTD casts, and significant differences in the hydrographic properties were measured. Both stations are characterized by an intense intrusion interleaving below 50 m depth. The whole water column reflects intense mixing processes (*Fig. 5.2*, stations LV29-35 and -38). The most outstanding feature was the appearance of a oxygen minimum layer at station LV29-38 at depths of 230-350 m. It is necessary to mention a very high temporal variability of the TS properties over a short time. Fortunately, we made urged temporal observations at approximately 300 m depth while waiting for the precise positioning of the ship above the vent. This record was made in the middle part of the warm intrusion at station LV29-35 (*Fig. 5.3*). During the observations the temperature values at this depth varied from -0.3°C to +0.2°C in a few seconds. The fine thermohaline structure of the warm intrusion supports the idea of an intensive mixing in the water column.

"Giselle flare" is situated in the conjunction point of two branches of the main current system of the Okhotsk Sea. One of them is the Northeast Sakhalin current along the Sakhalin coast and the other one is the northwestern periphery of the cyclonic circulation in the Derugin Basin. Additionally, tidal currents of diurnal type influence the mean flow. This is proved by the unstable character of the ship's drift during calm conditions.

Tab. 5.1: *Time of high and low sea level for place Moskalvo (53°36`N/143°30`E) nearest to cape Elizabeth (local time)*

Date	Time	Level
06/11	08:36	1.7 m
	23:31	**0.3 m**
06/12	09:12	1.8 m
	23:32	**0.2 m**
06/13	09:52	1.9 m
	23:32	**0.2 m**

Station LV29-35 was carried out on June 12th, 2002 at 22:52 p.m. local time and station LV29-38 on June 13th, 2002 at 15:07 p.m. According to *Table 5.1*, our observations were made in different phases of the tidal cycle: station LV29-35 was conducted during low water with minimum tidal currents, whereas station LV29-38 was carried out during maximum tidal currents.
The acoustic image of "Giselle flare" for the period of station LV29-35 demonstrated a straight vertical position of "Giselle flare" almost up to the surface. In contrast to this, the acoustic image of station LV29-38 demonstrated a strong inclination of the flare towards the south due to a reinforced mean flow. The flare lies almost horizontally along the bottom. By the way, this image represents the lowest inclination among all observed flares.
A possible explanation for the appearance of an oxygen minimum with regard to the temperature increase in the warm intrusion at station LV29-38 in comparison to LV29-35 might be the following: relatively warm waters with low oxygen values can be transported close to the slope from the western margin of the Derugin Basin during one tidal phase. This explanation is supported by the hydrographic properties of the offshore station LV29-47.
In order to understand these processes and their temporal variability, it would be necessary to carry out long-time observations at least in diurnal cycles.

5.4.2 Derugin Basin

A total of 21 CTD stations was carried out in the barite mineralization area in the vicinity of the "Barite Mounds". As in all parts of the sea during this time of the year, the vertical water column represented conditions of spring heating in the upper layer and a continuous ventilation (cooling) at intermediate depths. The vertical distribution of temperature and salinity indicates a well pronounced dichothermal subsurface layer. A more typical feature for all stations is the clearly expressed fine thermohaline structure (numerous intrusions of different vertical scales) in between the dichothermal layer and the intermediate temperature maximum (*Fig. 5.4*, station LV29-14). These features indicate internal interleaving, mixing and, in general, permanent ventilation and cooling of the water mass from cold surface (subsurface) layers. This means that the upper 500-600 m in the Derugin Basin do not represent a stagnant zone. Below these depths, the distribution of temperature and salinity is very monotonous up to the bottom.

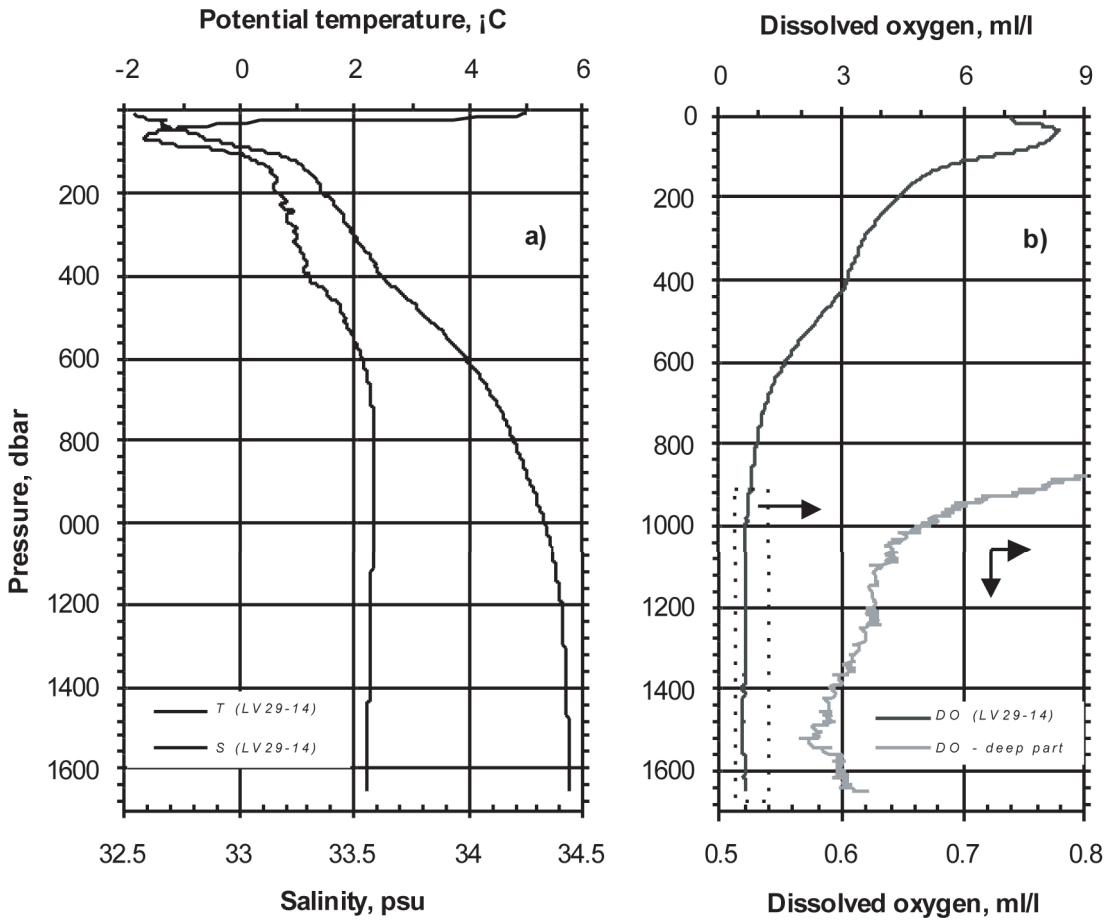

Fig. 5.4*: Vertical profiles of Potential temperature and Salinity (a) and Dissolved oxygen (b) at station LV29-14.*

Another important characteristic is the increasing oxygen concentration towards the bottom. Such features were found at almost all stations in the vicinity of the barite mineralization area. Of course, this data has to be confirmed by other chemical properties.
With regard to currents it should be mentioned that the good atmospheric conditions without wind during the observations resulted in a stable positioning of the ship without drifting.
Also, we would like to mention the phenomenon of the “red tide”, which took place during the observations. Obviously, it was caused by the spring bloom of dinoflagellates. This phenomenon was well pronounced and even led to a contamination of the CTD sensors and Niskin bottles.

6. METHANE INVESTIGATIONS

Anatoly Obzhirov and Olga Vereshchagina

6.1 Introduction

Methane was measured in the water column of the Okhotsk Sea on 6 expeditions within the KOMEX I project from 1998 to 2000 (Biebow & Hütten, 1999; Biebow et al., 2000). In this period, the following was discovered:

1. Several methane flares occur on the East Sakhalin slope and shelf. The water columns inside and near the flares contain methane concentrations from 1,000 to more than 20,000 nl/l. Methane bubbles emanate from the seafloor via fault zones rising up to 300-400 m in the slope area and up to the surface on the shelf.
2. The sources of methane are oil-gas-bearing sediments, dissociating gas hydrates and present bacteria-generating production.
3. Methane anomalies exceed the background concentration 10-10,000 times.
4. Especially in the shelf area, methane rises from the sediment via the water column and the sea surface into the atmosphere. This process intensifies in spring and autumn.
5. The flux of methane from the seafloor increases in periods of seismo-tectonic activity.
6. Water layers of the shelf containing methane anomalies intrude into water columns of the slope area.
7. Methane anomalies in the 70-100 m thick bottom water layer were found in the “Barite Mounds” area of the Derugin Basin and in other barite-bearing areas.

The main research targets of Leg 1 of RV *Akademik Lavrentyev* cruise LV29 were the following:

1. To study in detail the methane distribution in the water column in connection with methane flares on the Northeast Sakhalin shelf and slope.
2. To investigate formerly discovered flares and to find new flares on the Northeast Sakhalin shelf and slope.
3. To retrace the anomalous methane distribution of the bottom water layer (methane plume) in the “Barite Mounds” area of the Derugin Basin.
4. To compare the methane distribution in the water column with other chemical parameters.
5. To examine the source of methane in the “Barite Mounds” area.

6.2 Methods

Water samples for methane measurements were taken from Niskin bottles of the CTD-rosette without air contact. Gas was extracted from the water by a vacuum line and was analyzed by gas chromatography aboard the ship (Obzhirov, 1993). The accuracy of the hydrocarbon analyses is 0.00001%. To control the correctness of the analyses gas standards from the USA were used for calibration.

6.3 Methane distribution in the water column

6.3.1 Results

Methane concentrations in the water column of all stations are presented in Appendix 4. The stations were subdivided with respect to their location into the following groups: Terpeniya

Bay and the adjacent slope (2 stations), Northeast Sakhalin shelf and slope (8 stations), "Barite Mounds" area (21 stations).

6.3.1.1 Terpeniya Bay and slope

Station LV29-1 was carried out in an area about 20 nm to the east from stations monitored in KOMEX I. An anomalous high methane concentration was found here decreasing from the bottom water layer (1,605 nl/l, depth 74 m) to 636 nl/l at a depth of 11 m and to 99 nl/l at the surface. This is 2-3 times more than the usual methane content in Terpeniya Bay in spring except for the surface layer. At the sea surface, the methane distribution is similar to those measured during the KOMEX I investigations in this season.
Station LV29-66 is located on the slope near "Salyuk flare" about 40 nm in SW direction from station LV29-1. A high methane anomaly (2,791 nl/l) was found there at intermediate water depths (depth 137 m) and in the near-surface layer (963 nl/l, depth 50 m). Another, less high one was measured in the bottom waters (337 nl/l, depth 719 m). It is possible that the intermediate methane-containing water layer intruded from the Terpeniya Bay shelf into the water column of the slope area. As a result, a methane bubble flux formed in the bottom water of "Salyuk flare".

6.3.1.2 Northeast Sakhalin shelf and slope

The methane distribution in the water column is shown on the profile of stations LV29-39 – LV29-31 (*Fig. 6.1*).
Station LV29-31 is located on the slope at a greater depth (946 m) than the other stations of this profile. Here, the methane concentration almost equals the background concentration. Only the bottom waters (depth 946 m) contain a small methane anomaly of 192 nl/l. The methane concentration becomes less with decreasing depth and equals the background concentration at the sea surface (71 nl/l). At a water depth of 694-595 m, an intrusion was observed with a 2.5 times higher methane concentration (78 nl/l) than in the surrounding layers. It extends from the slope to the deeper part of the Derugin Basin.
Station LV29-47 was carried out at "Salomatin flare". This flare was firstly discovered during this cruise. Here, methane anomalies were found in the bottom water (1,013 nl/l, depth 863 m) and in the intermediate water layer (351 nl/l, depth 644 m). At the sea surface the methane concentration (93 nl/l) is about 20% higher than the background one.
Station LV29-29 is located in the area of "Obzhirov flare". Methane anomalies were measured here in the bottom water (468 nl/l, depth 683 m) and the near-bottom layer (3,726 nl/l, depth 674 m). Different layers from the bottom to a depth of 300 m with sharp variations in the methane concentrations from 1,300 nl/l to 35 nl/l occurred. This could be due to an irregular distribution of methane bubbles rising from the flare. In the surface layer, a background methane concentration (69 nl/l) was observed.
Station LV29-45 is located between "Giselle and Obzhirov flares". A slight anomaly of methane (269 nl/l, depth 504 m) was found here in the bottom water ascending up to a depth of 347 m. From this depth upwards, the methane concentration is at background level (60-80 nl/l), but at the surface it increases again to 129 nl/l.
Stations LV29-35 and -38 were carried out in the area of "Giselle flare": station LV29-35 almost inside the flare, station LV29-38 slightly outside. The methane anomaly of station LV29-35 is 3-10 times higher than that of station LV29-38. A maximum methane concentration was measured in both stations at a water depth of 288 m (9,338 nl/l and 2,784 nl/l, correspondingly). The methane concentrations in the bottom water (depth 372 m) strongly differ from each other 5,494 nl/l in LV29-35 and 359 nl/l in LV29-38, but in the surface water they are equal (83 nl/l).

Station LV29-43 is located between “Erwin and Giselle flares”. A methane anomaly was found in the water column from the seafloor (3,031 nl/l, depth 294 m) to a depth of 39 m (679 nl/l) and in the surface water (155 nl/l). It is likely that the observed anomalous methane concentrations in this area derived from both flares, but primarily from “Erwin flare” (from shelf to slope) and from the sediment via a fault zone.
Station LV29-32 is located almost inside “Erwin flare”. A methane maximum occurs in the bottom water (7,197 nl/l, depth 172 m). The methane concentration decreases slowly to 3,295 nl/l at 109 m depth and from this depth on sharply to 80 nl/l at 50 m depth.
Station LV29-39 was carried out in the shelf area. A methane anomaly was observed from the seafloor (3,942 nl/l, depth 123 m) to the surface (247 nl/l). Many little flares originating from oil-gas-bearing sediments are located in this area.

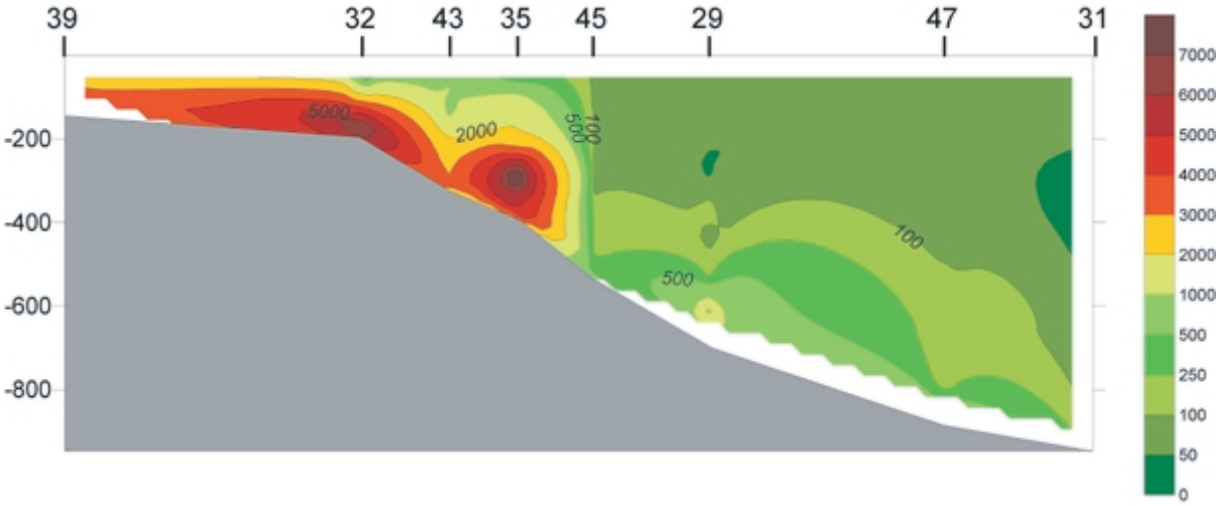

Fig. 6.1: *Methane distribution along the Sakhalin shelf and slope, stations LV29-31 - LV29-39.*

6.3.1.3 “Barite Mounds” of the Derugin Basin

In the “Barite Mounds” area, 21 stations were carried out. The methane distribution in the bottom water of this area is shown in *Figure 6.2*. A striking regularity in the methane distribution at all these stations is the presence of a thin bottom layer about 70-100 m thick with high methane concentrations of up to 1,000-6,000 nl/l. Stations LV29-2 and LV29-10 are located inside the barite-bearing area, and here, a methane anomaly was measured in the bottom water (1,213 nl/l, depth 1,478 m and 1,961 nl/l, depth 1,442 m, correspondingly). At all stations, the methane concentrations in the surface waters are almost at background level (60-80 nl/l).
During cruise GE99, a higher methane value (5,723 nl/l, depth 1,515 m) was measured in the bottom water near stations LV29-2 and LV29-10 (station GE99-32). Methane emanates via a fault zone from the sediment layers and basement rocks or from serpentine mantle rocks. Fluids enriched in barium and methane possibly rise from the earth interior to the seafloor. The change in the methane concentration of the bottom water from 1999 (GE99) to 2002 (LV29) may be caused by a changing activity of the fluid flow or by sampling in different points near the pathway of the fluid flow.
The methane investigations performed from 1998 to 2002 show that the methane plume is mostly distributed in a defined area above the barite-bearing hill which includes small sites of clams. The maxima in barite content and methane composition have an extension of about 10 x 5 nm (*Fig. 6.2*). On this cruise we investigated the area around the “Barite Mounds” in more detail. As a result, we found that the methane plume extends in N-E direction and that a new smaller plume centered in the area of station LV29-14 occurred. The methane

concentration in the bottom water of station LV29-14 amounts to 536 nl/l, and the number of barite fragments on the seafloor decreases in the aforementioned direction.

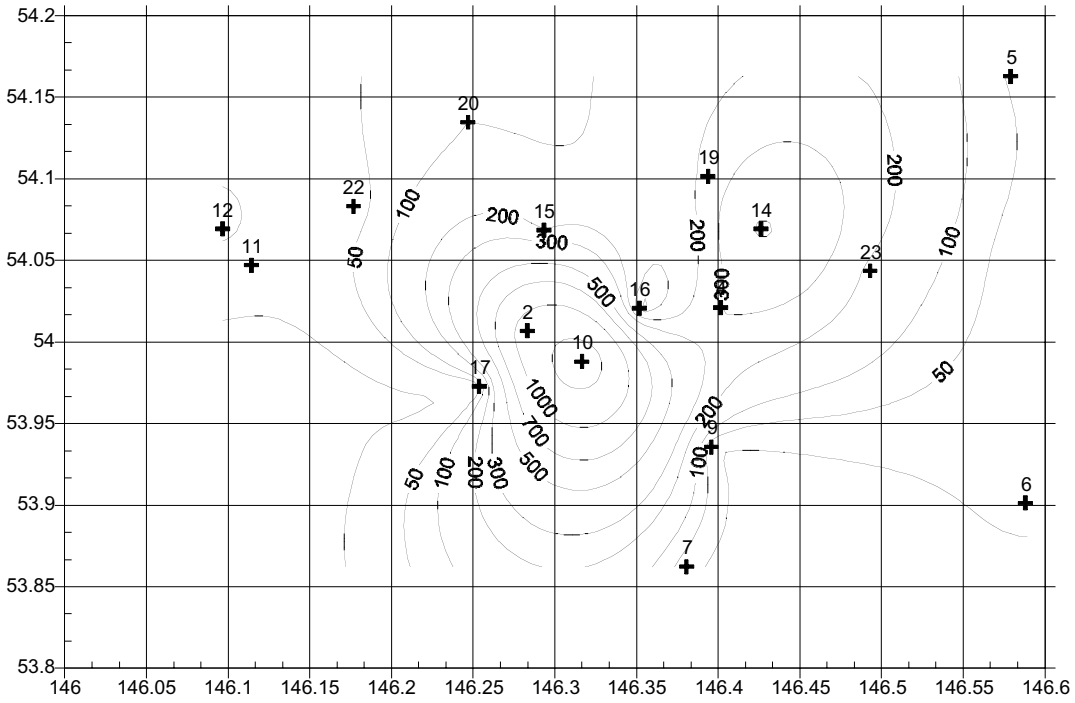

Fig. 6.2: *Methane distribution in the bottom waters of the "Barite Mound" area in the Derugin Basin.*

An unusual methane distribution in the water column was observed at station LV29-17. The methane concentration (10 nl/l, depth 1,516 m) in the bottom layer is at background level, but 100 m above the bottom the methane concentration increases to 955 nl/l (depth 1,417 m). This means that methane does not emanate from the seafloor, but is transported here by an intruded water layer possibly from the "Barite Mounds" area.
The methane distribution at station LV29-12 is different from the "Barite Mounds" plume area and therefore another small source of methane is supposed to exist in this area. There are two water layers (about 1,000 and about 500 m) with higher methane concentrations (70 nl/l, depth 990 m, and 49 nl/l, depth 495 m, respectively) than in the surrounding water column. This distribution pattern was observed at many stations in the "Barite Mounds" area, especially in its eastern part. It is possible that the two layers with higher methane concentrations intruded from the Derugin Basin. This means that methane emanates here from the seafloor and derives also from additional sources nearby.

6.3.2 Discussion

6.3.2.1 Sakhalin shelf and slope

The main objectives of these investigations are to determine the methane sources and how methane gets into the water column. There are three possible sources of methane: microbiological production, oil-gas-bearing sediments and dissociation of gas hydrates. The first one usually creates the background methane concentration in the water column – about 70-80 nl/l – in the surface as well as in the bottom water layer, if the sediment surface contains much organic matter (more than 1%), and 5-10 nl/l, if the content of organic matter is less. At the Sakhalin shelf and slope anomalous methane concentrations were found exceeding the background value 10-1,000 times (500-15,000 nl/l). Methane emanates from

oil-gas-bearing sediments and decomposing gas hydrates and migrates from the sediment into the water column mainly via fault zones.
Previous investigations (Obzhirov, 1993) and methane monitoring (Biebow & Hütten, 1999; Biebow et al., 2000) showed that the methane flux from the sediment into the water column increases in periods of seismo-tectonic activity during which the fault zones open and gas hydrates decompose. Thereby, methane gets into the water column and creates there sound-scattering flares (hydroacoustic anomalies) in the echogram. Inside the flares the methane concentration usually reaches 10,000-20,000 nl/l and more. In contrast, methane seeps from oil-gas-bearing sediment layers via fault zones into the water column without creating an hydroacoustic anomaly. In this case, a methane anomaly (500-2,500 nl/l) occurs in the bottom water and upper layers of the water column.
During Leg 1 of cruise LV29 many new flares were found. It is remarkable that they are located almost all in one line – a fault zone spreading in NE direction from the shelf to the slope and to the bottom of the Derugin Basin (*Fig. 6.3*). Some flares were observed in fissures which are crossed by the main fault. High methane contents (5,000-10,000 nl/l and more) were measured here. The methane distribution in the water column indicates that the sediment of this area is methane-enriched (oil and gas deposits and gas hydrates). Leg 1 of cruise LV29 was carried out during a period of seismic activity (June 2002) in which, for example, an earthquake happened on Sakhalin Island. Large amounts of methane rise from the sediment into the water column and the atmosphere at the Northeast Sakhalin shelf and slope. In the deeper part of the Derugin Basin the methane concentration in the water column decreases to the background level.

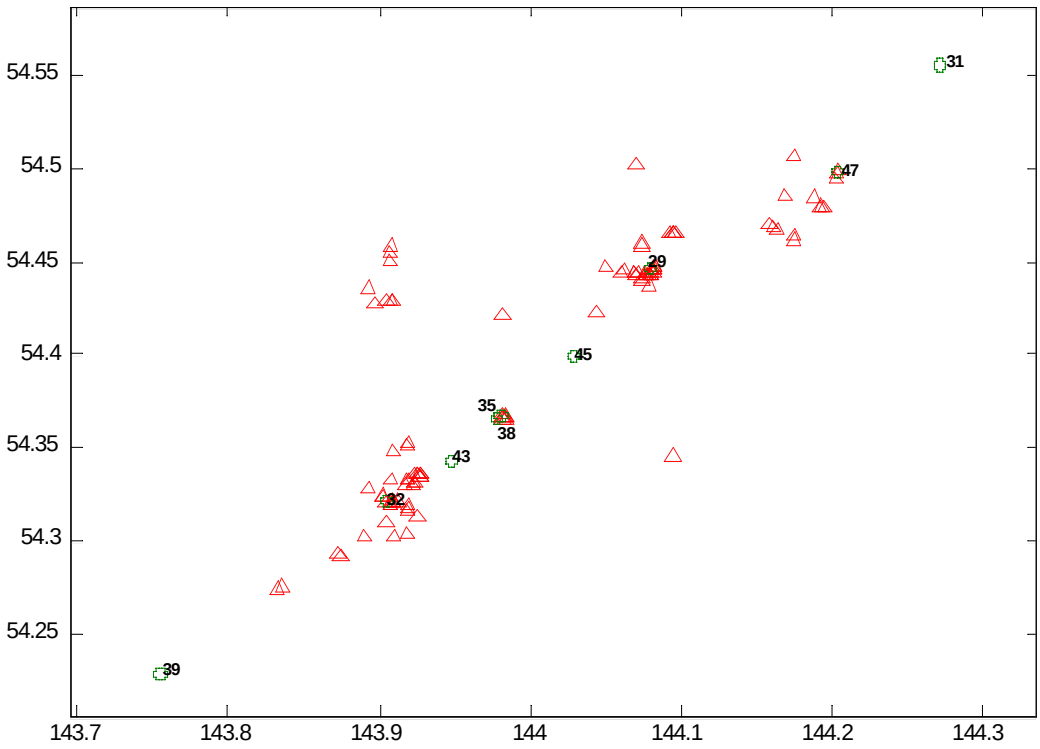

Fig. 6.3: *Map of the position of stations LV29-39 - LV29-31 and flares on the Sakhalin shelf and slope. Circles mark stations and station numbers; triangles mark flares.*

6.3.2.2 Barite area of the Derugin Basin

The source of methane in this area is yet unknown. It could be oil-gas-bearing sediment layers, metamorphic rocks of the basement, and methane derived from serpentinisation. The methane anomaly in the bottom water correlates well with the barite distribution. Therefore, it can be suggested that methane and barium rise together from the earth interior via fluid flow to the surface sediments. The area containing high barite and methane concentrations is located near a deep fault zone that goes down to the mantle (Gnibidenko, 1979). It represents the border between the Derugin Basin and the Kashevarov Rise. Stations LV29-2 and LV29-10 with methane anomalies in the bottom water are located in an area of the "Barite Mounds", where several faults extend from the interior to the sediment surface (see Chapter 4).
In this area, the top of a mantle diapir structure is located about 15-17 km below the seafloor (Gnibidenko, 1979). Several magnetic anomalies of about 3-5 nm in diameter were observed at the seafloor (see Chapter 12). There are traces of basaltic and (or) andesitic volcanic rocks near the sediment surface. The acoustic basement consists of basalt, andesite, tuff, green schists and other rocks (Gnibidenko, 1979). The green schists were formed when fluid containing methane and hydrogen passed through metamorphic rocks. In this process, barium is transported with the fluids from the metamorphic rocks and (or) from mantle rocks (basalt and andesite) to the surface thereby forming the barite chimneys. The hydrothermal processes including the barium and methane fluid flow took place several million years ago and have now ceased. Nowadays, barium is remobilized in the sediment and forms the barite crusts in the surface sediments. Clam fields are widespread in areas with methane seepage. Many dead clams were recorded by OFOS (see Chapter 9). The nowadays stable seismo-tectonic conditions in this area are possibly connected with the decreasing methane seepage.

6.3.3 Conclusions

The results of the methane investigation in Leg 1 of LV29 can be summarized as follows:

1. Many (more than 50) new flares were found in the area near "Giselle and Obzhirov flares". They create hydroacoustic anomalies at a water depth of 200-300 m above the seafloor. Inside the flares the methane concentrations amount to about 5,000-20,000 nl/l, whereas outside the flares they are about 500-3,000 nl/l.
2. The new flares are located mostly in the following line: "Erwin"-"Giselle"-"Obzhirov" from the shelf to the slope in NE direction (*Fig. 6.3*). This coincides with the orientation of a fault zone. Methane bubbles rise from oil-gas-bearing sediment layers via the fault zone and from decomposing gas hydrates into the water column and create a hydroacoustic anomaly like a flare.
3. The new flares seem to appear in the period of 2000-2002, because they were not observed in 1999 (Biebow et al., 2000). That means that this period was seismo-tectonically active. As a result, the fault zone has opened and methane emanates to the surface. The activity is confirmed by the earthquakes that happened in Sakhalin in 2000, 2001, and 2002.
4. A field with a high methane anomaly (5,000-10,000 nl/l and more) in the water column inside and outside the flares spreads from the shallow shelf to the slope at depths smaller than 400-500 m in the area of the northeast fault zone (line of stations LV29-39 – LV29-31, profiles 39-31, *Fig. 6.1*). The methane concentrations become less with increasing depth and increases only at the flares (methane vents).
5. There is a good correlation between the methane anomaly in the bottom water and the barite distribution in the "Barite Mounds" area of the Derugin Basin. Barium and methane are transported by fluid flow from the interior hydrothermal system via deep fault zones to the sediment surface. Today this area is tectonically stable, and only the methane flux continues to rise in the above-mentioned way.

6. An anomalous high methane concentration (500-2,500 nl/l) was found on the shelf and slope of Terpeniya Bay extending in SE direction. Its sources are oil-gas-bearing sediments on the shelf and possibly gas hydrates at the slope.

6.4 Methane distribution in sediment cores

The methane distribution in sediment cores was measured at 7 stations. Three stations (LV29-46, -50, -51) are located at the NE Sakhalin slope and four stations (LV29-53, -56, -59, -63) in the "Barite Mounds" area.
The main goal of this investigation was to study the methane concentration in sediment layers in areas inside and outside of gas hydrate deposits (Sakhalin slope) and inside and outside of areas with methane anomalies in the bottom water ("Barite Mounds" area).

6.4.1 Method

Two methods were used to extract the gas from the sediment: the Head Space method and the method of filling the sediment into impermeable plastic bags. Gas is taken from the bags by syringes. Gas analyzed in the gas chromatograph and methane extracted from the plastic bags are given in ppm; gas analyzed by Head Space is given in mM/kg or nl/kg. The sampling interval for gas measurement was 50 cm.

6.4.2 Results

The methane distribution in the sediment cores is presented in Appendix 4. Cores LV29-46 and LV29-50 were taken in "Obzhirov flare". Gas hydrates were sampled at station LV29-50 in the depth interval from 395 to 415 cm. The methane concentration in the upper layer from 0 to 150 cm is at background level (20-100 ppm). It sharply increases (35,000 ppm) in interval 200-250 cm and slightly decreases to the base of the core from 20,000 ppm (250 cm) to 4,000 ppm in layer 410 cm, where the gas hydrates were found. In core LV29-46 the methane concentration increases from background value (60 ppm) in interval 0-220 cm to 66,000 ppm at the base (510 cm). The methane distribution in both cores shows that the sediment in a gas hydrate area contains large amounts of methane at a depth of about 200 cm below the seafloor. Station LV29-51 is located outside "Obzhirov flare", but in an area with a new flare. The sediment in this area also has high methane contents (11,000 ppm), but less (from 400 cm) than in the gas hydrate area.
Cores LV29-53 and LV29-56 were recovered in an area with a high methane anomaly in the bottom water and a wide barite distribution at the seafloor. The sediments of these cores (especially of core LV29-56) have an anomalous high methane concentration. The concentration in the sediment of the upper layer 0-100 cm exceeds the background value about 10 times (0.004 mM/kg). The methane concentration in layer 150-250 cm is about 3.5 mM/kg. Down to the base of the core (300-600 cm) it decreases about 2-3 times. In this station sediment samples were taken by two methods: Head Space and plastic bags. A comparison of the methane distribution in the samples taken by the different methods shows that the two methods yield well correlating results.
Coring station LV29-59 is located outside the second area of barite distribution and LV29-63 inside of it. The methane anomaly (300-500 nl/l) in the bottom water is not very high, the barite crusts are thinner, and the surface sediment is stone-covered in this area. The methane concentration in all sediment cores outside station LV29-59 is at background level (0.0001-0.0003 mM/kg). The methane concentration at station LV29-63 increases from 0.0007 mM/kg (0 cm, seafloor) to 0.006 mM/kg (core base – 450 cm) and is 100 times less than at station

LV29-56 which is located in an area with a great methane anomaly in the bottom water and a wide barite distribution.

6.4.3 Conclusions

1. The methane distribution in sediment cores of the Sakhalin slope containing gas hydrates and of the “Barite Mounds” are nearly the same. The sediment cores of these areas yield high methane anomalies (about 1-3 mM/kg). It seems that the gas hydrate distribution in the sediments of the “Barite Mounds” area is the same as in the Sakhalin slope area.
2. Outside the gas hydrate and barite areas the sediment contains a background methane concentration (0.0001-0.0003 mM/kg).

7. HYDROCHEMICAL STUDIES OF THE WATER COLUMN ABOVE METHANE VENTS

Pavel Tishchenko, Galina Pavlova, Anatoly Salyuk, Valery Sosnin, Sergey Sagalayev, Natasha Khodorenko, Alexander Salomatin, Anatoly Obzhirov, Klaus Wallmann, Bettina Domeyer, and Janne Repschläger

7.1 Introduction

Currently, areas of the World Ocean in which gas hydrates occur are investigated intensively. These hydrate deposits contain enormous amounts of methane so that the upcoming shortage of fossil fuel might be overcome by the exploitation of gas hydrate reservoirs. Moreover, natural seeps increase the methane content in the atmosphere. Methane has a greenhouse effect; it therefore may play an important role in climate modulation. Monitoring of methane in the atmosphere and the study of natural sources of methane are thus necessary elements in the investigation of global warming processes. An additional interesting feature of methane venting areas are the authigenic mineral formations on the seafloor and its biological activity which develops in sediments around fluid vents.
On this cruise, we studied the carbonate system (pH, alkalinity, dissolved calcium), dissolved oxygen and nutrients in the water column above methane sources on the seafloor. The main goal of this study was to investigate the impact of methane venting on the carbonate system. Potential mechanisms, which may influence parameters of the carbonate system, are the following: a) microbiological oxidation of methane in the water column as shown by Valentine et al. (2001); b) transport of CO_2 by methane bubbles with subsequent dissolution in upper layers of the water column; c) water column mixing by a strong stream of methane bubbles.

7.2 Methods

pH measurements of sea water were carried out by means of a cell without liquid junction (Tishchenko et al., 2001; Tishchenko et al., 2002), composed of:

Glass-electrode-Na^+	test solution (standard solution)	H^+-glass-electrode

We used glass electrodes responding for hydrogen (ESL-43-G) and for sodium (ESL-51-G) ions which are manufactured by Gomel Plant (Belorussia). For the cell calibration a buffer solution of TRIS-TRIS·HCl-NaCl-H_2O (m_{TRIS}=$m_{TRISHCl}$=0.04, m_{NaCl}=0.4) was prepared. The pH values on "total" scale were calculated as:

$$pH_T = p(a_H / \gamma_{Na})_S + \frac{F \cdot (E_S - E_X)}{RT \ln(10)} + \log\left[\frac{(m_{Na})_S}{(m_{Na})_X}\right] - \log\gamma(_{Na})_X + \log\gamma(_H)_X$$

where E_S, E_X are electromotive forces of the cell in standard and test solution, respectively, and $(m_{Na})_S$ is the molality of sodium ions in standard solutions as defined in the recipe of the standard solution. The molality of sodium in test solutions (sea water) was calculated as:

$$(m_{Na})_X = \frac{13.872 \cdot S}{1000 - 1.00511 \cdot S}$$

Standard values of $p(a_H / \gamma_{Na})_S \equiv -\log(a_H / \gamma_{Na})_S$ in buffer solutions were tabulated previously (Tishchenko et al., 2001). The activity coefficients of sodium and hydrogen ions are also published (Tishchenko et al., 2001; Tishchenko et al., 2002). During the cruise, the formal standard potential of the usually daily calibrated cell was constant within −0.2 mV. Thereby, the error of pH_T measurements was about −0.003 pH unit.

Total Alkalinity (TA) in sea water was analyzed within 3 hours after sample retrieval by direct titration of 25 ml of sea water with 0.02 N HCl in an open cell. To remove carbon dioxide during titration the samples were flushed with a continuous stream of pure nitrogen. A mixture of methylene blue and methyle red was used as indicator, and the titration was completed when the green color of the solution turned to light pink (pH of the end point is equal to 5.4-5.5). This method is well-known as Bruyevich's method (Bruyevich, 1944) and recommended as standard operating procedure among oceanographers in Russia (Ivanenkov, 1978). The acid was standardized daily with Na_2CO_3 solution prepared from pre-weighted crystals dried at 280°C. The Brinkman/Dosimat 665 motor-driven piston burette reproducible to −0.001 ml in the delivered volume was applied for analysis. Based on analysis of sea water replicates, an analytical precision of −2.6 µM/kg (n=10) for TA was reached in this study.

Dissolved oxygen was determined by the modified Winkler method (Carpenter, 1965). Thereby, the end point was detected photometrically at a wave length of 350 nm. Automatic titration was carried out using a Dosimate burette, photometer and PC. Estimated from replicates, the precision of the oxygen analysis generally amounted to −1 µM.

Samples for *dissolved calcium* (Ca) in sea water were filled into 140 ml plastic flasks and preserved with hydrochloric acid to create pH = 2. These samples will be analyzed by complexometric titration of 10 g of sea water (Tsunogai, 1968) in the shore-based laboratory at POI. EGTA is used as titrant and GHA [glyoxal-bic (2hydroxyanil)], a sensitive reagent for calcium, is used as metal indicator at pH 11.7. Calcium is extracted into a small volume (4 ml) of organic solvent (n-Butanol) as its GHA-complex, and titrated with EGTA (9.714 mM/l). The end point is sharp and occurs when the red color of the organic layer vanishes. The EGTA is standardized daily with standard calcium solution prepared from 1.0309 g of highly pure calcium carbonate dissolved in hydrochloric acid and diluted to 1 liter after adding 13.114 g magnesium sulfate ($MgSO_4$ *7 H_2O) and 27.49 g sodium chloride. The solution is 10.30 mM in calcium, 53.20 mM in magnesium and 470 mM in sodium, as in sea water. A correction factor of 0.9946 is applied to account for Sr dissolved in sea water. The Brinkman/Dosimat 665 motor-driven piston burette reproducible to −0.001 ml in the delivered volume is applied for analysis. This method provides a precision of up to −0.1%.

Dissolved silicate was measured applying standard photometric procedures on a Perkin-Elmer Lambda 2 UV/VIS Spectrometer. A volume of 0.5 ml sample or standard was diluted to 5.0 ml with deionized Milli-Q water and 0.2 ml heptamolybdate solution. After 15 minutes, 0.2 ml oxalic acid solution and 0.2 ml ascorbic acid were added. After another 30 minutes, the blue-colored silicomolybdic complex developed and the absorbance was measured at 810 nm. A replicate analysis of the water column samples indicated a reproducibility of −3 %.

Dissolved phosphate and the sum of dissolved nitrate and nitrite (TNO) were measured using an auto-analyzer. Samples for TNO analysis were passed through a reductor column to convert nitrate into nitrite. Photometric reagents were added through plastic tubing's, and the adsorbance of the colored solutions was measured in flow-through photometric cells. A replicate analysis of the water column samples indicated a reproducibility of −10 % for both nutrients.

From each Niskin bottle, samples were analyzed for dissolved oxygen, pH, alkalinity and nutrients (silicate, TNO and phosphate). Dissolved inorganic carbon (DIC) and in situ pH were calculated using widely accepted procedures (Millero, 1995) and carbonic acid constants as suggested by Lucker et al. (2000).

7.3 Results and discussion

Hydrochemical data was collected along with hydrographic CTD data at 28 stations in three areas of the Okhotsk Sea. Two, seventeen and nine stations were conducted in Terpeniya Bay, the Derugin Basin and along the Sakhalin slope, respectively. All data is given in Appendix 3; the used abbreviations are listed in the table below.

Table 7.1: *Symbols, units, and abbreviations used in the figures and the table of hydrochemical properties.*

TA	Total alkalinity, mM/kg
NTA	Normalized total alkalinity, mM/kg (=TA*35/S)
$pH_t(15)$	PH_t measured at 15°C in "total" scale
$PH_{in\text{-}situ}$	pH at in situ temperature and pressure in "total" scale
DIC	Dissolved inorganic carbon, mM/kg
NDIC	Normalized dissolved inorganic carbon, mM/kg (=TCO_2*35/S)
pCO_2	Partial pressure of carbon dioxide, µatm
CO_3	Carbonate ion concentration, mM/kg
La	Aragonite saturation degree
Lc	Calcite saturation degree
O_2	Oxygen concentration, ml/l
AOU_b	Biological part of apparent oxygen utilization, µM/kg
SiO_2	Dissolved silica
PO_4	Dissolved phosphate (PO_4^{3-} + HPO_4^{2-} + $H_2PO_4^-$ + H_3PO_4)
TNO	Sum of dissolved nitrate and nitrite

7.3.1 Derugin Basin

The seventeen stations are situated very close to each other and from an oceanographic point of view it can be said that they are in one location (~54°N, 146.35°E). *Figure 7.1* presents the parameter profiles of the carbonate system and dissolved oxygen. The profile of normalized alkalinity shows that the consumption rate of dissolved $CaCO_3$ from sea water exceeds the rate of carbonate dissolution at water depths of 100-200 m due to biogenic $CaCO_3$ formation. Normalized alkalinity reaches a constant value (2.438 mmol/kg) at 1,430 m depth within experimental uncertainty. It is implied that biogenic $CaCO_3$ apparently does not reach the seafloor in the Derugin Basin. The saturation degree of calcite (Lc) is very low in deep water, and carbonate particles on the surface of the seafloor should dissolve. We tried to find a correlation between methane anomalies and carbonate parameters for deep-water samples but without success.

The nutrient distribution in the Derugin Basin is represented best by the dissolved nutrients measured at CTD stations LV29-11, -12, and -16 (*Fig. 7.2*). The concentrations of dissolved

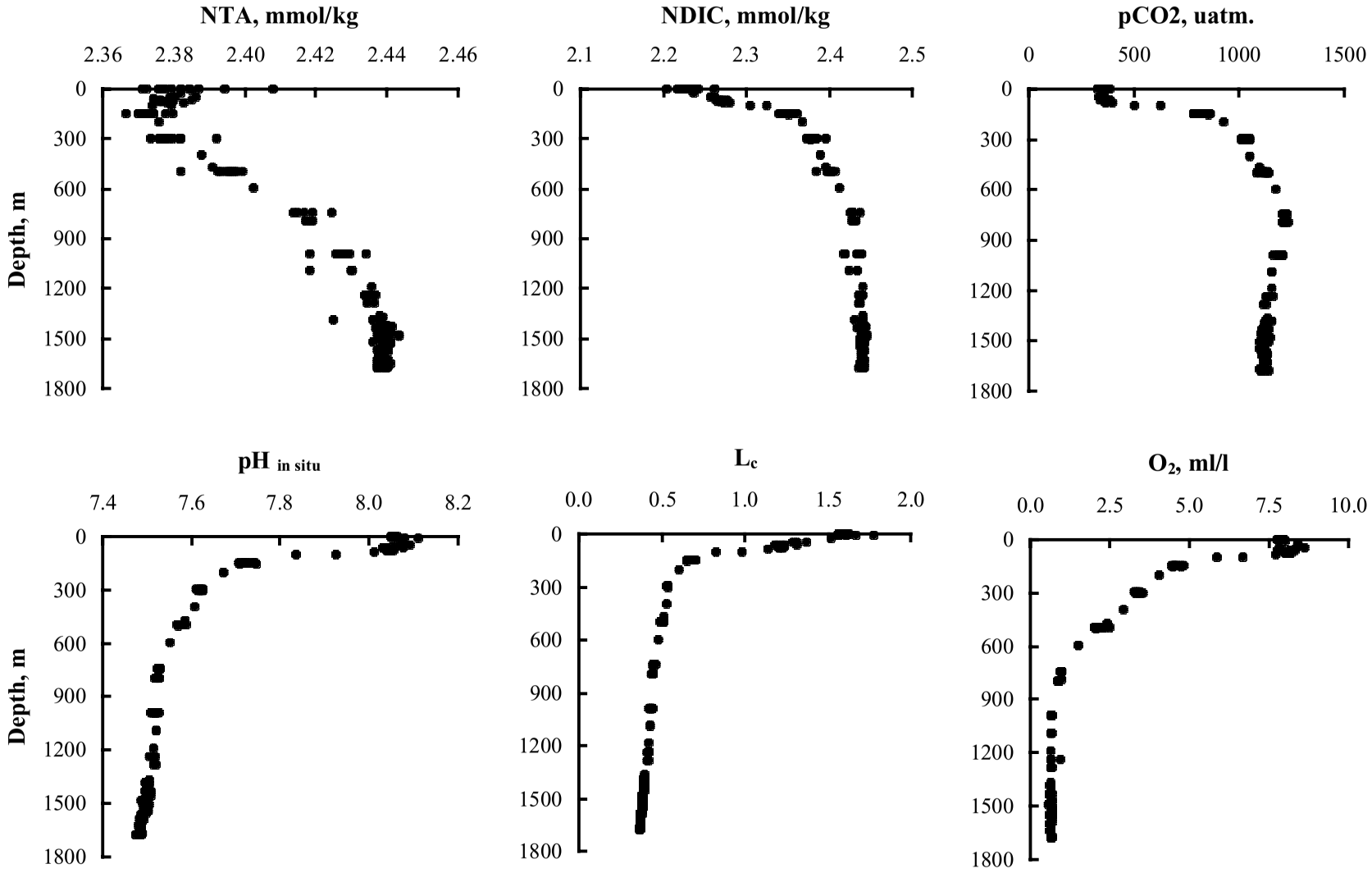

Fig. 7.1: *Profiles of normalized total alkalinity (NTA), normalized dissolved inorganic carbon (NDIC), CO_2 partial pressure (pCO_2), in-situ pH, saturation degree of calcite (L_c) and dissolved oxygen (O_2); all stations in the Derugin Basin.*

silicate decrease continuously with depth to values of up to 200 µM in the bottom waters. The concentrations of dissolved Ba in the sea water are tightly correlated with dissolved silica. Thus, the extremely high silica values also imply high concentrations of dissolved barium in bottom waters. Preliminary calculations of the saturation degree with respect to barite indicate that the bottom waters of the Derugin Basin are indeed close to saturation (Gramm-Osipov, pers. com.). Thus, the preservation of barite chimneys and precipitates in the "Barite Mounds" venting area seems to be favored by the unusually high concentrations of barium in the overlying bottom waters.

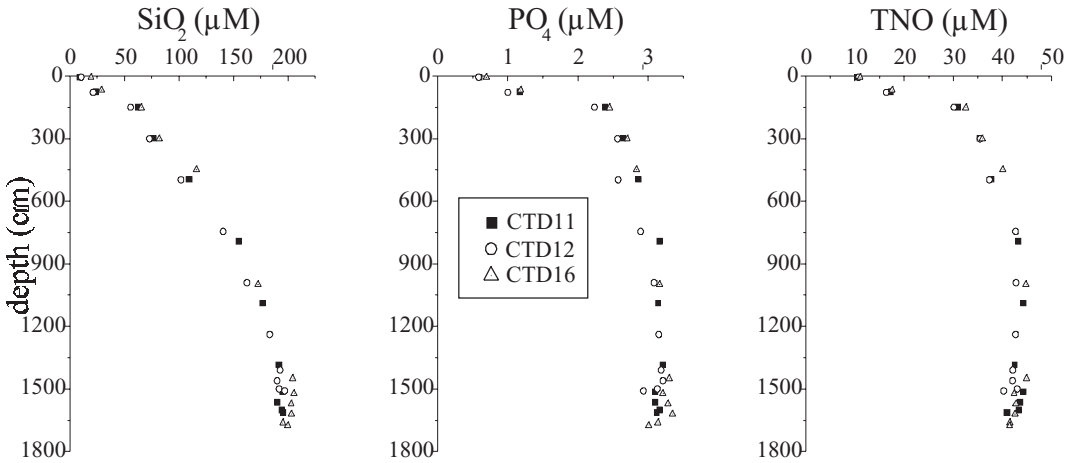

Fig. 7.2: *Profiles of dissolved silica (SiO_2), dissolved phosphate (PO_4) and the sum of dissolved nitrate and nitrite (TNO) at CTD stations LV29-11, -12 and -16 in the Derugin Basin.*

Dissolved phosphate reaches an almost constant level around 3.1 µM below a water depth of 1,000 m, whereas TNO shows a slight decrease below this depth (*Fig. 7.2*). The very low oxygen contents below 1,000 m (*Fig. 7.1*) suggest that TNO might by depleted by denitrification processes. A correlation plot of TNO versus phosphate taking into account the data of all measuring points in the Derugin Basin reveals that the average N : P ratio of the Derugin samples amounts to only 12.5 −0.3. This atomic ratio is significantly smaller than the average ratio observed in the World Ocean (15) confirming that the deep Derugin waters might have lost dissolved nitrate due to microbial denitrification. Surface waters contained rather high concentrations of dissolved silica (>10 µM), phosphate (>0.5 µM) and TNO (>10 µM) suggesting that primary production in the Derugin Basin was not limited by nutrient availability over the sampling period (June 2002).

7.3.2 Sakhalin slope

At the northeastern Sakhalin slope a field of flares is located at ~54°N. We tried to collect hydrochemical data inside "Erwin flare", "Giselle flare" and "Obzhirov flare". Additional samples were taken in between these flares, as well. The most unexpected results were obtained at stations LV29-35 and -38 situated nearest to "Giselle flare". Water samples were taken here within a lateral distance of only 160 m. The time lag between the sampling at the two stations was only 16 hours. *Figure 7.3* shows the profiles of pH and dissolved oxygen for these stations. Both parameters reveal a significant temporal variability which is also seen in the TA and dissolved silica profiles measured at the same stations (*Fig. 7.3*). Two hypotheses

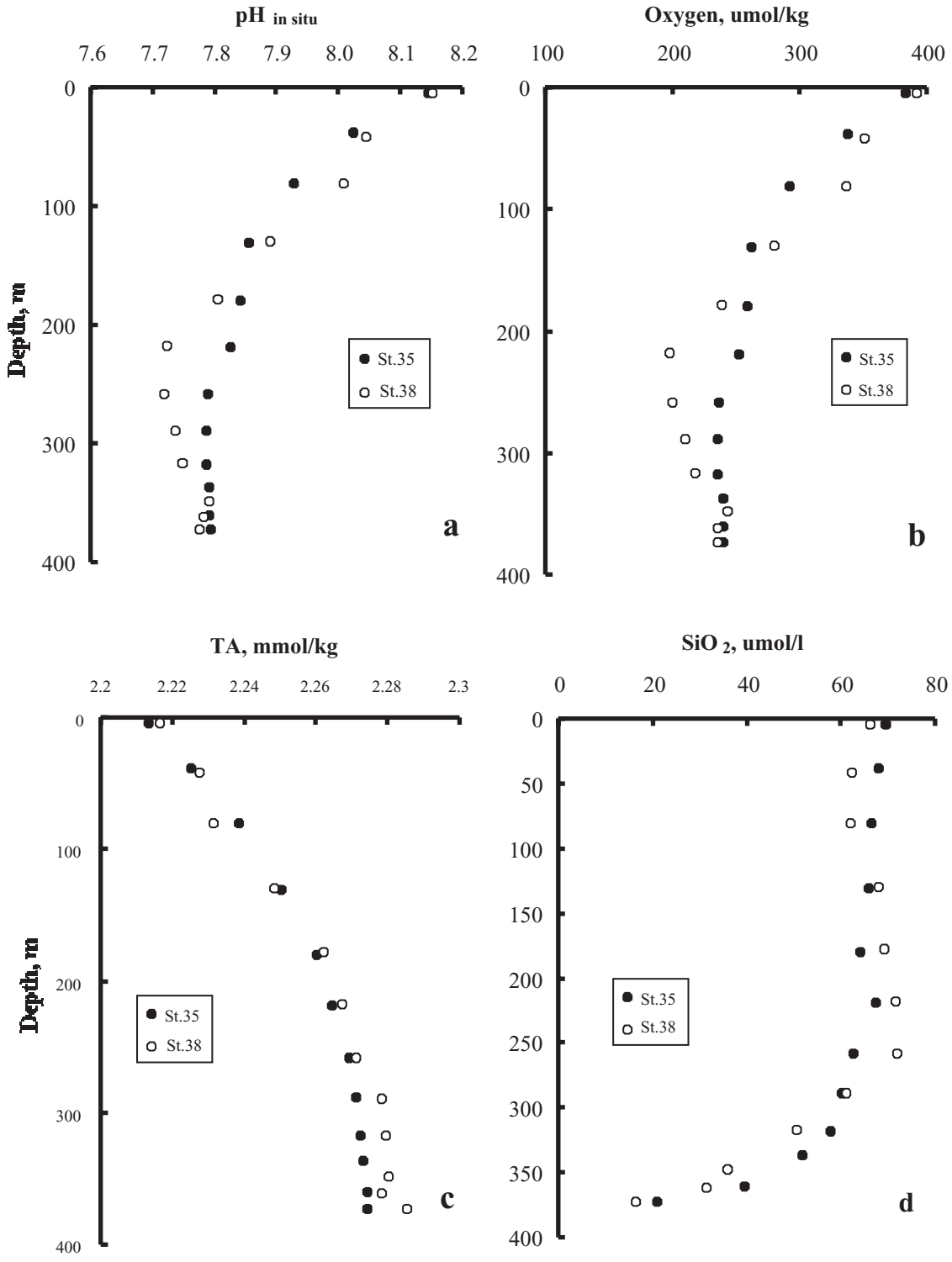

Fig. 7.3: *Profiles of pH (**a**), dissolved oxygen (**b**), alkalinity (**c**), dissolved silica (**d**) for stations LV29-35 and -38.*

have been made to explain this phenomenon. According to the first, a strong upward gas stream mixed the water column during sampling at station LV29-35. Hereafter, the water column was reconstructed so that an undisturbed water column was sampled at station LV29-38 16 hours later. The second hypothesis says that the variability is caused by other strong dynamic processes such as slope convection, tidal currents and eddy propagation. Sections of pH and dissolved oxygen show structures similar to that of the anticyclonic eddy situated near

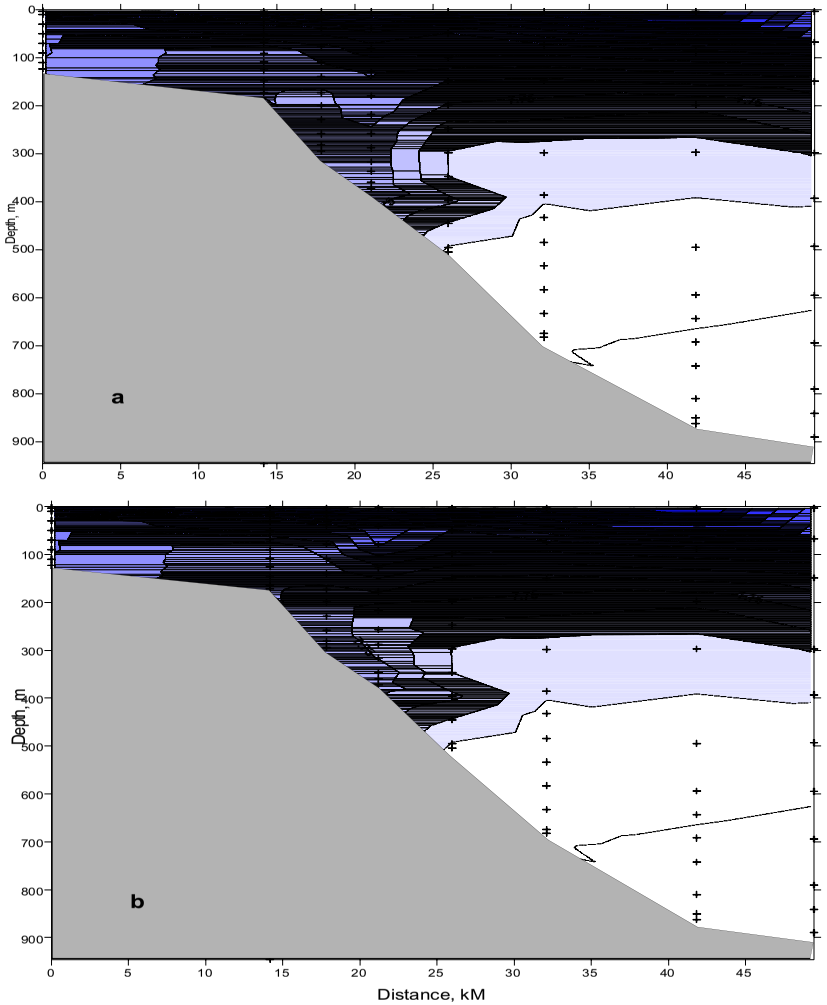

Fig. 7.4. *Sections of $pH_{in\text{-}situ}$ across stations LV29-29, -31, -32, -35, -39, -43, -45, -47 (**a**); and stations LV29-29, -31, -32, -38, -39, -43, -45, -47 (**b**). The deepening of isolines at central parts of the sections probably corresponds to anticyclonic mesoscale eddies*

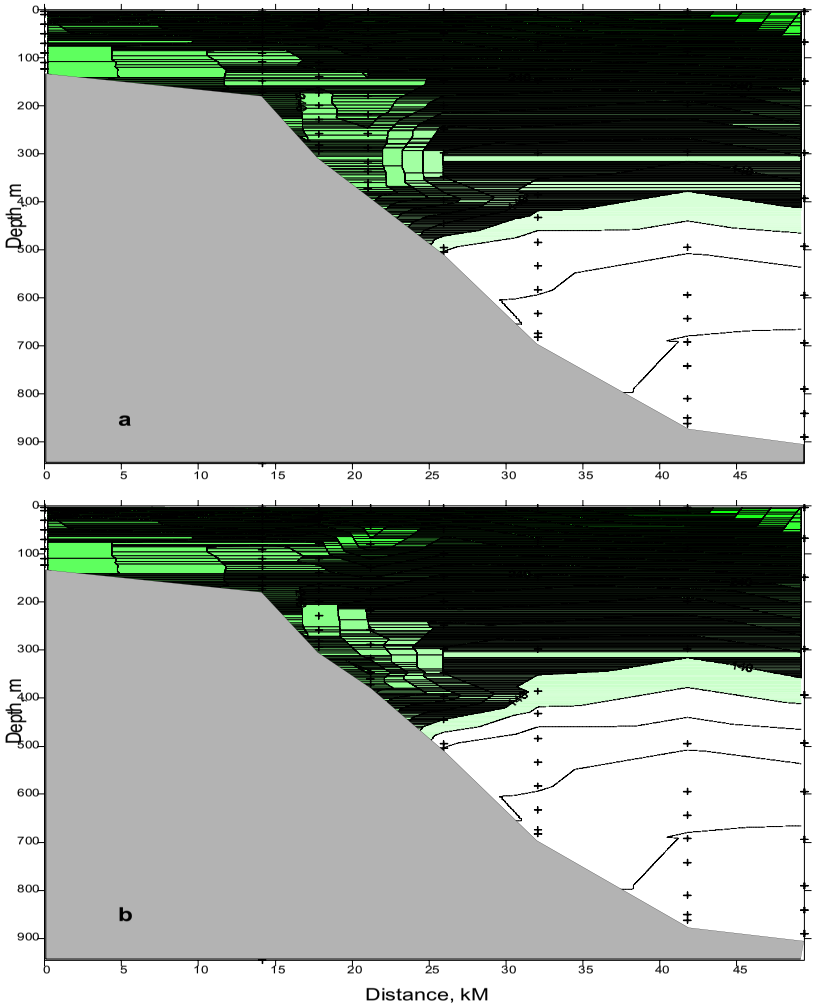

Fig. 7.5. *Sections of dissolved oxygen (µmol/kg) across stations LV29-29, -31, -32, -35, -39, -43, -45, -47 (**a**); and stations LV29-29, -31, -32, -38, -39, -43, -45, -47 (**b**).*

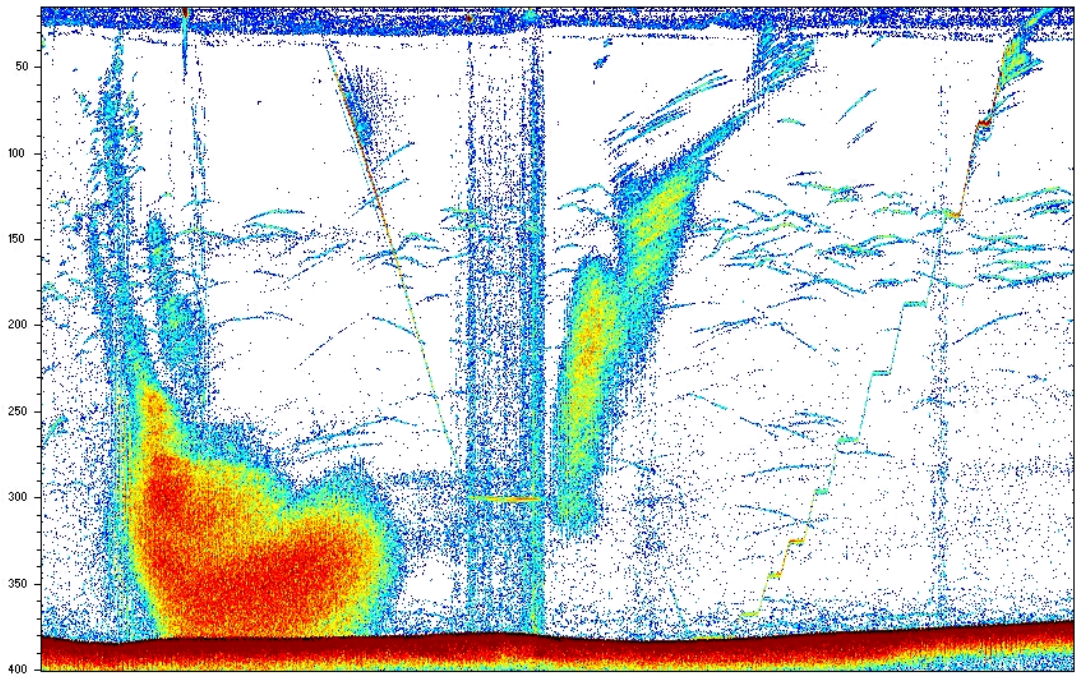

Fig. 7.6: *Acoustic images of "Giselle" Flare observed at station LV29-35.*

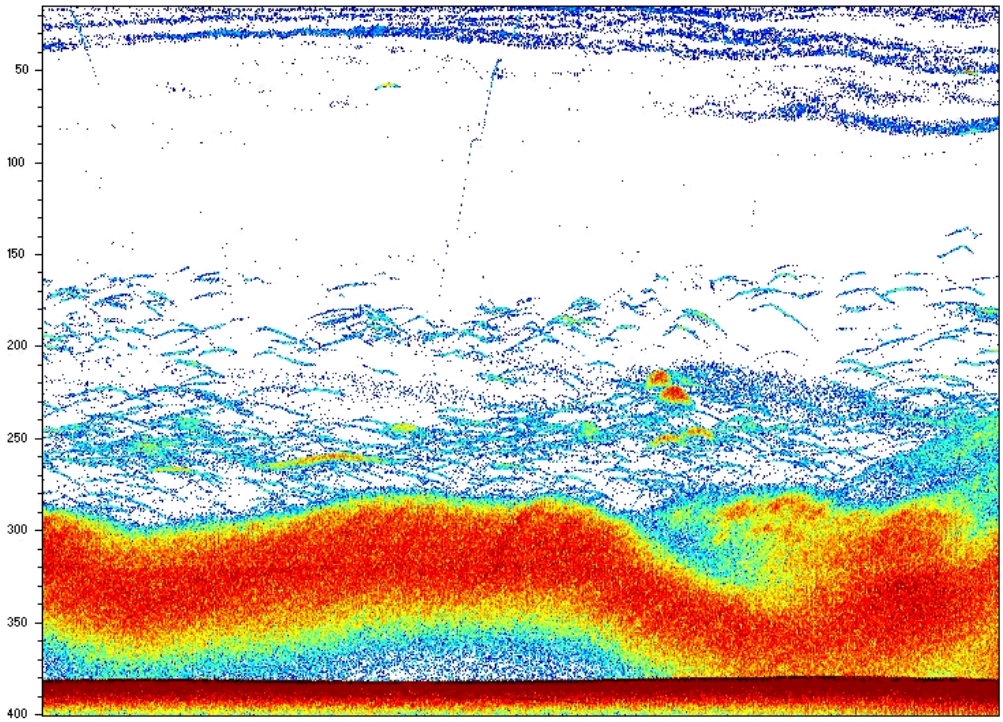

Fig. 7.7: *Acoustic images of "Giselle" Flare observed at station LV29-38.*

"Giselle flare" (*Figs. 7.4* and *7.5*). On the other hand, it is seen from *Figures 7.4* and *7.5* that fresh water penetrates along the slope near the bottom which might be regarded as an indication of slope convection. The tidal table for place Moskalvo (53°36'N/142°30'E) shows that our observations were made in different tidal phases. Station LV29-35 was conducted during low water when the tidal current is obviously nearly missing. This can be seen from hydroacoustic images of "Giselle flare" (*Fig. 7.6*). In contrast to this, station LV29-38 was carried out in the phase of maximum tidal current during which "Giselle flare" lies horizontally close to the bottom (*Fig. 7.7*). Future analyses are necessary for a final conclusion about which of the discussed processes governs the observed large temporal variability in hydrochemical parameters including the methane concentration on the Sakhalin slope.

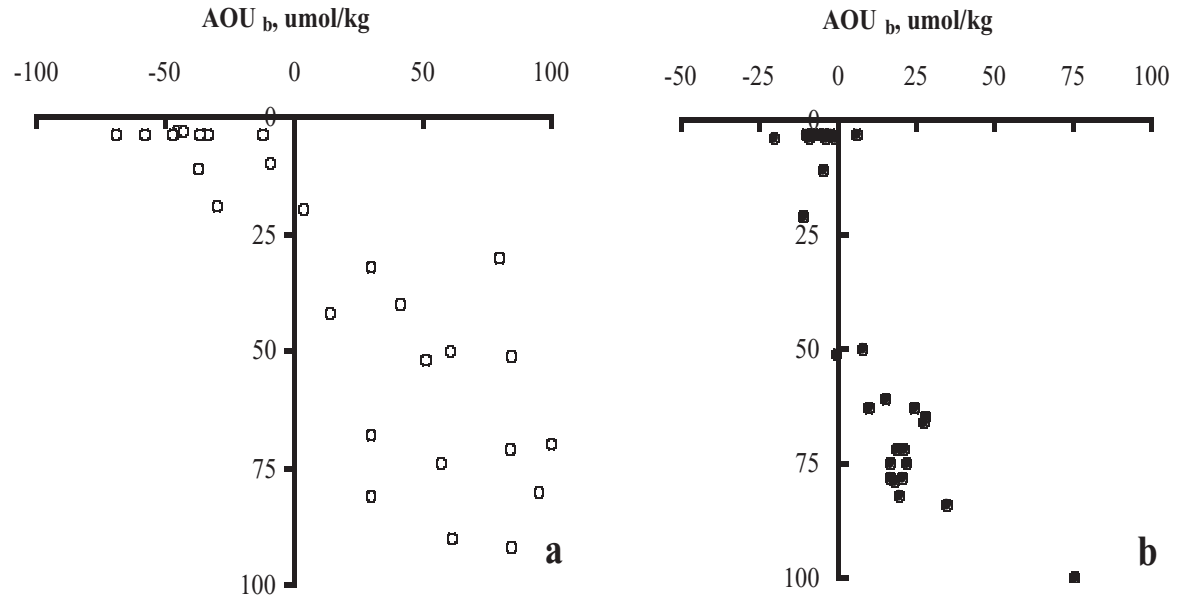

***Fig. 7.8**: Profiles of the "biological" term of apparent oxygen utilization (AOU_b) for the Sakhalin slope area (**a**) and Derugin Basin (**b**).*

The biological productivity in the upper water column is very important from a geochemical point of view, because in many cases, the main source of material for mineral formations is organic matter. There are different methods to estimate this productivity. The most simple quality estimation, the "biological" term of apparent oxygen utilization (AOU_b), was applied here (Tishchenko et al., 1998). A negative value of this parameter implies that the oxygen production by photosynthesis surpasses the oxygen consumption by respiration and oxidation of organic matter. AOU_b was calculated using data of dissolved oxygen and the measured parameters of the carbonate system. A comparison of the Sakhalin slope and Derugin Basin (*Fig. 7.8*) yields that the photosynthesis exceeds the decay of organic matter in the upper 25 m of the water column to a much greater extent on the Sakhalin slope than in the Derugin Basin. Obviously, the Sakhalin slope area is a much more productive region than the Derugin Basin.

7.4 Conclusions

Despite the high precision of our measurements, we did not find any effects of methane bubbles on the carbonate system parameters of the water column within the investigated

methane plumes. Only the exceptionally large temporal variability of hydrochemical properties of the water column in “Giselle flare” might be related to the mixing induced by gas bubbles. This variability will be subject to further investigations following this cruise.

The studied carbonate system of the water column provides useful information for the understanding of complex geochemical processes in the underlying sediments in form of the in situ pH near the bottom, the saturation degree of calcite in the water column, the character of the profile of normalized alkalinity, the estimation of the biological activity in the upper water column layer.

The nutrient data shows exceptionally high silica concentrations in the deep waters of the Derugin Basin suggesting that the bottom waters covering the “Barite Mounds” might be close to saturation with respect to barite, whereas the carbonate system data clearly demonstrate a strong undersaturation with respect to calcite and aragonite. It seems to be likely that these water properties exert a great influence on the chemical and mineralogical composition of the precipitates accumulating at the “Barite Mounds”. Moreover, the nutrient data shows that deep Derugin waters are subject to denitrification processes.

8. PORE WATER GEOCHEMISTRY

Klaus Wallmann, Pavel Tishchenko, Galina Pavlova, Bettina Domeyer, Janne Repschläger, Natasha Khodorenko, and Sergey Sagalayev

8.1 Pore water sampling and analysis

Sediment samples were squeezed in a cold room at 4°C temperature and 2-4 bar using a polypropylene apparatus pressurized by argon and equipped with 0.45 µm cellulose acetate membrane filters to separate the pore water from the sediment matrix.

Pore water samples were stored in the refrigerator at 4°C and sub-samples for sulfide determination, element analysis, and $\delta^{13}C$ measurements were taken and conserved within two hours after squeezing. Sulfide samples were conserved with 47.6 mM zinc-acetate solution, supra-pure HCl (50 µl of 30% HCl solution) was added to dissolved element sub-samples (4 ml), and $\delta^{13}C$ samples (1 ml) were given into gas-tight vials previously purged with nitrogen gas. All vials used for pore water storage were previously washed with acid and Milli-Q water to prevent sample contamination.

As pore water samples rapidly loose alkalinity and Ca during storage, these parameters were determined within some hours after sampling. The other nutrients and dissolved ions (phosphate, ammonia, silica, magnesium, and chloride) proved to be more stable and were thus analyzed during the following days.

8.1.1 Dissolved calcium

Samples for dissolved calcium (Ca) in pore water were analyzed 2-6 hours after squeezing by complexometric titration of 1 ml of pore water dispensed in 10 ml deionized water using the same procedure as with sea water analyses (Tsunogai, 1968). The correction factor concerning strontium (Sr) will be calculated after the analysis of pore water for Sr in the shore-based laboratory at GEOMAR. The Brinkman/Dosimat 665 motor-driven piston burette reproducible to ±0.001 ml in the delivered volume was applied for analysis. Based on the analysis in pore water replicates, an analytical precision of ±7 µmol/kg (n = 8) for calcium in pore water was achieved in this study.

8.1.2 Dissolved magnesium

The sea water of a salinity of 35 is approximately 0.055M in magnesium, 0.01M in calcium and 0.0001M in strontium, other divalent metals being present at the p.p.b. level. The concentration of magnesium can be derived from the total concentration of alkaline earth metals and determined calcium concentration. The total concentration of alkaline earth metals was determined by the photometric method with EDTA, with eriochrome black T as indicator. The procedure is the following: 1 ml of pore water, 5 ml of ammonium buffer, 0.1 ml indicator and 10 ml of pure water were added into a titration vessel, then a fiber optic cell was immersed into the titration vessel and the titration curve was recorded on a Brinkmann PC-2000 photometer at wave length 540 nm. The end point was calculated using the least square method for treatment of titration curve. IAPSO water with known concentrations of magnesium and calcium of 54 mM and 10.55 mM, respectively, is used as primary standard. Standard deviation of this method was found as 0.15%.

8.1.3 pH

pH is a master parameter in geochemical studies, because the solubility of minerals and the migration ability of different species are governed by this parameter. Therefore, precision and accurate measurements are highly desirable. Recently, we have shown that the main source of errors and thermodynamic uncertainty of pH measurements in the sea water is the liquid junction potential (Tishchenko et al., 2001), because commonly the cell with liquid junction is used

Ag,AgCl	Solution of KCl m≥3.5	test solution (standard solution)	H^+-glass-electrode	(A)

Owing to Pitzer's method (Pitzer, 1991) and the existence of highly stable and accurate ion selective electrodes, the cell without liquid junction has been proposed for pH measurements

glass-electrode-Na^+	test solution (standard solution)	H^+-glass-electrode	(B)

Thus, we executed Guggenheim's suggestions who wrote seventy years ago "... It must not be supposed that we mean in any way to disparage the many valuable results obtained by means of cells with liquid junctions of the type in general use for "p_H measurements". But these should be used only as a last resort and wherever possible discarded in favor of cells without liquid junctions. Thus cells of the type

$$H_2 \mid \text{solution} \mid HgCl \mid Hg,$$

if the concentration of Cl^- in the solution is known, may be used to measure $C_{H^+} f_{\pm}^2$ while cells of type

$$H_2 \mid \text{solution} \mid Na\ (Hg),$$

if the concentration of Na^+ in solution is known, measure approximately C_{H+}..." (Guggenheim, 1930).

On this cruise, we measured pH in the sediments by means of cell (B). For minimizing the degassing process in the sediments, measurements were carried out in a cool room with an ambient temperature about 5°C. Sediments samples were thermostated at 5°C for stations LV29-34, -46 and at 10°C for others. The other details of pH measurements are described in Chapter 7. All pH data is listed in Appendix 5.

For discussing the quality of our pH measurements in the sediments, profiles of pH, saturation degree of calcite and alkalinity are given in *Figure 8.1*. There is a strong scatter in pH data which amounts to more than 0.5 pH unit. This scatter is not correlated with smooth profiles of alkalinity, dissolved calcium and magnesium. It is not caused by unstable work of the electrodes and pH-meter, because the same system has been used for pH measurement of sea water where the reproducibility of pH profiles in the water column in the Derugin Basin was better than 0.01 pH unit. We assumed that this scatter is caused by degassing. Station LV29-59 probably had the lowest gas content of the sediments and pH is about 7.5. For this station, the saturation degree of calcite is less than 1. But for station LV29-56 the saturation degree significantly exceeds 1 everywhere. This means that unreliable pH data has been obtained. Sediments of this core contained abundant gases. Therefore, degassing was more intensive at station LV29-56. As result of the degassing, pH shifts to the high side and pore water becomes supersaturated with regard to calcium carbonate. Apparently, the existence of some

scatters in the alkalinity profile of station LV29-56 might be caused by carbonate precipitation during core recovery.
Our final conclusion is that the pH data of the gray sediments measured aboard is unreliable. And the carbonate system of pore water might be studied only by modeling diagenesis processes using more reliable data as nutrients, alkalinity, calcium and magnesium concentrations.

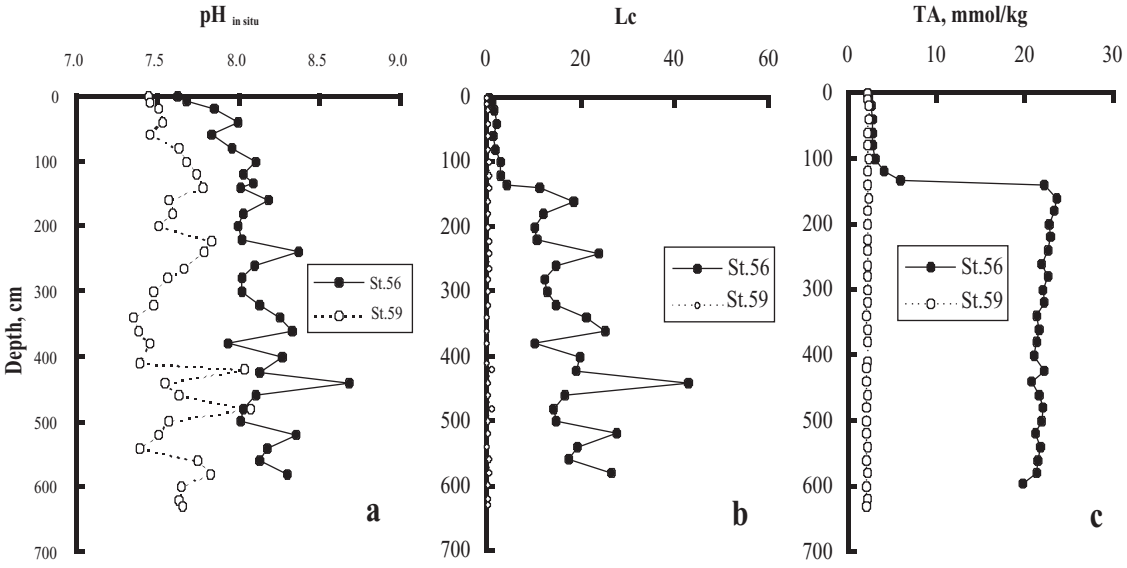

Fig 8.1: *Profiles of $pH_{in\ situ}$(**a**), saturation degree of calcite (**b**) and total alkalinity (**c**) for gravity corer stations (LV29-56-1, SL-R; LV29-59-1, SL-R).*

8.1.4 Total Alkalinity

Samples for Total Alkalinity (TA) in pore water were analyzed 2-3 hours after squeezing by direct titration of 1 ml of pore water dispensed in 10 ml deionized water with 0.02 N HCl in an open cell using the same procedure as with sea water titration (Bruyevich's method (Bruyevich, 1944)). Bruyevich's method is convenient to work with small volumes of the sample and allows to avoid the errors caused by H_2S oxidation during titration. The Brinkman/Dosimat 665 motor-driven piston burette reproducible to ±0.001 ml in the delivered volume was applied for analysis. Replicate measurements (n=8) indicated stable values, and an analytical precision of ±10 µmol/kg for TA in pore water was achieved in this study.

8.1.5 Total dissolved sulfide

Sulfide samples were conserved with zinc acetate gelatine solution (47.6 mM in Zn acetate) adding 0.1 ml solution to 1 ml oxic/suboxic pore water. For samples with intense H_2S odor, an aliquot of 0.5 ml was given into a solution composed of 4 ml Milli-Q water and 0.5 ml zinc acetate gelatine solution. The Zn-bearing solution was added to fix sulfide as colloidal zinc sulfide, whereas the water was used to inhibit ZnS precipitation. The resulting ZnS colloidal solution was mixed with 40 µl phenylen-diamin and 40 µl $FeCl_3*6H_2O$, and the absorbance was measured after 1 hour at 670 nm using a Perkin-Elmer Lambda 2 UV/VIS Spectrometer. A linear calibration curve was obtained in the concentration range of 0-57 µM $\sum H_2S$. The sulfide standard solution was titrated with sodium thiosulfate to determine the true concentration of the standard. Samples were diluted into calibration range before reagent addition.

8.1.6 Dissolved nutrients

Dissolved silicate, phosphate, and ammonia were measured applying standard photometric procedures on a Perkin-Elmer Lambda 2 UV/VIS Spectrometer. The analysis of nutrient concentrations was disturbed in anoxic samples with high ΣH_2S concentrations. Thus, sulfide-bearing samples were acidified with HCl (50 µl conc. HCl per ml sample) and stored in a cold room for two days prior to analysis. By this procedure sulfide was converted into hydrogen sulfide and transferred into the atmosphere.

Dissolved silica was determined diluting a volume of 0.5 ml sample (pore water and sea water) or standard to 5.0 ml with deionized Milli-Q water and 0.2 ml heptamolybdate solution. After 15 minutes 0.2 ml oxalic acid solution and ascorbic acid were added. The blue-colored silicomolybdic complex took an other 30 minutes to develop, before the absorbance could finally be measured at 810 nm.

For the analyses of phosphate, 2 ml of pore water sample or standard were diluted with 4 ml pure water; subsequently 0.1 ml ascorbic acid and 0.1 ml heptamolybdate reagent were added, and the absorbance was measured after 10 minutes at 880 nm.

To determine ammonia, 1 ml water sample or standard were made up to 5 ml using 4.8 ml Milli-Q water and 0.2 ml phenol solution. After 2 minutes 0.1 ml citrate buffer and 0.2 ml DTT reagent were added. After mixing, the samples were kept at room temperature protected from sunlight for about 24 hours, before the absorbance was measured at 630 nm.

Tab. 8.1*: Pore water sampling sites on cruise LV29*

Station	Location	Depth (m)	Working Area
34-1, HYC	54°19,202'N 143°54,576'E	182	Northern Sakhalin shelf, shelfbreak flare
46-1, HYC	54°26,492'N 144°04,600'E	684	Northern Sakhalin slope, “Obzhirov flare”
50-1, SL-R	54°26,811'N 144°04,870'E	695	Northern Sakhalin slope, “Obzhirov flare”
51-1, SL-R	54°28,812'N 144°11,561'E	825	Northern Sakhalin slope, deep flare
53-1, HYC	54°00,495'N 146°16,909'E	1493	Derugin Basin, “Barite Mounds”
56-1, SL-R	54°00,746'N 146°15,947'E	1470	Derugin Basin, “Barite Mounds”
59-1, SL-R	54°00,765'N 146°26,059'E	1425	Derugin Basin, “Clam Hill”
63-1, HYC	54°00,698'N 146°26,499'E	1431	Derugin Basin, “Clam Hill”

8.1.7 Chloride

Dissolved chloride was determined by titrating 0.1 ml sample dispensed in 5 ml Milli-Q water with $AgNO_3$ solution. As dissolved sulfide reacts with Ag^+ ions to form an Ag_2S precipitate, the chloride titration was performed only in aged samples with low sulfide content.

8.2 Results and discussion

Pore waters were separated from surface sediments recovered in 4 hydrocorer (HYC) and 4 gravity corer (SL(R)) deployments (*Tab. 8.1*). They were analyzed for dissolved nutrients (ammonia, phosphate, silica), alkalinity, sulfide, chloride, calcium, magnesium and pH as described in the methods section. A complete list of measured concentrations is given in Appendix 5.

8.2.1 Northern shelf and slope off Sakhalin Island

Sediments off North Sakhalin are sandy at water depths shallower than 300-400 m and silty at greater depths. They contain a terrigenous fraction delivered by Amur River and a biogenic fraction composed of biogenic opal and organic matter. Most of the fine-grained terrigenous particles delivered by Amur River are deposited at the mid-slope area inducing sedimentation rates of up to 100 cm kyr^{-1} (Tiedemann, pers. com.). Previously studied sediments from the mid-slope area (LV27-2-4, LV28-4-4, LV28-32-1, GE99 SL 24-2, GE99 SL 27-2, GE99 SL 29-3, GE99 SL 12-4, GE99 SL 26-2) have high particulate organic matter contents (1-2 wt-%) and high methane concentrations that document sulfate depletion and beginning methanogenesis at sediment depths of 3-6 m.

During cruise LV29, one sediment core was taken at the shelfbreak off northern Sakhalin within an area marked by an intense acoustic flare (HYC LV29-34-1). The core was very sandy and the pore water analysis revealed modestly reducing conditions at the core base. The low sulfide contents (<100 µM) and alkalinity values (<5 Eq. dm^{-3}) show that the sediments were not affected by gas or fluid venting at the coring site. Probably, the gas vents indicated by hydroacoustic data were missed during the coring operation.
Moreover, three sediment cores were retrieved in the northern mid-slope area (*Tab. 8.1*). Two of them were taken below "Obzhirov flare" (HYC LV29-46-1, SL LV29-50-1) where gas venting was documented on previous expeditions (Obzhirov, 1992; Biebow & Hütten, 1999; Biebow et al., 2000). One sediment core (SL LV29-50-1) contained gas hydrates that had previously been discovered at the same location by Ginsburg et al. (1993) and during the MV *Marshal Gelovany* expedition in 1999 (GE99). The top of the gas hydrate layer sampled in core LV29-50-1 was found in the core catcher at a sediment depth of 400 cm. In contrast, Ginsburg et al. (1993) found the gas hydrate top at a significantly shallower sediment depth of 30-120 cm, whereas gas hydrates were retrieved from a sediment depth of 300-320 cm during expedition GE99. The shift in the hydrate depth position is remarkable. It may either be due to a continuous deepening of the hydrate layer over the last 10 years or might be ascribed to lateral variability within the coring area. Continued hydroacoustic surveys suggest that gas venting first appeared in 1988 in the "Obzhirov flare" area (Obzhirov, pers. com.), whereas coring during GE99 recovered *Calyptogena* clam shells at various sediment depths documenting gas venting over extended periods of the Holocene. It might be envisioned that the historic venting re-started in 1988 and lost in intensity over the last decade inducing a continuous deepening of the hydrate deposition zone. Video-controlled coring and an enhanced positioning of the research vessel are needed to reveal the arial extend and structure of the venting area. Only with this enhanced data base and improved techniques, possible changes in the vent activity over time may be recorded.
One additional core (SL LV29-51-1) was taken at larger water depths north to the "Obzhirov flare" area. Here, hydroacoustic measurements showed a well developed flare and interesting seafloor structures suggesting strong venting activity. Nevertheless, the core contained no visible signs of venting such as massive carbonate crusts or gas hydrates. Thus, the venting site documented by the acoustic flare was again missed during coring.

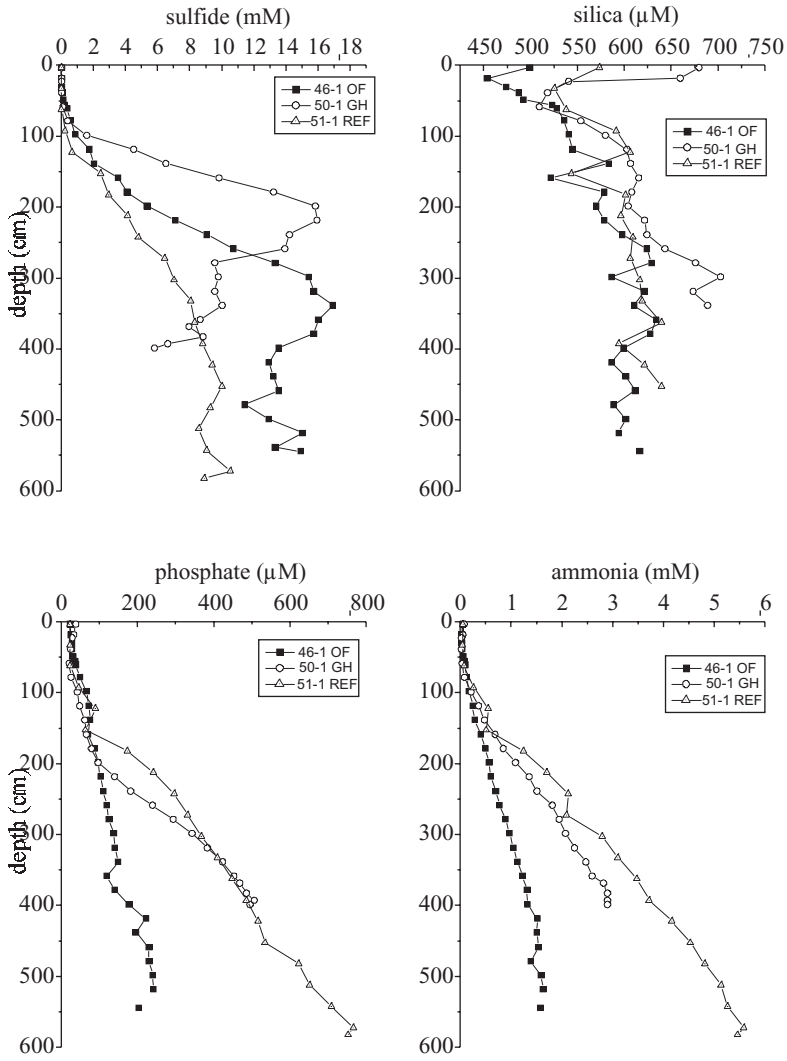

Fig. 8.2: *Concentrations of dissolved sulfide, silica, phosphate, and ammonia in Sakhalin slope sediments.*

Pore water data from the slope cores are summarized in *Figures 8.2* and *8.3*. The reference sediments taken to the north of "Obzhirov flare" (SL LV29-51-1) have high phosphate, ammonia, alkalinity, and sulfide values that document high rates of anaerobic organic matter degradation. The slope of the alkalinity profiles shows a distinct change at 400-450 cm depth that is accompanied by a sulfide maximum. This depth marks the lower boundary of the sulfate reduction zone and the upper boundary of the underlying methanogenic sediment column. Thus, methane production occurs at shallow depths in the northern mid-slope sediments as previously documented. Interestingly, the Mg concentrations begin to rise below a depth of 350 cm. The observation is surprising and might be related to de-sorption of Mg^{2+} ions from deep anoxic sediment layers caused by a change in solution composition.
In contrast to the reference core, sediments from "Obzhirov flare" (LV29-46-1, LV29-50-1) have enhanced sulfide concentrations and alkalinities in the upper 400 cm, whereas the nutrient values are generally diminished (*Figs. 8.2* and *8.3*). The hydrate-bearing core LV29-50-1 shows the highest alkalinity values accompanied by a strong sulfide maximum at shallow depth (200 cm) indicating high rates of anaerobic methane oxidation via sulfate reduction. The low Ca concentrations observed in the same core indicate intense carbonate precipitation processes.

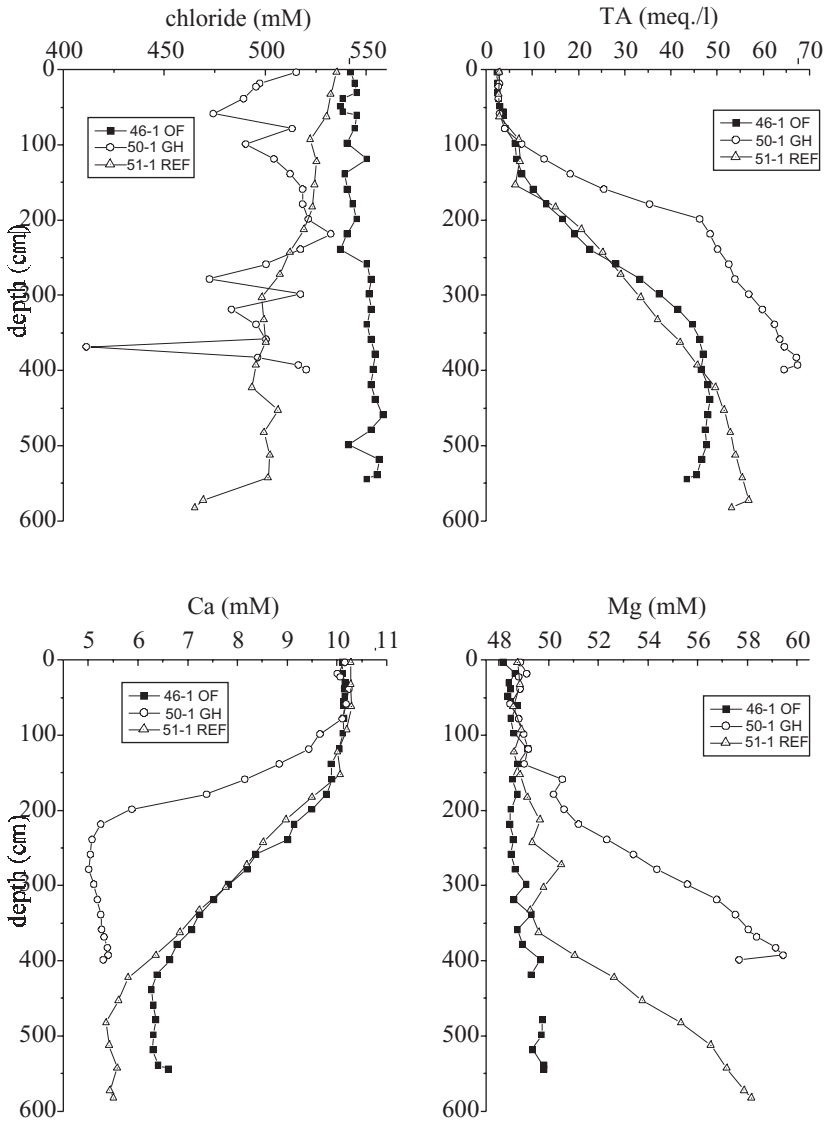

Fig. 8.3: *Concentrations of dissolved chloride, total alkalinity, calcium, and magnesium in Sakhalin slope sediments.*

A transport-reaction model was developed to simulate the processes occurring in the slope sediments. In this model, dissolved species are transported via bio-irrigation, molecular diffusion and burial, whereas solids are transported by burial only.

The model considers variable sediment porosity's as determined in cores taken during previous expeditions and depth-dependent transport coefficients. It simulates the distribution of two solid species (reactive POC, refractory POC) and six dissolved species (NH_4^+, SO_4^{2-}, CH_4, CO_2, HCO_3^-, Ca^{2+}) following the general approach outlined in Boudreau (1996), Luff et al. (2000), and Luff & Wallmann (subm.). The reactions and kinetic rate laws used in the model are summarized in *Table 8.2*. The model was implemented using MATHEMATICA Version 4.1. In this commercially available software, the system of coupled differential equation describing the depth profiles of solid and dissolved species is solved using the Method-of-Lines-Code, a finite difference procedure successfully used in previous models of early diagenesis (Boudreau, 1996; Luff et al., 2000).

Tab. 8.2: *Reactions and kinetic rate laws considered in the transport-reaction model for anoxic slope sediments.*

Degradation of particulate organic matter

via sulfate reduction: $2\ C(H_2O) + SO_4^{2-} => HCO_3^- + HS^- + CO_2 + H_2O$
via methanogenesis: $2\ C(H_2O) => CH_4 + CO_2$

Rate laws:
$R_{POC} = k_1 \times C_1 + k_2 \times C_2$
$R_{SO4} = 0.5 \times f_{POC} \times R_{POC} \times [SO_4^{2-}]/(M_{SO4} + [SO_4^{2-}])$
$R_{CH4} = 0.5 \times f_{POC} \times R_{POC} \times M_{SO4} /(M_{SO4} + [SO_4^{2-}])$
$R_{HS} = R_{SO4}$
$R_{CO2} = R_{SO4} + R_{CH4}$
$R_{HCO3} = R_{SO4}$
$R_{NH4} = (16/106) \times f_{POC} \times R_{POC}$

where R_{POC}, R_{SO4}, R_{CH4}, R_{HS}, R_{CO2}, R_{HCO3}, R_{NH4} are rates of POC degradation, SO_4^{2-} reduction, CH_4 formation, CO_2 formation, HS^- formation, HCO_3^- formation and NH_4^+ production, respectively. C_1 and C_2 are concentrations of reactive and refractory POC, k_1 and k_2 are the corresponding kinetic constants, f_{POC} is a function converting POC degradation rates from units wt-% POC yr^{-1} into units of µmol POC cm^{-3} yr^{-1}, $[SO_4]$ is the dissolved sulfate concentration, and M_{SO4} is a Monod constant (= 1 mM SO_4).

Anaerobic oxidation of methane

$CH_4 + SO_4^{2-} => HCO_3^- + HS^- + H_2O$

Rate law: $R_{SM} = k_{SM} [CH_4] \times [SO_4^{2-}]$

with k_{SM}: kinetic constant, []: concentrations in $mmol/dm^3$.

Carbonate precipitation

$Ca^{2+} + HCO_3^- => CaCO_3 + CO_2 + H_2O$

Rate law: $R_P = k_P \times (L_C - 1)$

with $L_C = [HCO_3]^2 \times [Ca]/([CO_2] \times K_{SP})$

where R_P is the carbonate precipitation rate, k_P is a kinetic constant, L_C is the saturation index with respect to calcite, and K_{SP} is the solubility product of calcite.

The model was first applied to sediment core LV29-51-1 to simulate the processes in slope sediments not affected by gas or fluid venting. The modeling procedure started with the simulation of POC and ammonia profiles. The kinetic constants of organic matter degradation (k_1 and k_2) and the penetration depth and intensity of non-local transport were varied until the resulting model curves fitted the available data. POC measurements in slope sediments cored during previous expeditions showed that the POC contents are close to 2 wt-% at the surface and decrease to 1.5 cm at 4-6 m sediment depth. These concentrations and the exponential decrease in POC concentrations observed in previous cores were taken as constraints to the model POC curve. Ammonia profiles were fitted to the data measured in core LV29-51-1 as

shown in *Figure 8.2*. Subsequently, the methane concentration at the base of the model column and the rate constant of anaerobic methane oxidation were varied until the calculated dissolved sulfide profile fitted the measured data. Finally, the rate constant for carbonate precipitation was varied to reproduce the measured Ca data. As a further control to the model results, the measured TA profiles were compared to the sum of HCO_3^- and HS^- concentrations calculated in the model.

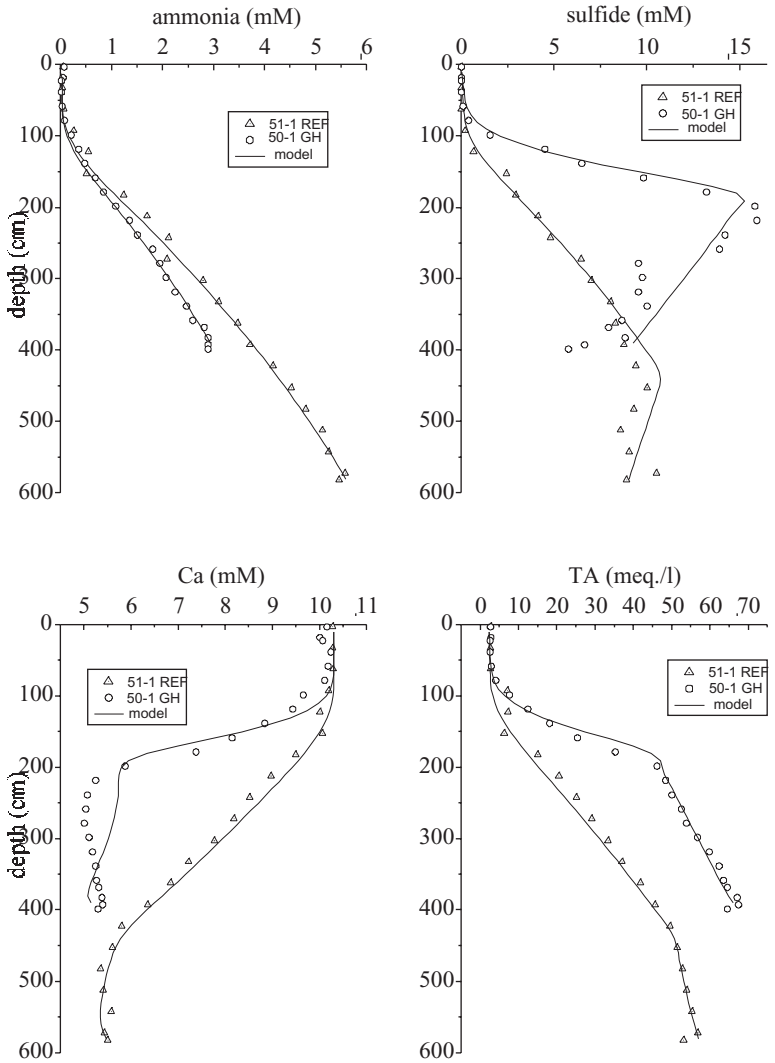

Fig. 8.4: *Dissolved ammonia, sulfide, calcium, and magnesium concentrations in sediment cores 51-1 and 50-1. Data versus model results.*

Figure 8.4 shows that the measured profiles were reproduced well by the model. The model results plotted in *Figure 8.5* indicate methane production below a sediment depth of 430 cm due to organic matter degradation and a methane concentration of 6 mM at the core base. The pore water data and the model thus confirm that methane is produced in sediments throughout the mid-slope area off North Sakhalin Island. Seismic measurements reveal a well developed BSR across the continental margin off North Sakhalin Island and thus demonstrate the presence of gas hydrates and free gas in the investigation area (Wong, 1999). Due to the extremely high input of organic matter and fast sedimentation, gas bubbles and gas hydrates are to be expected at shallow sediment depth. As the overlying sulfate reduction zone is rather thin (3-6 m), methane may escape into the bottom water throughout the northern mid-slope

area. The high methane background concentrations in bottom waters off North Sakhalin Island (Obzhirov, pers. com.) may be caused by an extended and diffuse input of methane from underlying sediments.

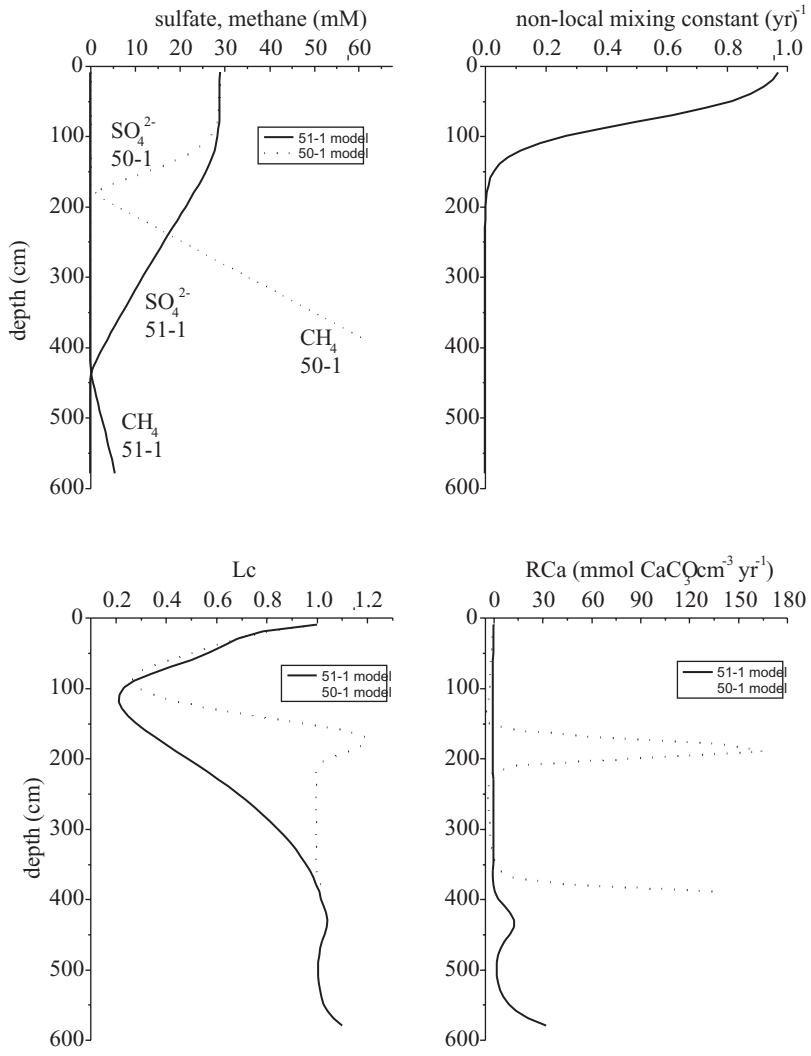

Fig. 8.5: *Results of the transport-reaction model applied to sediment cores LV29-51-1 and -50-1. Concentrations of sulfate and methane, depth-profile of the non-local mixing constant, saturation state with respect to calcite (Lc), and rate of calcite precipitation (RCa).*

Moreover, the model strongly suggests that the upper 150 cm of the sediment column were affected by non-local mixing processes (*Fig. 8.5*). The mechanisms responsible for this mixing are unknown. The mixing might be induced by deep-dwelling benthic infauna or might be caused by gas bubbles rising through the upper sediment layers. It induces a rapid exchange with the overlying bottom waters and thereby a strong nutrient depletion in the upper sediment horizons. Sediment cores from the Sakhalin slope retrieved during the previous LV28 and GE99 expeditions also had a depleted surface layer with unusually low nutrient contents overlying undisturbed and nutrient-rich sediments indicating that this distribution is a characteristic feature of the studied area.

According to the model, the pore fluids are close to saturation with respect to calcite (*Fig. 8.5*). The upper layers are undersaturated due to the CO_2 release upon microbial sulfate reduction and $CaCO_3$ precipitation, whereas the deeper layers are oversaturated due to the anaerobic oxidation of methane. The model result is also affected by the different molecular

diffusion coefficients of CO_2 and HCO_3^-. Thus, dissolved CO_2 diffuses much faster than HCO_3^- so that CO_2 escapes more rapidly towards the surface to induce undersaturation in the upper sediment horizons. The low saturation values produced by the model are more realistic than the extremely high values derived from pH measurements (*Fig. 8.1*). The rates of carbonate precipitation shown in *Figure 8.5* may thus be regarded as a realistic estimate even though the carbonate system implemented in the model has been strongly simplified to save computation time. A more sophisticated model (C.CANDI, Luff & Wallmann (subm.)) will be applied to the data during the shore-based analysis to derive well defined precipitation rates and pH values.
The model was also applied to the gas hydrate-bearing sediment core LV29-50-1 using the same parameter values as before. Only, the concentrations at the upper and lower boundaries of the model column were adjusted to reproduce the measured data. *Figure 8.4* shows that the model curves fitted the data very well even though no fluid advection was considered in the model. Thus, the model results confirm that the "Obzhirov flare" sediments are not affected by fluid venting but rather by gas venting. The resulting methane concentration at depth (62 mM, *Fig. 8.5*) is close to the theoretical concentration in equilibrium with gas hydrate for ambient pressure and temperature conditions again confirming the validity of the model approach. The model strongly suggests that the distribution of pore water species above the hydrate horizon is mainly controlled by the release of methane from hydrates and the diffusive transport of methane towards the sediment surface. Moreover, carbonate precipitation proceeds at a high rate where the upwards diffusing methane meets the sea-water sulfate infiltrating the sediments from above. The upper 150 cm of the sediment column are again affected by non-local mixing presumably induced by rising gas bubbles (Haeckel, pers. com.).

The vigorous gas venting at "Obzhirov flare" may be related to fractures that can serve as gas conduits and are reported to cut through the sedimentary deposits of the northern slope area. The source depth of the rising gas is currently unknown. The gas hydrates recovered by Ginsburg et al. (1993) are of biogenic origin (C_1/C_2 ratio 37 000, $\delta^{13}C$ = -64.3‰, δD = -207‰). Thus, it may be concluded that the oil and gas deposits off Sakhalin Island that are presumably of thermogenic origin are not the major source of the venting methane gas. It seems likely that the gas-bearing sediments below the BSR are the most important gas reservoir taped in the "Obzhirov flare" area. These sediments are located several hundreds of meters below the sediment surface but well above the deep gas deposits commercially exploited at the Sakhalin shelf and slope. Additional methane may be extracted from the extended Holocene sediment cover which generates methane at shallow depths.

8.2.2 Derugin Basin

Four sediment cores were recovered from the Derugin Basin on cruise LV29. Core LV29-53-1 was retrieved close to a site where barite- and fluid-bearing sediments were recovered during the previous GE99 expedition (core GE99-32-2). Core LV29-56-1 was taken at the base of the slope of the "Barite Mounds" where an OFOS survey revealed extended fields of *Calyptogena* and isolated barite build-ups. Both cores (LV29-53-1 and LV29-56-1) contained gas-rich sediments with a strong H_2S odor below sediment depths of 300 cm and 100 cm, respectively. The gas-rich sediments contained abundant crusts and authigenic precipitates of carbonate and barite. Cores LV29-59-1 and LV29-63-1 were taken at the slope of the "Clam Hill", an elevation situated east of the "Barite Mounds". Core LV29-59-1, which was taken further up the mound, showed no signs of venting and may thus be regarded as a reference sediment affected only by early diagenetic processes. Core LV29-63-1 was taken at the lower slope where a previous OFOS survey revealed dense and extended clusters of *Calyptogena*

clams. It contained sulfide-rich sediments at the base, again reflecting the upward flow of reducing fluids.

Core LV29-59-1 may be used to characterize the diagenetic processes prevailing in the Derugin Basin (*Figs. 8.6* and *8.7*). Previous studies showed that the Derugin Basin is the least productive area of the Okhotsk Sea and has sedimentation rates which are one magnitude order lower than at the Sakhalin shelf and slope (Biebow & Hütten, 1999). The nutrient and sulfide data confirms these results showing that organic matter degrades only very slowly within the sediment. Thus, ammonia, phosphate and sulfide concentrations are orders of magnitude lower than at the Sakhalin slope and are comparable to pore water data found in deep-sea environment. Chloride, alkalinity, Ca and Mg concentrations remain close to ambient sea-water values confirming the low diagenetic activity in these reference sediments (*Fig. 8.7*). The sulfide-bearing fluids at the bases of cores LV29-53-1, LV29-56-1, and LV29-63-1 are, thus, not formed in their present environment but at greater depths.

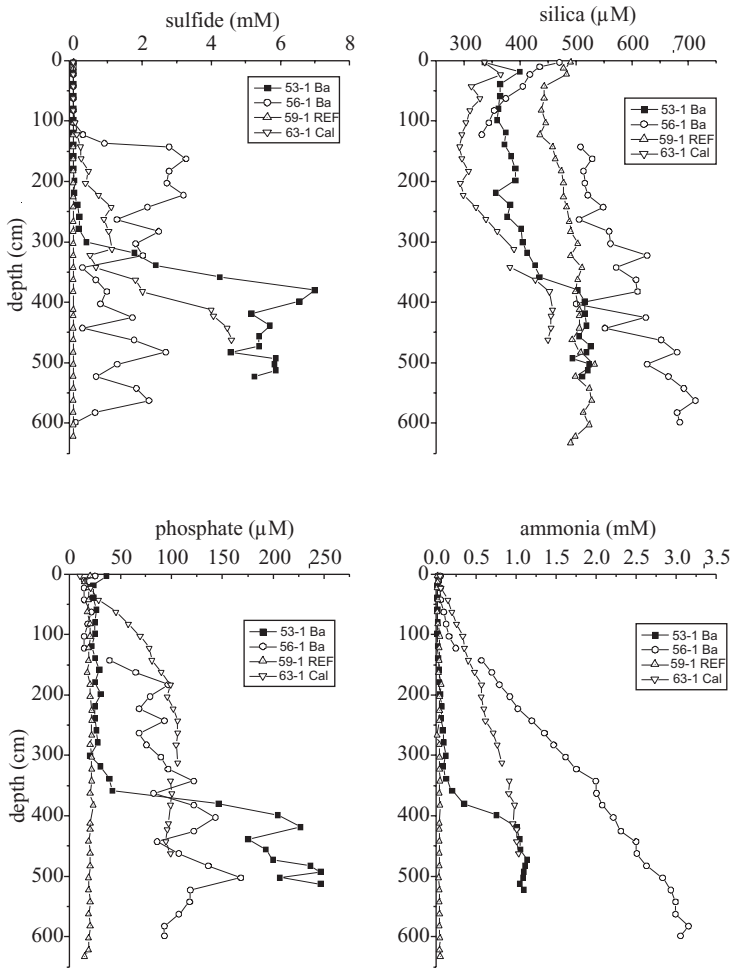

Fig. 8.6: *Concentrations of dissolved sulfide, silica, phosphate, and ammonia in sediment pore waters from the barite area.*

The most unusual concentrations and profiles were found in the gas-bearing sediment core LV29-56-1. Here, the chloride and magnesium concentrations were extremely low below sediment depths of 140 cm and increased sharply to sea-water values at 140-120 cm depth. The low concentrations indicate a deep origin of the fluids. They may be diluted with fresh water released from sediments by the diagenetic de-watering of biogenic opal and via

smectite-illit transformation. The chloride values were biased by a malfunction of a pipette, whereas the Mg data are of very high quality. The latter data shows little scatter and thus suggest that the freshening is not due to the dissociation of gas hydrates during core recovery. Hydrates were not found in the sediment core even though the presence of small amounts of micro-hydrates can not be discounted. The extreme gradients at 120-140 cm depth may again be caused by rapid non-local mixing in the surface sediments as already observed in the Sakhalin slope sediments. A rapid exchange with bottom waters is also suggested by the low dissolved-silica concentrations which are even more depleted than in the diagenetically almost inert reference core LV29-59-1.

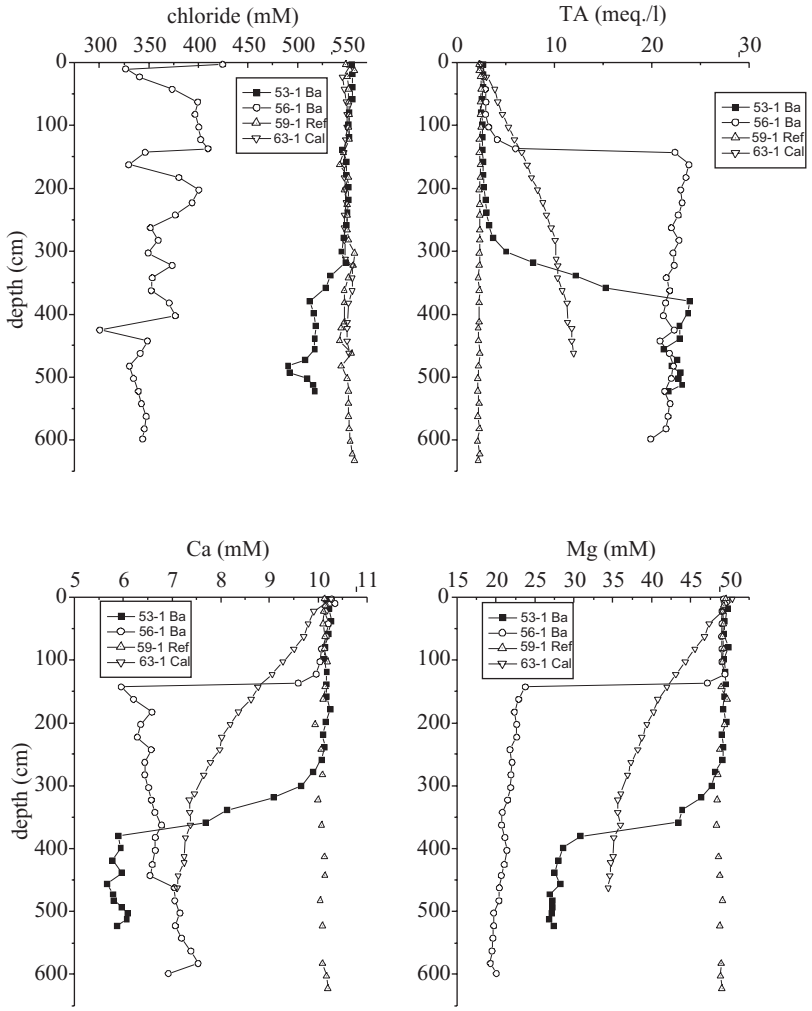

Fig. 8.7: *Concentrations of dissolved chloride, total alkalinity, calcium, and magnesium in sediment pore waters from the barite area.*

Sediment core LV29-56-1 had a similar signature even though the deep fluids seem to be more diluted with ambient pore waters and are only found in deeper sediment layers. Core LV29-63-1 taken at the “Clam Hill” shows increased sulfide and nutrient concentrations towards the base and decreasing Mg concentrations which again indicate a deep origin of the rising fluids. In contrast to the other fluid-bearing cores, the profiles were more continuous and showed no sharp gradients.

The cores taken during the expedition confirm that the barite area is affected and probably formed by deep fluids rising to the surface. Further shore-based analyses of the pore fluids will allow for a detailed exploration of fluid sources and hydrological processes prevailing in the barite area.

9. OFOS OBSERVATIONS

Giovanni Aloisi, Klaus Wallmann, Boris Baranov, Alexander Derkachev, Hartmut Hein, Harald Bohlmann, and Carl-Ulrich Noeske

9.1 Introduction

22 OFOS (Ocean Floor Observation System) lines were run on the Sakhalin shelf and slope and in the Derugin Basin area, looking for seafloor evidence of present or recent methane emission activity. In all but one of the explored areas, sound biological and/or geological evidence was observed in the form of benthic chemoautotrophic megafauna and/or authigenic mineral precipitates.
The position of OFOS lines was chosen based on the location of methane plumes, as mapped by echosounding and water column chemical surveys, and promising geological structures, identified during bathymetric and seismic surveys. For this, existing data collected during previous KOMEX cruises was integrated with data collected in newly explored areas during cruise LV29. OFOS lines were carried out drifting, taking advantage of the currents (0 to 1.4 knots) present both on the Sakhalin shelf and in the Derugin Basin. Currents are mostly along-coast on the Sakhalin shelf, (about N35 or N200, depending on the time of day); they are less predictable in the Derugin Basin area, where they may be affected by seafloor topography.
OFOS imaging confirmed to be a particularly effective method for the investigation of areas of cold seeps and provided a good intermediary between large-scale geophysical and geochemical surveys and bottom sampling operations. Biologists being absent aboard, considerations regarding the benthic macrofauna observed are limited in this report. A more accurate evaluation of the biological information collected during OFOS observations will be possible during land-based study of OFOS videos and photographs.

9.2 “Erwin flare”

6 OFOS lines were run across the newly discovered “Erwin flare”, located on the outer Sakhalin shelf (*Fig. 9.1*). These lines were aimed at crossing areas of methane emissions mapped during echosounder surveys earlier on the cruise.
The substrate in the “Erwin flare” area consists of coarse sand. Clouds of sediment, which form when the seafloor is hit by the OFOS frame, settle rapidly. The seafloor is littered with rounded cobbles, typical for this high-energy shelf environment. Less often, boulders a few decimeters across are present, possibly deriving, together with parts of the cobbles, from the shoreline of the Okhotsk Sea. Debris of this kind is typically trapped during winter time in ice forming at the shoreline of the Okhotsk Sea, is then transported by ice rafting to the shelf and beyond and is deposited as dropstones when the ice melts.
Benthic macrofauna is abundant. Amongst the most common organisms are crustaceans, starfish and anemones. Fish are also present. Shells are visible, although their abundance is difficult to appreciate, because scattered white debris is common on the seafloor and sometimes indistinguishable from shells.
In one part of the flare, white, massive, irregular build-ups up to 2 m high are present; several tens were seen in all but one of the OFOS lines. These build-ups protrude from the seafloor and sometimes have secondary, columnar bodies about 0.5 m long extending from them. A considerable amount of sediment is associated with these build-ups so that the overall appearance is of a massive, gray body covered by white decimetric patches. The seafloor around the build-ups is littered with white debris, forming an apron 2 to 3 m wide. The debris is composed of particles 5 to 10 cm across, presumably originating from the break-down of the build-ups.

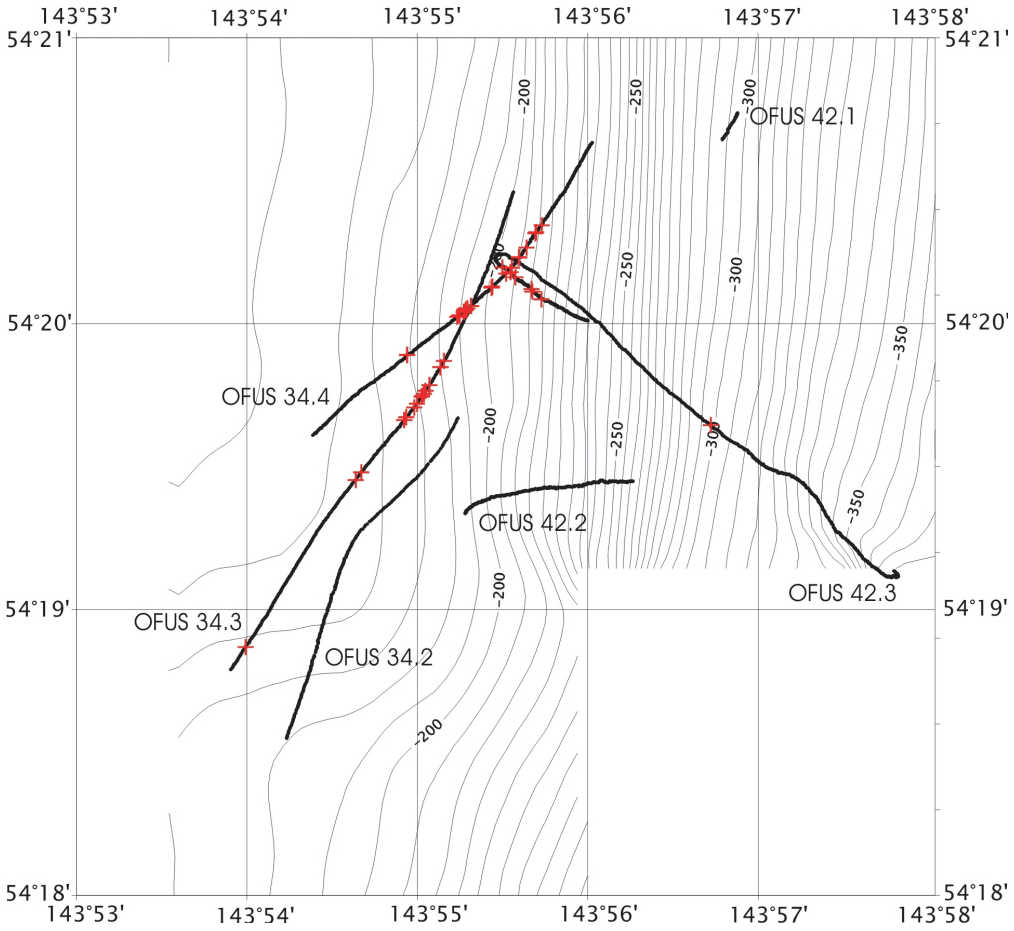

Fig. 9.1: *OFOS line run on the "Erwin flare" area. Crosses mark the occurrence of white, columnar build-ups.*

At present, the origin of the build-ups, biologic or abiotic, is not clear. One possibility is that they are built by colony-forming organisms bearing a calcareous shell. The recovery of aggregates of organisms composed of hard, calcareous, flower-shaped shells suggestive of a colonial mode of life are in favor of a biological origin. Alternatively, the build-ups are abiotic, and consist of authigenic carbonate precipitates. The fact that cold-seep authigenic carbonate formation is limited to anoxic pore waters, would require that build-ups form in the sediment and are subsequently exposed by erosion.
Bacterial mats, reported from another flare site on the outer Sakhalin shelf (Sahling et al., subm.), were not observed in the video recordings. In conclusion, no definitive evidence for methane emissions was seen during OFOS surveys of "Erwin flare".

9.3 "Obzhirov flare"

4 tracks run during the LV29 cruise in the "Obzhirov flare" area (*Fig. 9.2*) were aimed at expanding observations performed here during cruise LV28 (Biebow & Hütten, 1999). At "Obzhirov flare", situated on the intermediate continental slope, the substrate is fine-grained (silt-mud); rare debris, mainly cobbles, some of which are possibly ice-rafted, is present on the seafloor. The bottom waters are, however, turbid and the origin of some objects seen on the seafloor (e.g. black spots, which are common here) is uncertain.
Benthic macrofauna unrelated to fluid seepage is less abundant than at "Erwin flare". Fish, holothurians and crabs are the most commonly occurring large organisms. Infauna is thought

to be present too, and may be abundant, as suggested by the many centimeter-sized holes in the sediment.

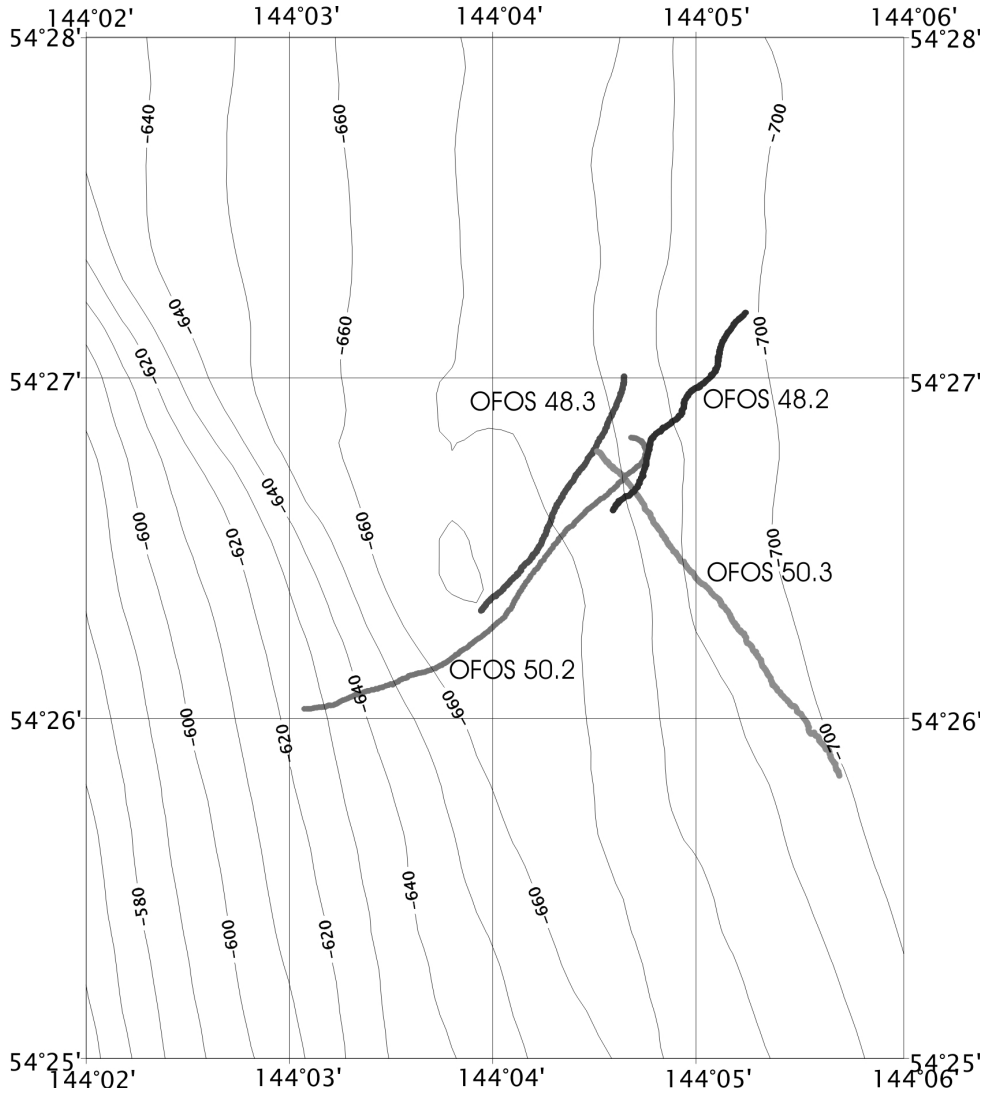

Fig. 9.2: *OFOS line run on the "Obzhirov flare" area.*

In addition to this fauna, extensive clam fields are present. These very likely consist of chemosynthesis-based species (*Calyptogena* and/or *Conchocele*?) which have been previously reported from this flare area (Sahling et al., submitted), and are indicative of active methane emission. Clam fields are up to 10 m across and can be very densely packed with clams which, in most cases, are partly buried in the sediment. Plenty bivalve shells lying on the seafloor are also present, single or in clusters, marking locations of recent methane emission. The areas of clam occurrence correlate nicely with flare images recorded with the echosounder.

In the areas most densely populated by clam colonies, a hard, irregular substrate is visible, covered by a few centimeters of soft sediment. It is not clear whether this is composed of sediment-covered clams or authigenic carbonate precipitates.

One area about 10-15 m wide, crossed on line LV29-50-3 (time on tape 3:05:00), is very densely covered by round, black and white patches of sediment. These occur next to what appears to be fields of living clams. Similar black patches in other areas of fluid seepage (e.g. the Mediterranean ridge) are composed of reduced sediments and represent single seeps; white patches, associated to the black ones, are bacterial mats. The examination of

photographs might reveal whether also the patches observed in “Obzhirov flare” are seep-related.

9.4 Derugin Basin

9.4.1 “Barite Mounds” area

The most spectacular evidence for the seepage of fluids was observed in the Derugin Basin. A ridge richly covered by authigenic barite that was first described on cruise LV28 (Greinert et al., 2002) was extensively mapped during cruise LV29. OFOS observations served to appreciate the extent of the authigenic barite, as well as that of the associated seep-related terrain. Altogether, 10 OFOS lines (*Fig. 9.3*) were run in this area; three types of terrain, described separately in this section, were defined by this survey: background seafloor, fringe areas of fluid seepage and areas of barite build-up. This OFOS survey is used to better constrain the extent of barite build-up deduced from the distribution of the “upper barite reflector” seen on the echosounder survey. Together, the echosounder and OFOS surveys are used to estimate the lateral extent and the volume of authigenic barite present at the “Barite Mounds”.

9.4.1.1 Background seafloor

The background seafloor in this part of the Derugin Basin consists of mud. 2-5 cm wide holes, often with a 10-15 cm rim of accumulated sediment particles surrounding them are very frequent. Often, the accumulated sediment surrounding the holes is white. The holes and the accumulated sediment are consistent in size throughout the whole investigated area. The most likely explanation is that these are holes made by burrowing organisms (clams, worms?). Sparse debris is also present on the seafloor and consists of brecciated particles of variable size, from centimeters to several decimeters across, to which benthic sessile organisms attach. These particles are probably of ice-rafted origin. Occasionally, trails several centimeters wide are seen. These are most probably traced by large (10 cm) gastropods which were observed at the end on some of such trails. Benthic macrofauna (crabs, starfish) are more rare here than in the shelf and slope areas.

9.4.1.2 Fringe areas of fluid seepage

These areas are similar to the background seafloor areas, except for the occurrence of seepage-related clams (*Calyptogena*?) that occur singularly and in clusters. Usually, approaching the fringe area of seepage from the background seafloor area, the first indication of fluid seepage is represented by clam shells. Moving towards the areas of barite build-up, living clams appear, and clusters become more frequent and contain a larger number of clams (typically from 3-4 to a few tens of individuals). The seafloor is often crossed by clam trails which lead to clusters of clams; these trails are narrower (2-3 cm) than those left by the passage of gastropods.
In the fringe area, barite debris can be seen on the seafloor. Sometimes it is hard to distinguish between barite debris and regional ice-rafted debris. However, debris increases considerably in abundance and size towards the barite build-ups (boulders of more than 1 m across are common) suggesting that considerable amounts originate from the break-down of authigenic barite constructions. The fringe area of fluid seepage is limited towards that of barite build-ups by the first occurrence of an in-place barite build-up.

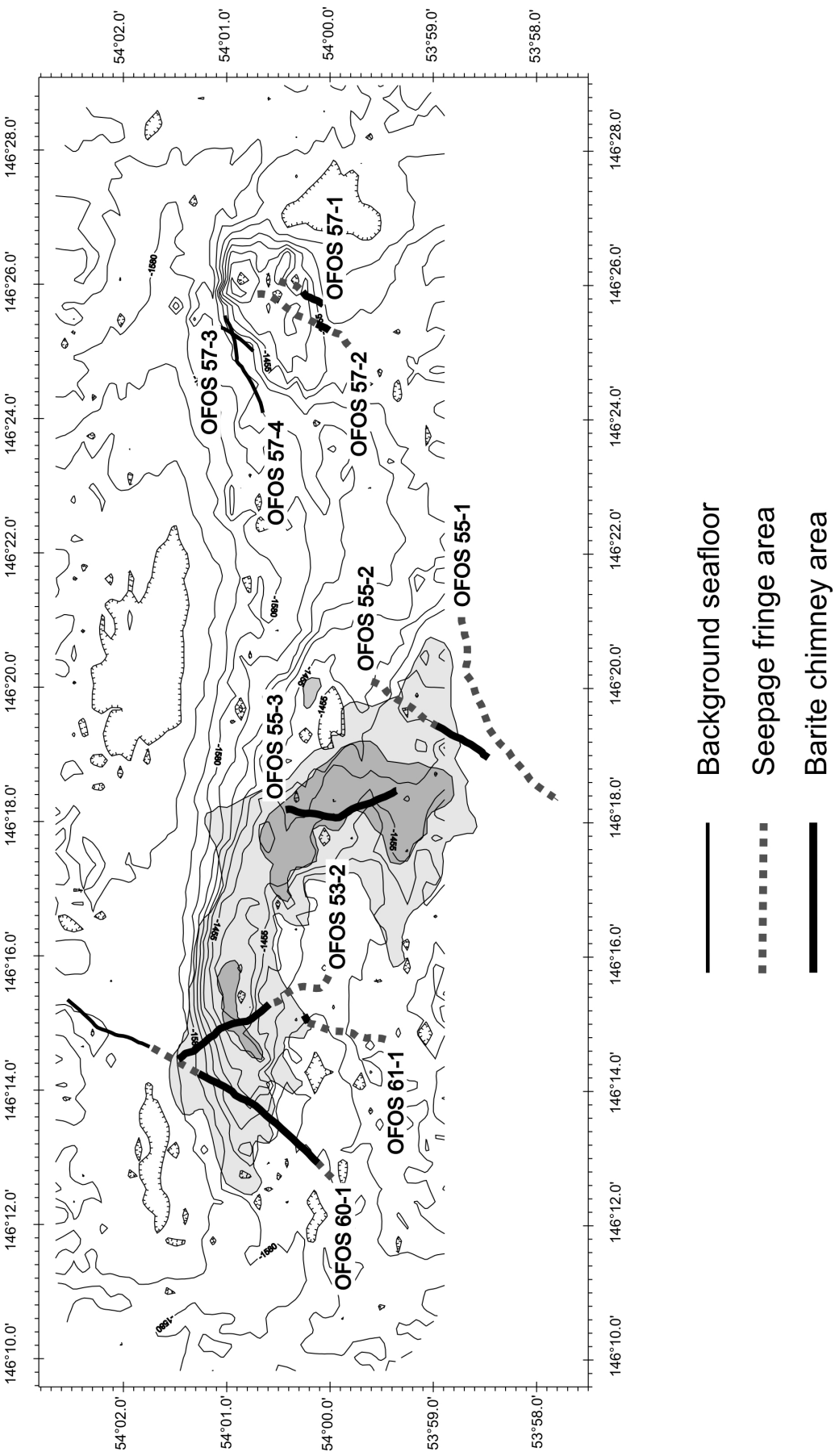

Fig. 9.3: *OFOS line run on the "Barite Mounds" area. Three types of terrain are distinguished based on OFOS observations. Shaded areas correspond to the extent of the barite build-ups as inferred by the distribution of the "upper barite reflector" seen on the 12 kHz echosounder.*

9.4.1.3 Area of barite build-up

In this area, massive barite build-ups (both massive and chimney-like) up to more than 20 m high dominate the landscape. They are separated by stretches of "fringe-type" seafloor (including the seep-associated macrofauna) a few to 40 m across. The alternation of flat, reflective seafloor with topographically rough areas of barite results in the presence of a secondary, weak reflector over the seafloor on echosounder tracks run in this area.
Often, authigenic barite build-ups are as wide at the base as they are high, giving the impression of a truncated pyramid construction (massive barites). Less often, they build vertically elongated, slim columnar structures (chimneys), a few meters in diameter and up to 20 m high. Commonly, the surface of the authigenic barite is dark due to an authigenic manganese oxide layer deposited on the barite. White patches of authigenic barite occur in decimetric to metric barite protrusions in the upper part of the barite chimneys and in cracks and fissures in the massive barites, showing that these are current locations of fluid seepage and authigenic barite precipitation. In patches of white barite, barite precipitation seems to occur in distinct centimeter-sized areas which give a mottled aspect to some parts of the chimneys, probably reflecting the highly porous nature of the barite fabric (Greinert et al., 2002) which offers a high number of distinct pathways the fluids can follow to reach sea water. Freshly built, recent barite deposits can thus be recognized on the basis of their white color.
The slope at the base of the barite build-ups is covered by a chaotic accumulation of barite blocks. Moving away from single build-ups, barite debris decrease in abundance and size.
The slope morphology in this area is strongly affected by the presence of barite precipitates. When going upslope, the OFOS often encounters vertical walls of barite up to 20 m high. Once the OFOS has risen over the top of these obstacles, it then descends typically half the distance it has risen, before touching the seafloor again. Terraces limited downslope by walls of barite are common and may be of tectonic origin. In this case, the barite walls develop on fault scarps which produce the terraces and which could be preferential pathways for the migration of fluids.
4 OFOS lines explored the mound to the east of the "Barite Mounds", where a variant to the barite build-up terrain was observed. Although authigenic barite occurs as chimneys, the height of which does not exceed a few meters, most of the authigenic precipitate seems to occur as decimeter-thick crusts. This landscape is more similar to that of cold-seep areas worldwide, where carbonate precipitates more commonly form. In addition, the most impressive accumulation of dead clams occurs here. The seafloor between barite precipitates is often white due to the presence of a layer of shells.

The distribution of seafloor types according to the OFOS observations is plotted in *Figure 9.3*, along with the distribution of the "upper barite reflector" seen on the echosounder survey. The distribution of the barite build-ups as observed by OFOS is generally consistent with that inferred by the distribution of the "upper barite reflector". Minor inconsistencies can, however, occur and are due to the different footprint of the OFOS video system (a few meters) and of the 12 kHz echosounder (about 200 m at 1,600 m water depth):

1) Barite chimneys were observed in OFOS lines which extend outside the "upper barite reflector" area (e.g. SW part of OFOS LV29-60-1). In these areas, barite chimneys are very rare in the OFOS record and likely are not abundant enough to produce a reflection in the echosounder signal. Similarly, in the eastern mound area explored during OFOS LV29-57-1 and LV29-57-2, although no reflector has been recorded, barites occur, mainly as crusts, but also as chimneys generally not higher than a few meters.

2) Parts of OFOS lines ascribed to the fringe area of fluid seepage (e.g. SE part of line LV29-53-2) fall within the area of barite chimney occurrence as inferred from the presence of the "upper barite reflector". Along these stretches of seafloor, no in-place barite chimneys were observed, but the seafloor is littered with large-scale debris of barite chimneys, indicating the presence of barite build-ups next to the track. The density of barite chimneys in these areas is very likely much greater than that in areas described in point 1, above.

In addition to better constraining the distribution of the barites, the OFOS surveys convey useful information on the extent of fluid seepage outside the "Barite Mounds" area. From OFOS lines LV29-61-1, LV29-53-2 and LV29-55-1, it is clear that the area of the seafloor affected by seepage of fluids is greater than that occupied by barite build-ups. It is difficult to estimate the extent of the fringe area of fluid seepage, since only OFOS line LV29-60-1 marks the border between this area and the background area. Large stretches of seafloor covered by the 'fringe-type' seafloor on lines LV29-61-1 and LV29-55-1 suggest, however, that it could be at least as big as the area of barite build-up.

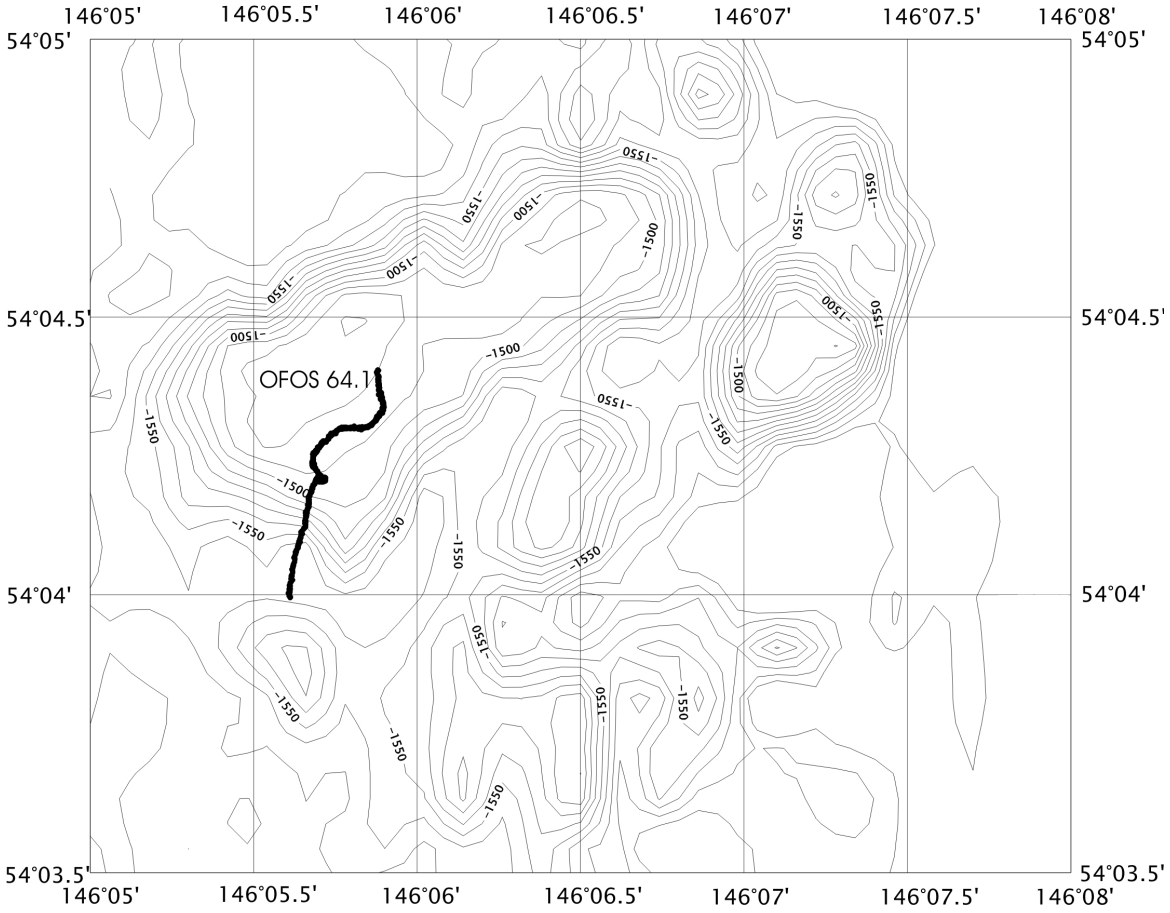

Fig. 9.4: *OFOS line run on the "Baranov high".*

9.4.2 "Baranov high"

One OFOS line explored the "Baranov high", a bathymetric high to the west of the "Barite Mounds" (*Fig. 9.4*) that shares its seismic and morphological characters, possibly indicative of active or recent seepage of fluids. The observed seafloor is of the 'fringe seepage type', confirming that the seepage of fluids is presently active. In addition, a considerable amount of debris (boulders up to 60 cm across occur), resembling fragments of barite chimneys were observed. No in-place barite precipitates were found, however, and it is not clear whether they

do occur, along with fluid venting, at this site. Evidence for fluid seepage decreased in the last part of the track towards the base of the southern slope.

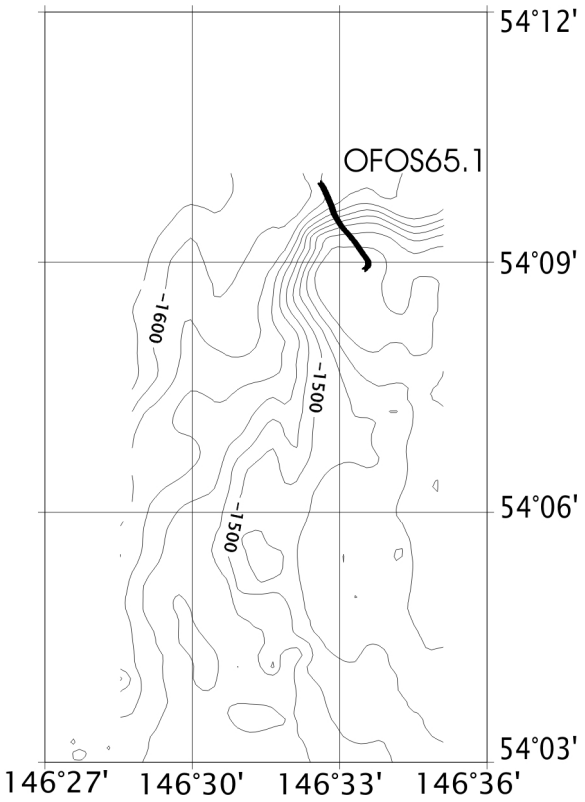

Fig. 9.5: *OFOS line run on the northeastern ridge.*

9.4.3 NE Ridge

This ridge culminates in a bathymetric high (*Fig. 9.5*) and is interpreted - on the basis of seismic data - as a tilted block. An OFOS line was run on this ridge to check the hypothesis that, in contrast to the other explored areas and as suggested by its distinct seismic character, this structure is devoid of fluid seepage. Seafloor typical of the background type was seen all along the OFOS line. Plenty debris occurs along this line, too.

10. SEDIMENTS AND AUTHIGENIC MINERALIZATION OF COLD-SEEP AREAS

Alexander Derkachev, Natasha Nikolayeva, Anatoly Botsul, and Giovanni Aloisi

10.1 Slope and shelf of Sakhalin Island

Five cores with a length from 55 to 580 cm and two dredges were taken on the shelf and slope of Sakhalin Island. For core descriptions see Appendix 6.
Coring stations LV29-34-1 and LV29-42-5 are located in a water depth of 182-191 m in the "Erwin flare" area. The cores recovered sediments of up to 100 cm in thickness, which consist of coarse-grained sand with an admixture of dropstones. In the lower part of core LV29-34-1 (interval 75-90 cm), the sediments are well sorted and contain a large amount of dropstones. Below 90 cm, they are suddenly replaced by silty clay, which probably is of lagoonal origin. In this core, a small fragment (about 1 cm in diameter) of sandstone with calcite cement was discovered at 20 cm. Carbonate debris probably of authigenic origin occurs in the entire core in minor quantities. The sediments of core LV29-42-5 are better sorted and contain more dropstones than core LV29-34-1. In the lower part of the core, they are replaced by gravel-pebble deposits with an admixture of sand and dark brown wood pieces.
Dredges LV29-40-1 and LV29-42-6 yielded sandy sediments with a large amount of dropstones. The bottom fauna is abundant and includes mollusks, crabs, starfish, and worms. One carbonate concretion of 6 x 1,5 cm in size consisting of dense massive calcite-cementing sandy particles was found. It has the same composition like the carbonate fragment from core LV29-34-1.

Two cores were taken in the "Obzhirov flare" area. One of them (core LV29-46-1 from 684 m water depth) recovered sediments typical for marginal areas of methane seeping. They are represented by terrigenous-diatomaceous silty clay and clayey silt of olive-green and greenish-gray color. The sediments are mottled and bioturbated; in sections 60-70 cm, 220-225 cm and 280 cm small shell fragments were discovered. For this core, small laminas and lenses of hydrotroilite and an H_2S odor are characteristic. From 430 cm on, the sediment becomes saturated with respect to gas and water and yields a typical lumpy-brecciated texture (Ginsburg & Soloviev, 1994; Derkachev et al., 2002). Fragments of *Calyptogena* and small (up to 1-1,5 cm in size) branchy carbonate concretions were discovered in the surface sediments.
Core LV29-50-1 was taken in direct proximity to a gas flare. It recovered sediment typical for areas of gas emanations (cold-seep areas): the sediments are bioturbated and contain lenses and laminas of hydrotroilite and carbonate concretions. Here, water-saturated and gas-saturated horizons with a characteristic lumpy-brecciated texture as well as fragments of *Calyptogena* and gas hydrate layers are significant. Carbonate concretions of different morphology and size were discovered at interval 148-320 cm. In the upper part of the horizon (148-200 cm), concretions of primary carbonate formation occur frequently. They are soft, slightly dense, and of 0.3-0.6 cm in diameter. Fragments of *Calyptogena* were discovered here, too.
Dense, massive concretions of flattened and branchy shape dominate in the lower part of the horizon. Besides, worm tubes with an empty or sediment-filled central channel were rarely observed here, as well. These up to 10 cm large concretions are located inside the sediments parallel to stratification. Concretions cementing shell fragments were found at 205 cm. A similar sedimentary section was discovered in this area on the MV *Marshal Gelovany* cruise in 1999 (Biebow et al., 2000; Derkachev et al., 2002) (*Fig. 10.1*).
Gas-saturated sediments were traced from 240 cm downwards, which turn into a gas hydrate-bearing horizon (395-405 cm). Gas hydrates are represented by thin interlayers and lenses of white color within massive sediments.

Station LV29-51-1 was conducted on the slope at a water depth of 825 m in a newly discovered area with a gas anomaly situated not far from "Obzhirov flare". The core contained terrigenous-diatomaceous sediments from the marginal part of gas seeping, which is indicated by a characteristic pore water geochemistry (see Chapter 8).

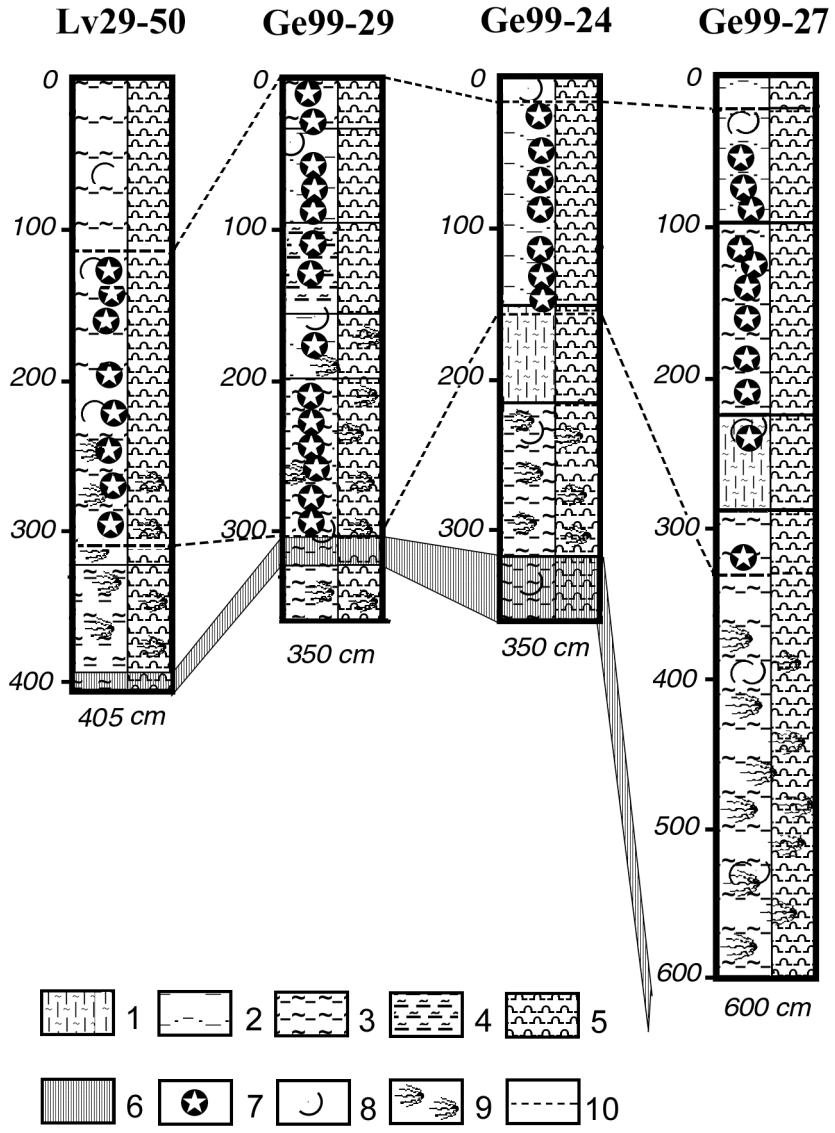

Fig. 10.1: *Distribution of carbonate concretions and gas hydrates in sediments from the area of active gas emanations on the Sakhalin slope (Obzhirov flare) and texture peculiarities of these sediments.*
1 - sand-silt-clay, 2 - sandy silt, 3 - clayey silt, 4 - silty clay, 5 - diatomaceous sediments, 6 - horizon with gas hydrates, 7 - carbonate concretions, 8 - shell fragments, 9 - texture of gas-saturated sediments, 10 - upper and lower boundaries of the distribution of carbonate concretions in the sediments.

10.2 Derugin Basin

Sediments and types of carbonate-barite precipitates, their mineral, chemical and isotopic composition were studied in detail on previous cruises in the Okhotsk Sea (Biebow & Hütten, 1999; Biebow et al., 2000; Derkachev et al., 2000, 2002; Greinert et al., 2002). These investigations allowed to conclude that carbonate and barite mineralization is widely

distributed not only at the sediment surface, but also inside the sediments of the "Barite Mounds" (Derugin Basin) covering an area of more than 10 km^2.

On GE99 cruise, an anomalous chemical composition of the pore waters connected with high barium concentrations was discovered (station GE99-32). The mineralogical and chemical composition of sediments and authigenic precipitates of core GE99-32 were studied, too (Derkachev et al., 2002). The obtained data allowed to suppose that the center of gas-fluid emanations with a marked flow of deep fluids is situated in the area of this station.

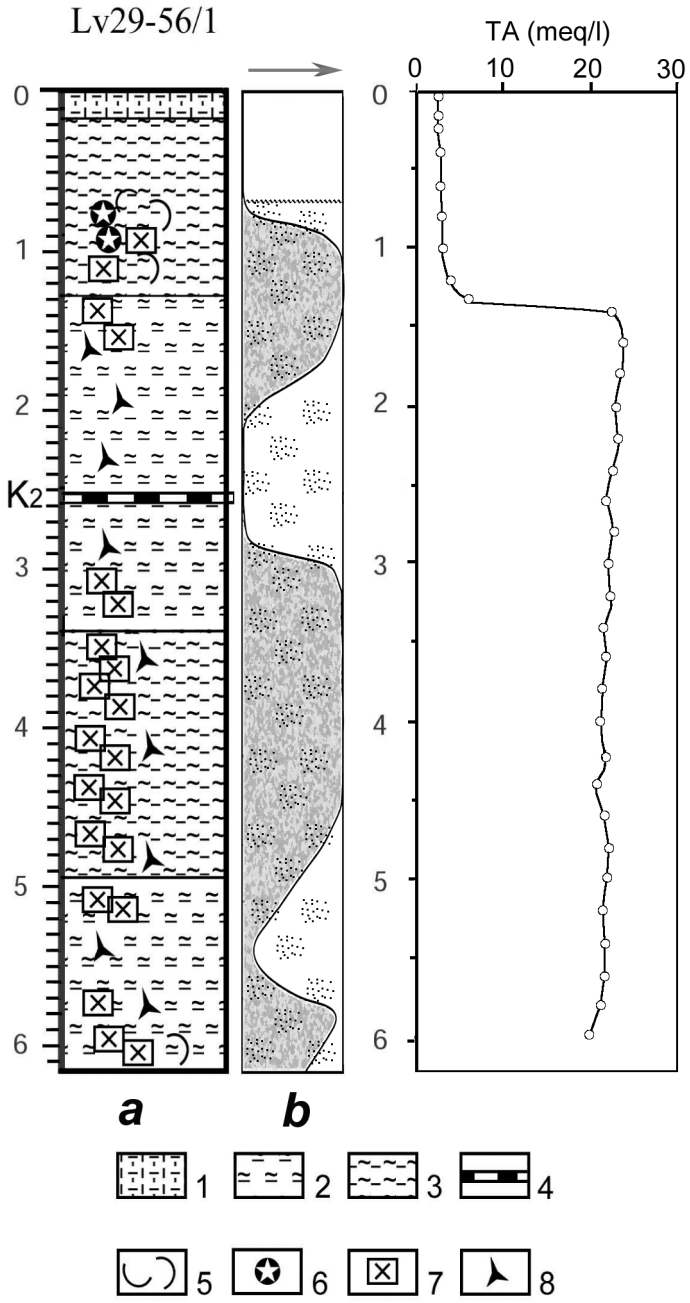

Fig. 10.2: *Manifestation of carbonate and barite mineralization in the sediments of core LV29-56.*
a - lithological column, b - distribution of carbonate (gray background) and barite (rare dots) mineralization in the core, TA - total alkalinity (see Chapter 8).
Wavy line shows upper boundary of authigenic barite distribution; arrow shows the trend of intensity increase for carbonate mineralization.
1 - sand-silt-clay, 2 - silty clay, 3 - clayey silt, 4 - volcanic ash layer, 5 - shell fragments (Calyptogena), 6 - carbonate concretions, 7 - barite-carbonate crusts, 8 - barite and carbonate tubular bodies.

For determining the origin and composition of fluids and their influence on processes of authigenic mineral formation, investigations were carried out close to the well known area of active seeping. Two cores (LV29-53-1 and LV29-56-1) taken here recovered a section of Holocene-Pleistocene sediments up to 615 cm thick, which contain a large quantity of varying carbonate and barite precipitates. Core LV29-100 was taken in Leg 2 of cruise LV29 in the southern part of the "Barite Mounds" and recovered sediment with authigenic carbonates and barites even at 10 cm depth.

Up to now, only core LV29-56-1 and partly core LV29-53-1 were analyzed in detail. Due to the fact that both cores are located relatively close to one another, their sediment composition is similar, but there are differences mainly expressed in the distribution of the mineral-morphological types of carbonates and barites.

The sediments consist mainly of terrigenous clayey silt and silty clay with a large sand admixture. Dropstones are common. Ash layer K2 discovered at 176-178 cm (LV29-53-1) and at 251-252 cm (LV29-56-1) is a good stratigraphic marker and consists mainly of volcanic glass, pumice fragments and crystalloclastics (crystals of plagioclase, pyroxenes and magnetite embedded in volcanic glass).

Two textural horizons of these cores can be divided: an upper horizon represented by soft or moderately dense sediments with slight bioturbation, and a lower horizon consisting of gas-saturated and water-saturated sediments with a typical lumpy-brecciated texture (at 382-530 cm in core LV29-53-1, at 115-615 cm in core LV29-56-1).

Authigenic carbonates and barites were observed throughout the entire cores except for the upper 60-70 cm (*Fig. 10.2*). In core LV29-53-1 the first carbonate concretions appear at 63 cm, they are represented by branchy bodies with smoothed edges (2 x 5 x 0,5 cm in size). Downcore, their content increases; horizons 290-305 cm and 373-385 cm are enriched by them. Their size varies from 1 to 10 cm. Many concretions have swells and tubes filled with authigenic barite. Below 380 cm, carbonate crusts of up to 5-10 cm in size occur frequently (especially at 400-425 and 450-480 cm). The upper part of the crusts usually has a flat rough surface; the lower part has cavities. They also contain barite worm tubes.

The first carbonate concretions in core LV29-56-1 appear at 76 cm (*Fig. 10.2*). These are small (up to 2-4 cm in diameter) precipitates oval in shape, which differ from the surrounding sediment by a lighter color. Authigenic bodies with an unusual morphology were discovered at interval 90-130 cm. They are represented by angular, very hard fragments of up to 10 cm in size consisting of an agglomerate from both highly bioturbated sediments and large fragments of *Calyptogena* and *Provanna.* The entire mass is impregnated with calcite and cryptocrystalline barite cement.

A predominance of carbonate crusts of different size and shape (individual fragments are 3-12 cm in size) is characteristic for core LV29-56-1. Branchy concretions with smoothed edges typical for core LV29-53-1 and other stations carried out in the "Barite Mounds" (Biebow & Hütten, 1999; Biebow et al., 2000; Derkachev et al., 2000) occur rarely. A lot of carbonate crusts were noticed at 370-510 cm. Usually, they have a flat, rough surface on one side (sometimes with an inclusion of dropstones) and cemented tubes filled with barite. Their other side is angular and contains numerous swells. The crusts are rather fragile; they easily crumble forming small angular fragments. Many fragments have a granular structure of carbonate cement consisting of numerous calcite, dumbbell-shaped aggregates. We previously observed similar aggregates in other cores (*Fig. 10.3*). Usually they are characteristic for bacterially induced carbonates (Buczynski & Chafetz, 1991; Gonzalez-Mucoz et al., 2000).

Some carbonate crusts contain shapeless and crustate precipitates of authigenic barite incrusting cavities in the sediment and worm tubes. Barites of this type are represented by aggregates of lamellar colorless or yellowish-brown crystals. There is also cryptocrystalline barite cement in the carbonate crusts, but for understanding its relation with carbonate mineralization special mineralogical investigations are required. Carbonate mineralization is distributed unequally. Even barite crusts without carbonate cement occur here.

The analysis of the distribution of different types of carbonates and barites showed that authigenic barite mineralization is pronounced within all recovered sediment layers except for the upper horizons (60-70 cm) (*Fig. 10.2*). The authigenic barites observed in core LV29-56-1 are of different morphological types: microconcretions with a rough surface and their aggregates, tubular bodies, crusts, cryptocrystalline cement in barite-calcite crusts. They formed apparently at the lower boundary of the sulfate reduction zone. The presence of authigenic barite in the entire core may indicate a long period of delivery of barium-saturated fluids from deep sediment horizons. The quantity and variety of the morphological types of barite precipitates depend on the intensity of gas-fluid flow. Barites are probably an earlier stage of authigenic mineral formation than calcite; numerous tubular bodies filled with barite and covered by a thin calcite coat prove this.

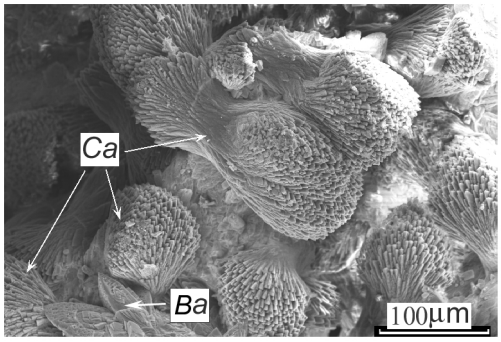

Fig. 10.3: *SEM-images of bacterially induced Mg-calcite (aggregates of dumbbell crystals) in the sediment of core GE99-32.*

If methane is the main source of carbon for the formation of carbonate concretions (Derkachev et al., 2000, 2002; Greinert et al., 2002), there was certainly a cyclicity in the delivery of methane by fluid flow. This periodicity of carbonate mineral formation was proven in core LV29-56-1 by the presence of horizons enriched with respect to carbonate precipitates (*Fig. 10.2*). One of them is horizon 80-210 cm containing carbonates and fragments of fauna (*Calyptogena*, *Provanna*) typical for areas of gas-fluid emanations.
The primary development of carbonate crusts can be observed in horizon 280-510 cm. The existence of carbonate crusts with a specific flat surface may provide evidence on their formation at the sediment surface close to the water-sediment boundary. Carbonate crusts are known in many areas of the World Ocean with active gas emanations (Kulm & Suess, 1990; Sakai et al., 1992; Jorgensen, 1992; Stakes et al., 1999; Aloisi et al., 2000; Greinert et al., 2001; etc.). Further analyses of the pore water geochemistry, sediment and authigenic precipitates will show to what extent our assumption about the cyclicity of carbonate mineral formation is correct.

On cruise GE99, an isolated submarine hill with an elevation of 150-170 m above the surrounding basin (Biebow et al., 2000) was mapped in a 5 km distance from the "Barite Mounds" close to the area with a prominent heat flow anomaly (Hayashi, 1997). As we believe that barite mineralization occurs at this structure as well, 4 OFOS profiles were run on this hill ("Clam Hill"). Two profiles (stations LV29-57-1 and LV29-57-2) crossed the southeastern slope of this structure, where large clusters of chemosynthetic fauna were discovered.
The dredging carried out in Leg 2 (station LV29-99) along the OFOS transect LV29-57-1 was very successful. Flat barite crusts, *Calyptogena* shells and their fragments of up to 10 cm size were recovered in large quantities as well as some living specimens of this specific fauna.
The size of the barite crusts varies from 8 to 22 cm. Besides, many small fragments (1-5 cm) were discovered. All these crusts are covered by a thin (0.1-0.2 mm) dark brown coat of both

iron and manganese hydroxides. Many of them have such a coat not only on the inner but on the outer surface too. This proves their prolonged exposure at the seafloor. Most likely, these crusts are fragments of build-ups and slabs which are more homogeneous in morphology and structure than those observed during OFOS records. Some crusts have a gray color and inclusions of soft sediments on the inner side showing their exposure on the sediment surface. All crusts are composed of barite, but it is possible to distinguish different morphological types:

1. Thin, flat lamellar fabrics of 1-2 mm in thickness and of 5-8 cm in length with a rough surface.
2. Crusts with a flattened surface complicated by tubular swells 0.7-2.0 cm thick. Their inner side is represented by numerous branching pillars and swells (*Fig. 10.4 c,d*). All of them consist of closely intergrown barite spherulites.
3. Multilayer crusts 1.5-3 cm thick and up to 15 cm long (*Fig. 10.4 b*). They consist of 2-3 flattened crusts of the first or second type; the space between them is filled with numerous compactly packed lamellar-globular aggregates of gray barite.
4. Crusts up to 2-2.5 cm thick. Their inner and outer surfaces represent dense interweaving of branchings and columnar barite fabrics some millimeters across and 0.5-2 cm high. On some of them, there are tubular fabrics of 0.5-0.8 cm in diameter with a pronounced channel, the walls of which are incrusted by brushes of lamellar yellow barite. These tubular fabrics are most likely remnants of barite-containing fluids filling up the channels in the surrounding sediments. The largest fragment (about 22 cm) recovered by dredging may be classified as this morphological crust type (*Fig. 10.4 a*). Among a dense network of branching, intergrown tubes and swells, it contains numerous holes not filled with barite.

Despite the considerable variety of crust morphology, the crust's composition and inner structure are relatively constant. It consists of barite represented by lamellar gray and yellow crystals; colorless crystals occur seldom. These crystals often form spherulitic aggregates and their growth products. The massive cryptocrystalline or spherulitic texture of closely intergrown barite aggregates is visible on fractures of thin crusts and swells; these aggregates cement the surrounding sediments. Often, the crusts contain inclusions of not only sandy clastic particles, but also both dropstones and shell fragments. The whole barite-containing mass is impregnated by numerous elongated tubes of about 0.1 mm diameter orientated in different planes, sometimes forming dense clusters. Their patterns are also visible on the surface of the crusts. Usually, the tubes are completely or partly filled with colorless lamellar and closely packed aggregates of barite. Most probably, these thin tubular fabrics are pseudomorphs of remnants of tubular worms or bacterial mats consisting of the filamentous bacteria *Beggeatoa*.

As shown by the OFOS observations at stations LV29-57-1 and LV29-57-2 and by dredging, an earlier unknown center of gas-fluid emanations was discovered in the southeastern part of "Clam Hill". The presence of mainly dead colonies of chemosynthetic fauna indicates a reduction of gas-fluid venting at present. The barite crusts here are covered by a coat of iron and manganese hydroxides showing their long exposure on the seafloor. It is remarkable that in contrast to the "Barite Mounds" neither fragments of barite chimneys nor carbonate crusts, concretions or carbonate-barite fabrics were observed (Derkachev et al., 2000, 2002; Biebow & Hütten, 1999; Biebow et al., 2000; Greinert et al., 2002). The different morphological types of barite crystals typical for barite chimneys are missing even in the fine sediment fractions.

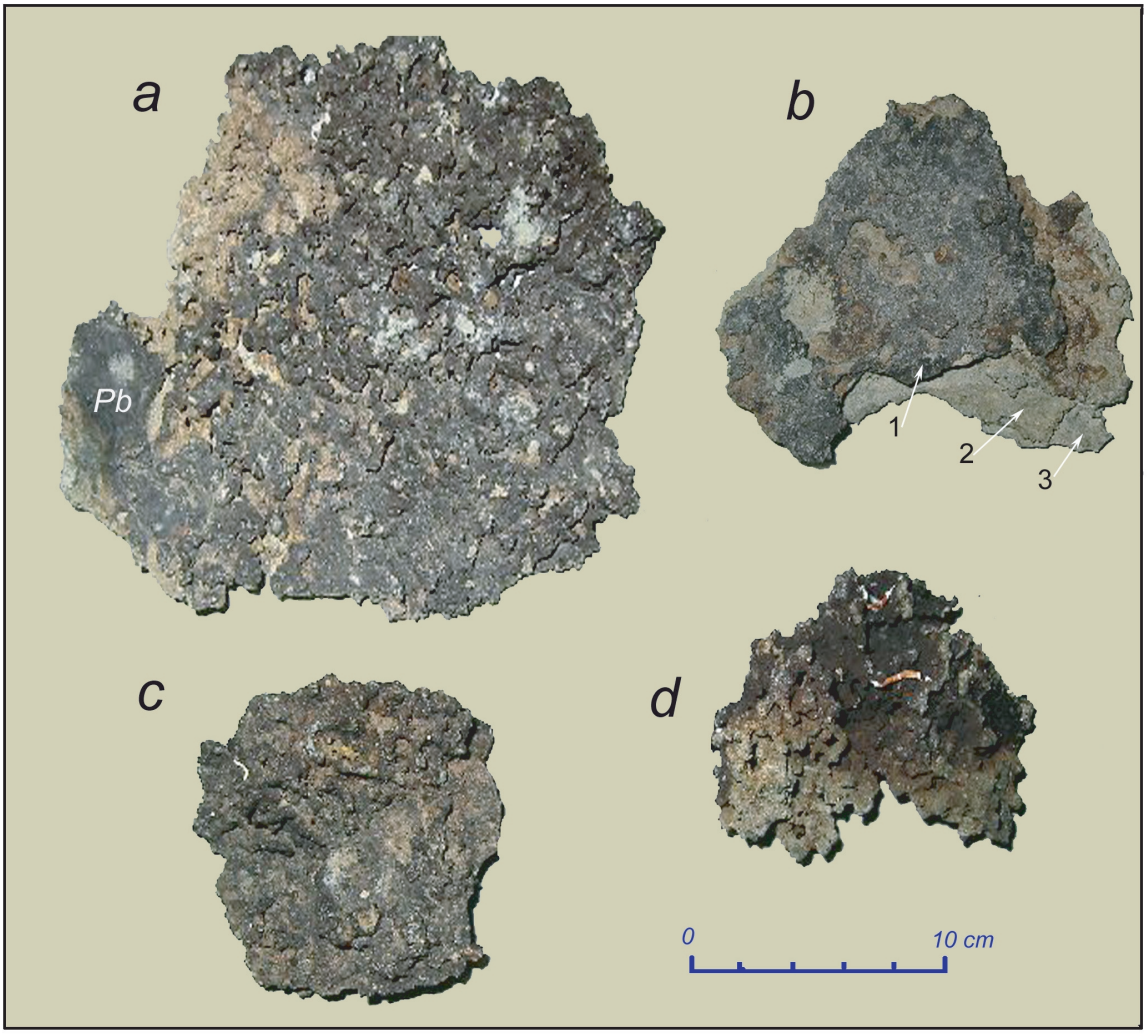

Fig. 10.4: *Photographs of barite crusts.*
a, c, d - fragments of flat barite crusts with numerous swells on their surface covered by a thin coat of iron and manganese hydroxides. These crusts cement enclosing sediment including gravel and pebble (Pb) of ice rafting; b - multilayer (laminas 1, 2, 3) barite crusts with a rough surface.

According to their morphology and inner structure, the barite crusts were formed near the sediment surface close to the water-sediment boundary. They were partly eroded by near-bottom currents, and later on, they formed slabs and crusts on the surface. Probably, barite crusts are formed in areas with a slow fluid flow, that is enriched with respect to barium and sulfide. In comparison to the gas-fluid expulsions of the “Barite Mounds”, the fluids of “Clam Hill” contain low methane concentrations, which is confirmed by the absence of carbonate mineralization.
Cores LV29-59-1 and LV29-63-1 taken in the “Clam Hill” area contain Late Pleistocene sediment typical for the Okhotsk Sea with large amounts of dropstones (sand, gravel, pebble). Core LV29-63-1 is located not far from the seeping area which can be seen from its pore water geochemistry.
It is likely that build-ups of barite chimneys occur also in the northern part of this hill. Rare findings of barite crystals, characteristic for chimney build-ups, in smear slides of the sediments from cores LV29-59-1 and LV29-63-1 are indicative of this.

Thus, summarizing all available information on the distribution of barites and carbonates in the studied area (Biebow & Hütten, 1999; Biebow et al., 2000; Suess et al., 1999; Derkachev et al., 2002; Greinert et al., 2002), we have convincing data that in the Derugin Basin ("Barite Mounds" and "Clam Hill" areas), a long-living and giant center of cold seeping exists. Similar vast manifestations of barite mineralization have not yet been found in other areas of the World Ocean.

11. CORE TEMPERATURE MEASUREMENTS AND PHYSICAL PROPERTIES OF SEDIMENTS

Jeffrey Poort, Tatyana Matveyeva, and Alexander Bosin

11.1 Objectives

The objectives of core temperature measurements were two-fold: to constrain the thermal conditions near venting systems off Sakhalin and in the Derugin Basin, and to detect temperature heterogeneities of sediments caused by dissociation of disseminated gas hydrates. In addition, thermal conductivity and magnetic susceptibility were measured on half cores providing us two important physical properties of the sediment column. Thermal conductivities further deliver us the information necessary to calculate heat flow from the thermal gradients. All data is listed in Appendix 7.

11.2 Core temperature measurements

11.2.1 Method

Temperatures were measured practically on all cores recovered by gravity and hydrocoring during Leg 1 of cruise LV29. Temperature measurements were performed within 10 min after core retrieval. Although complicated temperature paths may be induced during the core recovery process (generally 30-35 minutes from penetration to arrival on deck), the cold water and air temperatures provided optimal conditions with limited temperature changes. Because the process of core retrieval is fairly uniform, the temperature profiles at neighboring cores should be relatively consistent unless there are additional heat sources or sinks.
Temperature measurements were performed at intervals ranging from 20 cm to 100 cm. Needle thermometers were inserted in the sediments through holes in the polyethylene sediment core packing or on half cores (diameter of the cores: 10-14 cm). Temperature measurements were always started from the cores` upper interval downcore. Two different thermometers were used, both measuring temperatures using thermistor (semiconductor) sensors. The portable Japanese Technol Seven D617 with a resolution and accuracy of 0.01 and 0.1°C, respectively, allowed easy and quick handling. For more accurate measurement the LITOS device with an accuracy of 0.01°C was used. At several control points, the temperature was measured repeatedly to get an estimation of the temperature paths during the measurement procedure.

11.2.2 Preliminary results and discussion

11.2.2.1 Sakhalin slope

Core temperature measurements were performed on three cores from the Sakhalin slope area: LV29-46-1, LV29-50-1, LV29-51-1. The first two cores were taken in the “Obzhirov flare” area, a known site of near-surface hydrate occurrence located at a water depth of 690-700 m. The third core was recovered from a newly discovered acoustic flare situated northeast of “Obzhirov flare” at a water depth of 825 m. On these cores we used the portable thermometer and measured at small intervals of 20-25 cm (sometimes 50 cm) trying to detect zones where small pieces of hydrates left a cold thermal anomaly due to the endothermic dissociation process. The measured temperatures are shown in *Figure 11.1*. The corresponding near-bottom water temperature of 2.14°C taken from the nearby CTD station was plotted, too. The two cores from “Obzhirov flare” revealed near-vertical temperature profiles of 2.04°C and 2.06°C with overall thermal gradients of 5 mK/m and –19 mK/m for LV29-46-1 and LV29-50-1, respectively. In the latter, gas hydrates were recovered at the base of the core at 390 cm

subbottom depth. As the hydrates were immediately sampled for later laboratory measurement, no temperature measurements could be conducted here. A small negative anomaly of about 0.1°C in interval 30-50 cm above the hydrate-bearing sediments could indicate that some disseminated gas hydrate was present there, too. Core observation also suggested an increased gas content in this interval. In the first core a larger negative temperature anomaly was measured: the sediments there are up to 3.5°C colder than the over- and underlying ones. This is probably largely the result of sediment disturbance caused by pulling the sediment core out of the gravity corer on deck. However, near-bottom temperature variations could also have played a role. For hydrate dissociation, there were no indications.
Station LV29-51-1 at the new flare at 825 m water depth shows a linear temperature increase with depth of 50 mK/m up to 480 cm subbottom depth. From 480 cm up to the base of the core (580 cm) the thermal gradient suddenly increases to a highly anomalous value of 400 mK/m. Gas hydrates were not found in this core.

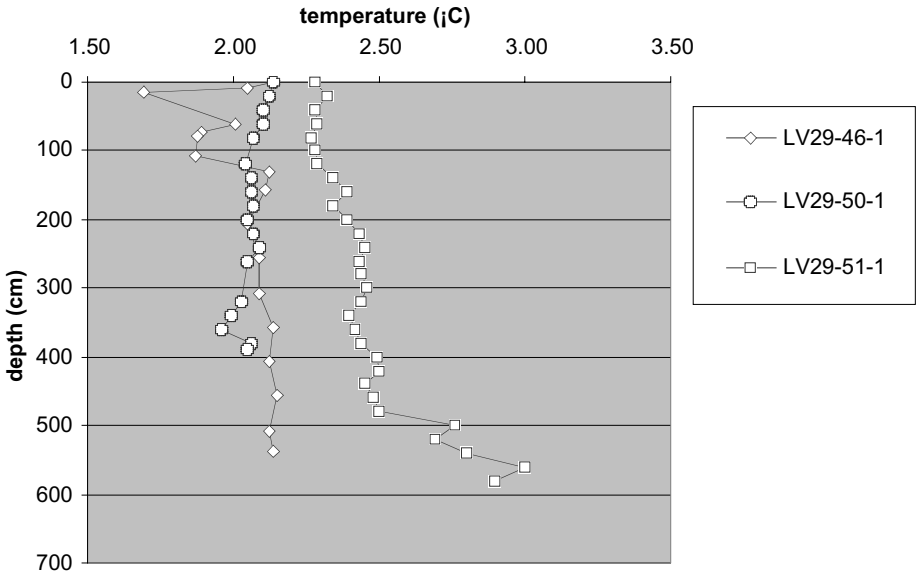

Fig. 11.1: *Temperatures measured on sediment cores from the Sakhalin slope.*

11.2.2.2 Derugin Basin

In the Derugin Basin 4 cores 450 to 600 cm long were recovered. Two cores were taken close to each other on the Barite Mounds at a water depth of about 1,500 m: LV29-53-1 and LV29-56-1. The other two cores were taken on the "Clam Hill" at water depths of 1,536-1,580 m: LV29-59-1 and LV29-63-1. Here, temperatures were measured at larger intervals of 50-100 cm with the LITOS thermometer in order to reduce the measuring time and get most accurate information on the thermal gradient and heat flow in this large venting area. Hydrate accumulations were previously not encountered here, but as the necessary stability conditions were given here, careful attention was paid to negative temperature anomalies. The measured subbottom temperatures are plotted in *Figure 11.2*. The near-bottom water temperatures measured by CTD were about 2.23°C.

All cores from the Derugin Basin show increased thermal gradients ranging from 142 to 243 mK/m for full core length averages. In all cores, and in particular in those of the "Barite Mounds", a general trend of higher gradients closer to the sediment surface was observed. The gradients in the upper intervals amount to such large values as 630-500 mK/m, whereas the gradients in the lowest intervals do not exceed 78-160 mK/m. This concave upward curving of geotherms is typical for areas with upward fluid flow.

Within this general trend, some intervals with colder temperatures can be recognized. The largest negative temperature anomaly (0.25°C) is expressed in the "Barite Mounds" core LV29-56-1 at a subbottom depth of 200 cm at which also anomalous high methane and water contents were found (see Chapter 6.4.2). All these indications suggest that disseminated gas hydrate was present in the interval of 150-350 cm and dissociated before the core was exposed for analysis. The core also appeared to have very low chlorinity values, but this information has to be confirmed by further analyses. Cold temperatures were also measured in cores LV29-63-1 and LV29-53-1 at subbottom depths of 250 and 300 m, respectively. These negative anomalies are, however, not larger than 0.1-0.15°C. Again, the dissociation of hydrates might have caused them, but this has to be confirmed by other proxies.

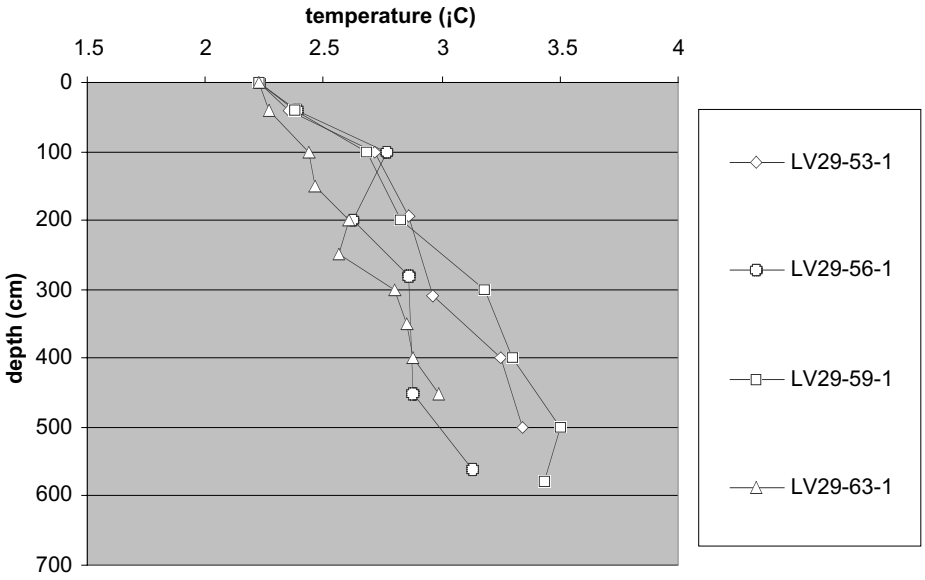

Fig. 11.2: *Temperatures measured on sediment cores from the Derugin Basin.*

11.3 Thermal conductivity

11.3.1 Method

Thermal conductivity data was collected on all cores at intervals of 0.5 to 1 m. The measurement was performed 20-40 min after core arrival on deck by inserting a needle probe in the half cores. Thermal conductivity was measured with the LITOS needle probe applying the continuous heating method. Errors are typically between 5-10%; corrections for temperature and pressure conditions were not made.

11.3.2 Preliminary results and discussion

The measured thermal conductivities are plotted in *Figure 11.3*. The range of measured thermal conductivities amounts to 0.54-1.07 W/m/K and the average is 0.76 W/m/K. Most cores yielded thermal conductivity values of about 0.70 W/m/K at 1 m depth with an increase or decrease of 0.1 W/m/K up to 4 m subbottom depth. These values are normal for diatomaceous silty clays.

Three cores show a different picture.

1) In core LV29-59-1, the thermal conductivities are much higher over the whole length of the core, ranging between 0.86 and 1.07 W/m/K. These high values probably reflect the

high sand content in the core. Also, the water content in this core was much lower than in the other cores.

2) Cores LV29-56-1 ("Barite Mounds") and LV29-50-1 ("Obzhirov flare") display a pattern that can best be explained by the presence of gas hydrates that were already dissociated during core recovery. In core LV29-56-1 the lowest thermal conductivity was measured: 0.54 W/m/K at 2 m subbottom depth. The low value is believed to result from the very high water content in this interval. 1 m upcore, a thermal conductivity of 0.88 W/m/K was obtained, corresponding to a low water content. This observation supports the suggestion that gas hydrates were present in this interval: the high water content resulted from the dissociation of hydrates during core retrieval, while the low water content and high thermal conductivity of the overlying layer resulted from water segregation during the hydrate formation process in situ. A similar pattern, but less profound was observed in core LV29-50-1. In this core from "Obzhirov flare" gas hydrates were visually observed at the core base.

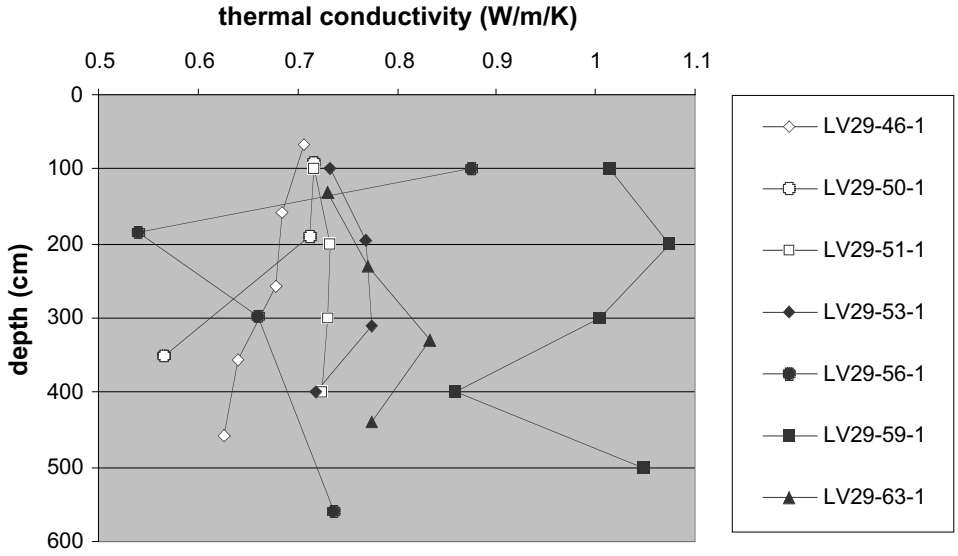

Fig.11.3: *Thermal conductivities measured on sediment cores from the Sakhalin slope (open marks) and the Derugin Basin (filled marks).*

11.4 Magnetic susceptibility

11.4.1 Method

Low-field magnetic susceptibility was measured on each half core. We measured with a Bartington MS2 susceptibility meter, which was calibrated each time with a sample of 1% Fe_3O_4. Measurements were performed in 5 cm intervals. It should be noted that the measurements were sometimes conducted not immediately and continuously on the whole core length, but in two or three sessions depending on core availability. In general, in these cases an important shift to higher values was observed at the start of a new session. These artifacts were not corrected.

11.4.2 Preliminary results

The results of the magnetic susceptibility measurements are plotted in *Figure 11.4*. The measured susceptibility varies in general between -20.10^{-6} and 40.10^{-6} CGS, with the exception of core LV29-63-1 and local high peaks in the other Derugin cores corresponding

to dropstones. For the three cores taken on the Sakhalin slope (LV29-46-1, LV29-50-1 and LV29-51-1), a general trend of maximum values near the surface (0 to 20.10^{-6}) was observed decreasing towards values of -20.10^{-6} at the core base. The larger values near the surface are probably the result of small amounts of authigenic magnetite. In three of the four cores from the Derugin Basin (LV29-53-1, LV29-56-1 and LV29-59-1) a similar decreasing trend was observed in the upper 2-3 m of the core, but with slightly higher values (from 20.10^{-6} - 40.10^{-6} to -20.10^{-6} - 0). Below 2-3 m subbottom depth, susceptibilities start to increase again. For

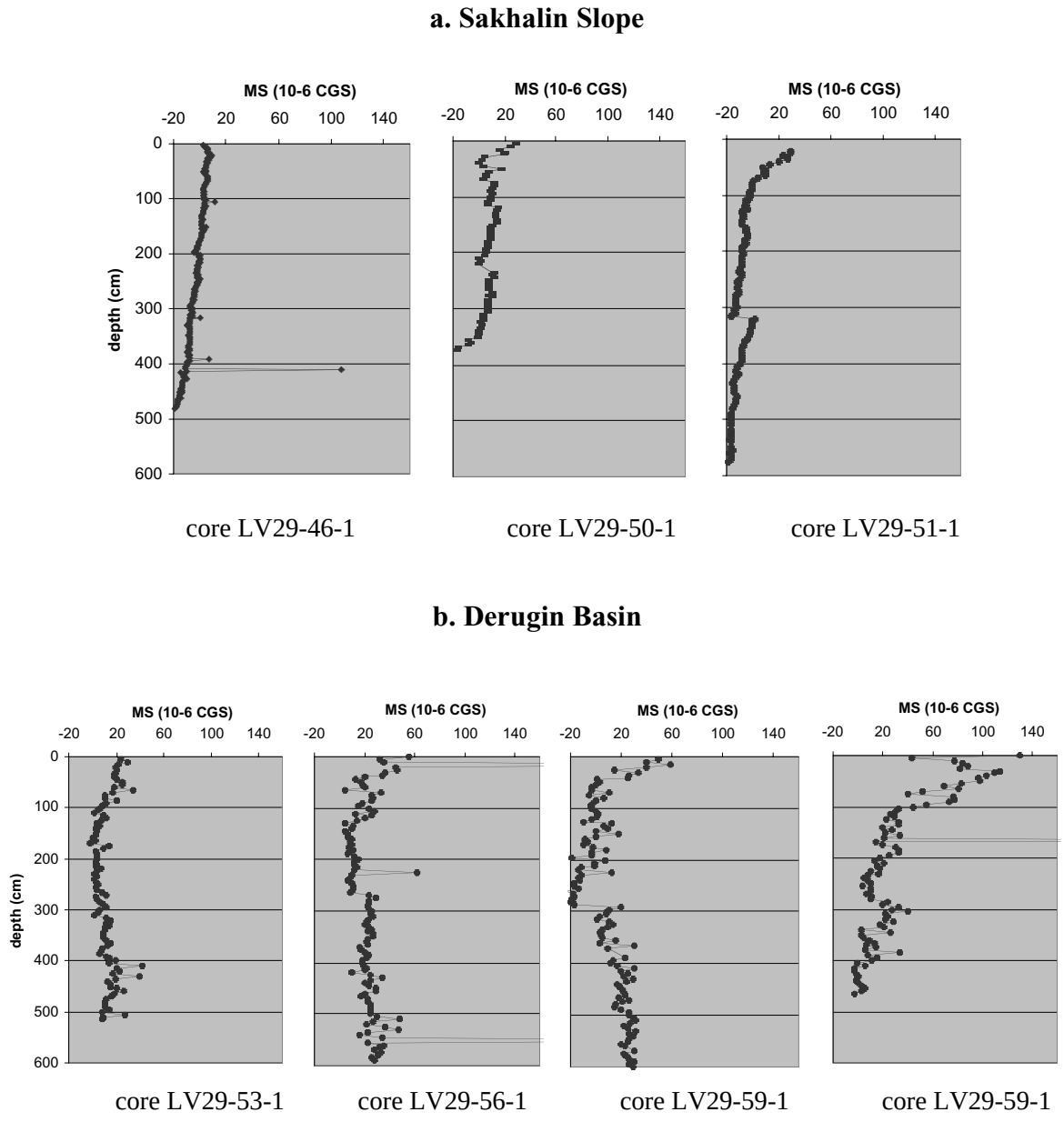

Fig. 11.4: *Magnetic susceptibility determined on half cores from the a) Sakhalin slope and b) Derugin Basin.*

interpretation we need information on pore water element and mineralogical composition. Only core LV29-63-1 revealed higher values than the other cores: the susceptibility first increases in the upper 35 cm from 43.10^{-6} to 114.10^{-6}, and then also decreases to the base of the core.

11.5 Summary

Core temperature measurements and determinations of thermal conductivity and magnetic susceptibility were performed on three sediment cores from the Sakhalin slope (in "Obzhirov flare" and flare 72) and on four cores from the Derugin Basin ("Barite Mounds" and "Clam Hill"). Temperatures were measured immediately after core arrival on deck and physical properties were measured within one hour. The thermal measurements revealed the following features:

1) The flares on the Sakhalin slope show non-elevated temperatures and very low to negative heat flow values in the upper 4-5 m of the sediment column (-13 to 36 mW/m^2). This could indicate a mixing process with sea water.

2) All sampled sites in the Derugin Basin are characterized by high overall heat flow values (100-243 mW/m^2). In general, heat flow decreased from a value of 450-550 mW/m^2 in the upper meters to 65-155 mW/m^2 at 4-5 m subbottom depth. This concave upward curving of temperature profiles is typical for areas with relatively strong upward fluid flow.

3) In two cores the presence of gas hydrates, dissociated during core recovery, was indicated at a specific interval by both temperature and thermal conductivity data. One core corresponds to "Obzhirov flare", where hydrates were also visually observed. The other core was recovered from the "Barite Mounds" in the Derugin Basin. Gas hydrates have never been visually observed in the Derugin Basin. We suggest that the chlorinity data should be used to confirm the gas hydrate interpretation based on thermal indications.

12. BARITE-CARBONATE MINERALIZATION, METHANE ANOMALIES AND GEOPHYSICAL FIELDS IN THE DERUGIN BASIN

Ruslan Kulinich and Anatoly Obzhirov

12.1 Introduction

Barite-carbonate mineral associations discovered in the eastern part of the Derugin Basin more than twenty years ago were first described as a product of hydrothermal activity by Astakhova et al. (1987) and Astakhova et al. (1990). Detailed studies on the origin and geochemical composition of these mineral associations have already begun during the joint Russian-German cruises LV28 (August-September, 1998) and GE99 (July-September, 1999) within the KOMEX I project.
The results of these expeditions indicate that the earlier found barite samples are only single fragments of massive barite-carbonate chimney-like build-ups up to 5-10 m in height and several meters in diameter. Barite build-ups and barite crusts are widely distributed in the so-called “Barite Mounds” area. Anomalous high methane concentrations were measured in the near-bottom waters of this area, as well (Biebow & Hütten, 1999). Mineralogical and geochemical investigations already carried out within KOMEX I indicate that deep fluid venting plays an active role in barite-carbonate diagenesis and in the occurrence of high methane concentrations. There are also signs for a recent continuation of this process. The structural control on barite mineralization could also be identified (Biebow et al., 2000).

Nevertheless, the following questions have remained unclear:
1. What are the sources and mechanisms of the fluid ascent - cold seeping or deep hydrothermal processes connected with magmatic activity?
2. How large is the area affected by these processes?
3. Why is the strong methane emission on the shelf and slope of Sakhalin not accompanied by barite-carbonate mineralization as observed in the Derugin Basin? Obviously, this is due to different methane sources in these two areas.

12.2 Preliminary results and discussion

The investigations of these questions were continued during the 29th cruise of RV *Akademik Lavrentyev*. Additionally, the spatial and causal relationship of barites and gas anomalies with the structural pattern of the acoustic basement and the overlapping sediments was investigated and a correlation with gravity and magnetic anomalies was performed. The correlation of the aforementioned geophysical fields with the distribution of the barite-carbonate mineral associations was made to better understand the structural patterns of the investigated area and to estimate the degree of magmatic activity, which took place here in the past, and thus to make a contribution to the understanding of the initial (deep) sources of the strong gas emanations and barite mineralizations. For this purpose, maps of gravity and magnetic anomalies obtained during the 16th cruise of RV *Professor Gagarinsky* were used. *Figure 12.1* shows the map of gravity and free-air anomalies.
To determine the nature of the gravity anomalies, they were correlated with the acoustic basement relief mapped during the same expedition. This correlation shows that the acoustic basement structure and the bathymetry are the main sources of the gravity anomalies. Thereby, positive anomalies reflect basement uplifts and negative ones areas of depressions. According to this, a vast area of negative anomalies was observed in the Derugin Basin, whereas the Central Okhotsk Rise, a morphostructure with a very thin sediment cover, is characterized by the highest amplitudes of gravity anomalies. The studied area is part of the

Kashevarov Rift Zone (Gnibidenko, 1990), which is located between them. In accordance with the obtained seismic data, the gravity map illustrates a mosaic of near-latitudinal horsts and grabens forming the Kashevarov zone.

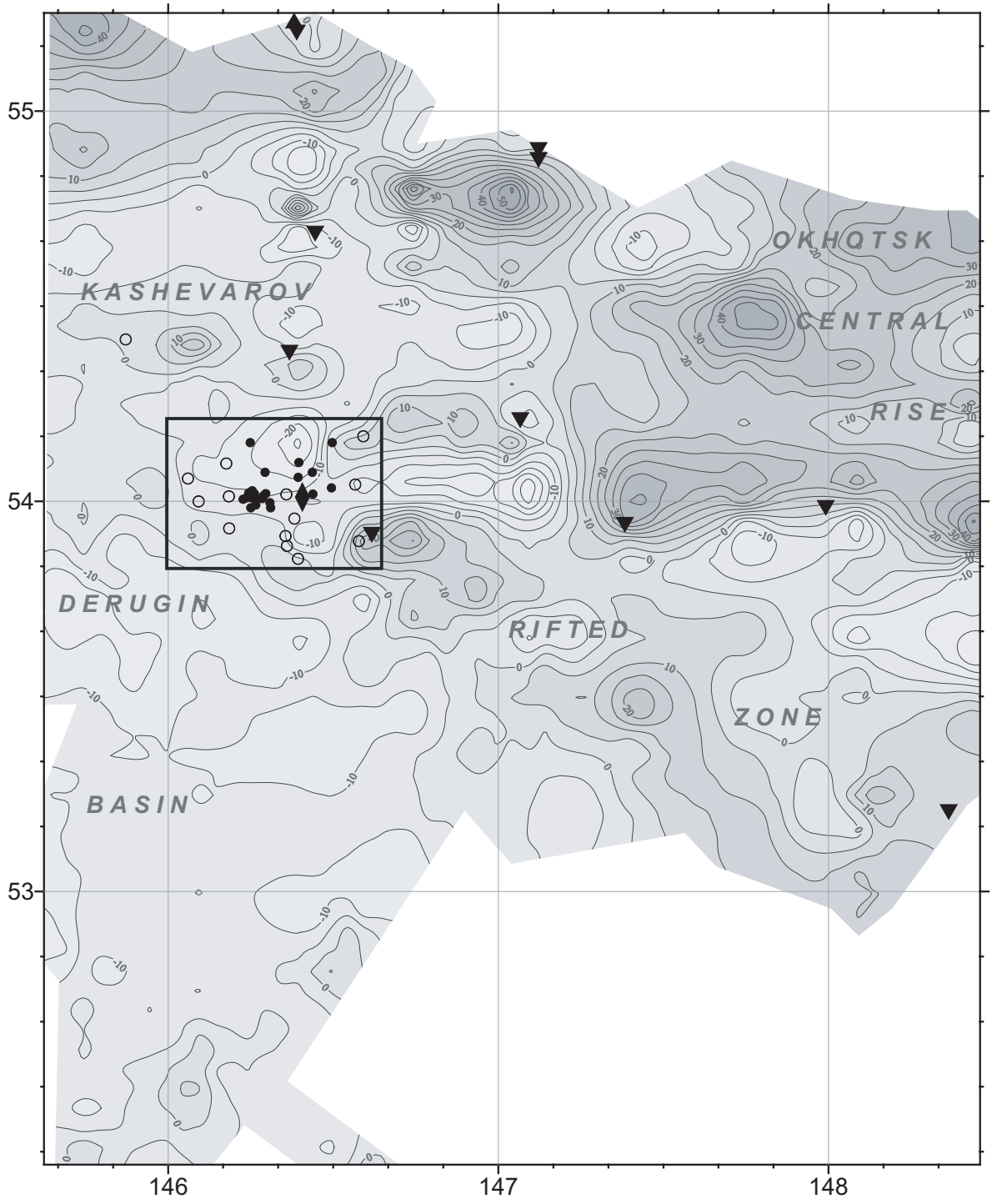

Fig. 12.1: *Gravity free-air anomaly map. Gravity data was obtained during the 16th cruise of RV Professor Gagarinsky. Filled circles indicate position of stations with methane anomalies in the bottom water. Open circles indicate stations without methane anomalies. Diamond marks the position of high heat flow values. Triangles indicate dredging sites carried out before KOMEX cruises. The investigated area is limited by a rectangular.*

The formation mode and basement composition are important indicators to understand the present conditions of this zone. The results of dredging carried out along the western part of the Central Okhotsk Rise and in the Kashevarov Rift Zone are the only data source on the

basement's composition. Dredging was carried out in the investigation area already in previous years (Catalog of dredging sites in the Okhotsk Sea, 1982). The location of the dredge sites is shown on the gravity anomaly map (*Fig. 12.1*). Apparently, almost all these sites are located within the gradient zones of gravity maximums that correspond to the flanks of basement uplifts. The samples recovered during dredging include mainly volcanic and plutonic rocks of intermediate and basic composition. Volcanic rocks are mainly represented by andesites, andesite-basalts, basalts, diabases, quartz porphyrites, dacites and tuffs. Plutonic rocks consist of diorites, granodiorites, and less often of granites. These rocks have a high average density (2.67 - 2.90 g/cm^3) and may be a source of the positive gravity anomalies.

The spatial consistence of the recovered rocks with the observed gravity maximums indicates that they are autochthonous, dominate the basement composition and are the source of these gravity disturbances. Assemblages of similar rocks were also recovered by dredging in other areas of the Kashevarov Rift Zone. The sites dredged during the 13th cruise of RV *Dmitry Mendeleev* are located nearest to the investigated area. Petrological analysis of samples recovered during this expedition (Korenbaum et al., 1981) showed that volcanic and plutonic rocks of intermediate and basic composition prevail in the investigated area. Volcanic rocks are mainly represented by andesite-basalts and andesite-dacites; plutonic rocks include most of all granodiorite and diorite. Acid types of magmatic rocks were found here less often. Pre-Cenozoic sedimentary rocks are formed mainly due to erosion of the basic and intermediate volcanic and plutonic complexes. All types of rocks show signs of methamorphic and hydrothermal alterations. The studied magmatic rocks are mainly of Upper Mesozoic to Paleogene age. The age of the youngest basalts is 11.9 Ma.
Thus, the area of barite mineralization and methane anomalies is located in a zone in which tectono-magmatic activity probably started in Mesozoic times. Transtensional tectonics which took place in the Oligocene to Miocene (Kharakhinov, 1998; Worrall et al., 1996) destroyed the existing lithosphere and resulted in riftogenic conditions with intensive heat and mass transfers towards the upper crust. In this context, the Cenozoic rebuilding of the basement is not only expressed by the development of horst and graben patterns, but also by a new activation of deep magmatic processes initiating a new stage of volcanic and hydrothermal activity. This stage ended in the Pliocene in connection with a switch from extensional to compressional tectonics (Biebow et al., 2000). The dominance of magmatic components in the basements is perfectly reflected by its high magnetic anomalies (*Fig. 12.2*).

The structural position of the "Barite Mounds" earlier determined by seismic data (Biebow et al., 2000) can be specified using anomalous gravity and magnetic fields. According to the map of gravity anomalies (*Fig. 12.1*), the area of barite mineralization is located on the northern flank of a sublatitudinal basement uplift (horst), to the north of which an almost isometric depression is situated. According to our calculation, the depth of the basement descending in relation to the surrounding uplifts is here about 3,000 m. The depression formed at a crossing point of several faults trending in EW, NW and NE directions. With regard to this, the basement of the depression is considered to be very permeable for fluids. Actively disturbed and high magnetic anomalies observed above this depression indicate the presence of volcanic formations in the sediments and basement. Taking this into account, the specified structure is most likely of volcanogenic-sedimentary origin.
Thus, the barite mineralization and anomalous emanations of methane are closely correlated to this magmatic structure. Barite mineral associations are concentrated on the margin of this structure, whereas the distribution of methane anomalies covers a much larger area. According to the results of the present expedition, high methane concentrations occur in the whole area of this depression, but do practically not exceed its borders. Thus, it is likely that the methane emanations and barite mineralization are related to the earlier formed volcanogenic structure.

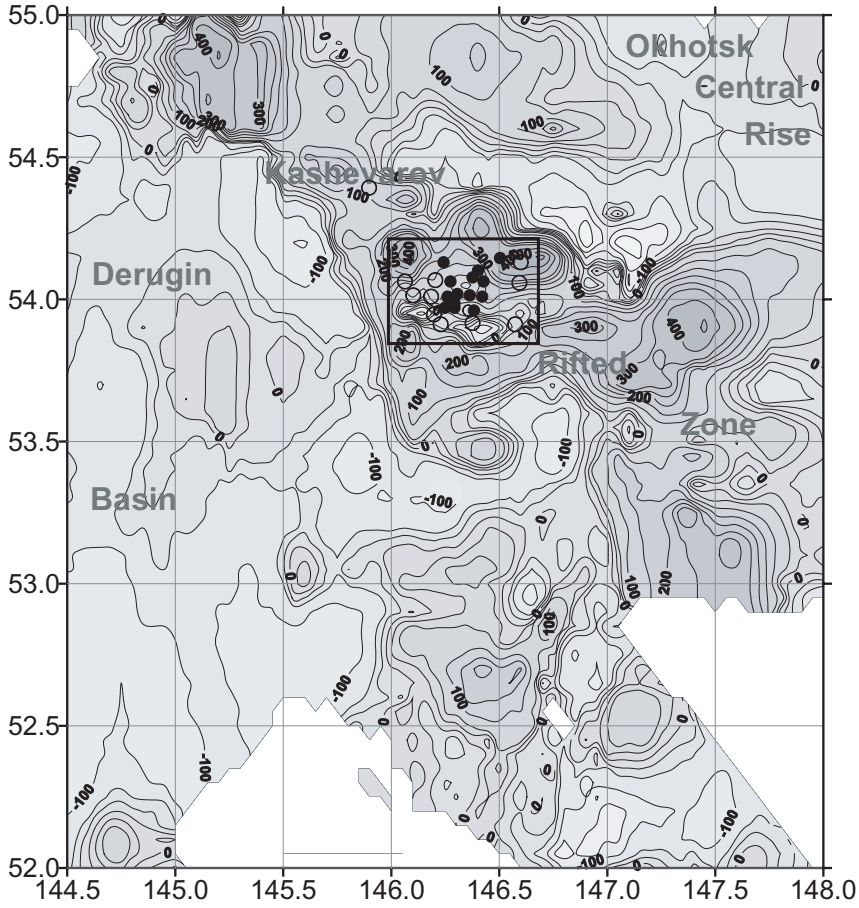

Fig. 12.2: *Magnetic anomaly map. Magnetic data was obtained during the 16th cruise of RV Professor Gagarinsky. Rectangular indicates investigated area of barite mineralization and methane anomalies. Filled circles indicate location of methane anomalies. Open circles indicate sites without methane anomalies.*

At present, it is difficult to determine the time of the last magmatic activation in this region. As mentioned above, the main magmatic processes ended possibly in Miocene or Pliocene times. However, the distinct localization and the high magnitude of the magnetic anomalies in the study area indirectly indicate a younger age of the formation of the magmatic rocks. The observed signs of fluid venting, the high heat flow near the investigation area (109.3; 155.5; 90.3 mWt/m^2), and the active emission of methane can be an indicator of remnant postmagmatic low-temperature processes. The barite-carbonate mineralogenesis is likely to be a secondary effect of the aforementioned processes.

12.3 Conclusions

The following conclusions can be drawn:

1. The barite-carbonate mineralization and anomalous concentration of methane in the bottom water of the investigated area are located within a volcanogenic-sedimentary depression formed at the crossing point of several faults. The main tectono-magmatic activity, which formed this structure, took place during the Oligocene to Miocene, but there is evidence that this activity ended much later.
2. The recently observed fluid venting, active emission of methane and high heat flow recorded near the study area can be indicative of remnant postmagmatic lowthermal processes within the borders of this volcanogenic structure. Barite-carbonate mineralogenesis can be a secondary effect of the above-mentioned processes.

13. REFERENCES

Aloisi, G., Pierre, C., Rouchy, J.-M. et al., 2000. Methane-related authigenic carbonates of eastern Mediterranean Sea mud volcanoes and their possible relation to gas hydrate destabilization. Earth and Plan. Scie. Lett., 184, 321-338.

Astakhova, N.V., Lipkina, M.I. & Mel'nichenko Yu.I., 1987. Hydrothermal barite mineralization in the Derugin Basin of the Sea of Okhotsk. Doklady Akademii Nauk SSSR (Talks of the Academy of Science of the USSR), 295, 1, 212-215 (in Russian).

Astakhova, N.V., Narnov, G.A., & Yakusheva, I.N., 1990. Carbonate-barite mineralization in the Derugin depression (Sea of Okhotsk). Tikhookeanskaya geologiya (Pacific geology), 3, 37-42 (in Russian).

Baranov, B., Werner, R., Hoernle, K., Tsoy, I., Bogaard, P.v.d. & Tararin, I., 2002a. Volcanological, geochemical, paleo-oceanological and geophysical evidence for compressionally-induced high subsidence rates in the Kurile Basin (Okhotsk Sea). Tectonophysics, 350, 63-97.

Baranov, B.V., Wong, H.K., Dozorova, K.A., Karp, B.Ya., Lüdmann, T. & Karnaukh, V., 2002b. Opening geometry of the Kurile Basin (Okhotsk Sea) as inferred from structural data. The Island Arc, August, 2002.

Biebow, N. & Hütten, E. (eds.), 1999. Cruise Reports: KOMEX I and II: RV Professor Gagarinsky cruise 22, RV Akademik M.A. Lavrentyev cruise 28. GEOMAR Report, 82, 188 pp.

Biebow, N., Lüdmann, T., Karp, B. & Kulinich, R., 2000. Cruise Reports: KOMEX V and VI: RV Professor Gagarinsky cruise 26, MV Marshal Gelovany cruise 1. GEOMAR Report, 88, 296 pp.

Boudreau, B.P., 1996. Diagenetic Models and their Implementation. Berlin: Springer Verlag.

Bruyevich, S.V., 1944. Determination alkalinity of small volumes of sea water by direct titration. In: Instruction of chemical investigation of sea water. Moscow-Leningrad: Glavsevmorput, 83 pp.

Buczynski, C. & Chafetz, H.S., 1991. Habit of bacterially induced precipitates of calcium carbonate and the influence of medium vicosity on mineralogy. J. Sedim. Petrol., 61 (2), 226-233.

Carpenter, J.H., 1965. The Chesapeake Bay Institute technique for the Winkler dissolved oxygen method. Limnol. Oceanogr., 10, 141-143.

Catalog of dredging sites in the Okhotsk Sea, 1982. Yuzhno-Sakhalinsk: Far Eastern Center of Academy of Sciences of the USSR Press, 101 pp. (in Russian).

Derkachev, A.N., Bohrmann, G., Greinert, J. & Mozherovsky, A.V., 2000. Authigenic carbonate and barite mineralization in sediments from Derugin Basin (the Sea of Okhotsk). Lithology and Mineral Res., 6, 568-585 (in Russian).

Derkachev, A.N., Obzhirov, A.I., Bohrmann, G., Greinert, J. & Suess, E., 2002. Authigenic mineral formation on the sites of a cold gas-fluid emanations at the bottom of the Sea of Okhotsk. In: Conditions of the generation of bottom sediments and related mineral deposits within marginal seas. Vladivostok: Dalnauka, 49-63 (in Russian).

Ginsburg, G.D. & Soloviev, V.A., 1994. Submarine gas hydrates. St. Petersburg: VNIIOkeangeologiya, 200 pp. (in Russian).

Ginsburg, G.D., Soloviev V.A., Cranston R.E., Lorenson, T.D. & Kvenvolden, K.A., 1993. Gas hydrates from the continental slope, offshore Sakhalin Island, Okhotsk Sea. Geo-Marine Letters, 13, 41-48.

Gnibidenko, G.S., 1990. The rift System of the Okhotsk Sea. - Proceeding of the First International Conference on Asian Marine Geology, Bejing: China Ocean Press, 73-81.

Gnibidenko, G.S., 1979. Tectonics of the seafloor from the far east marginal seas. Moscow: Nauka, 163 pp. (in Russian).

Gnibidenko, G.S., Hilde, T.W.C., Gretskaya, E.V. & Andreev, A.A., 1995. Kurile (South Okhotsk) Backarc Basin. In: Taylor, B. (ed.). Backarc Basins: Tectonics and Magmatism, New York: Plenum Press, 1995, 421-448.

Gonzalez-Mucoz, M.T., Ben-Chekroun, K., Ben-about, A., Arias, J.M. & Rodriguez-Gallego, M., 2000. Bacterially induced Mg-calcite formation: role of Mg 2+ in development of crystal morphology. J. Sedim. Res. Sec. A., 70 (3), 559-565.

Greinert, J., Bohrmann, G. & Suess, E., 2001. Gas hydrate-associated carbonates and methane-venting at Hydrate Ridge: Classification, distribution and origin of authigenic lithologies. Natural Gas Hydrates: Occurence, Distribution and Detection. AGU. Geophysical Monograph, 99-113.

Greinert, J., Bollwerk, S.M., Derkachev, A., Bohrmann, G. & Suess, E., 2002. Massive barite deposits and carbonate mineralization in the Derugin Basin, Sea of Okhotsk: precipitation processes at cold seep sites. Earth and Planetary Science Letters, 203, 165-180.

Guggenheim, E.A., 1930. Studies of cells with liquid-liquid junctions. Part II. Thermodynamic significance and relationship to activity coefficients. J. Phys. Chem., 34, 1758-1766.

Hayashi, T., 1997. The study of thermal structure and tectonic history of the Derugin Basin, Sea of Okhotsk. Master's thesis. Tokyo: Tokyo University, 39 pp.

Ivanenkov, V.N. & Bordovsky, O.K., 1978. The methods of hydrochemical investigation of the ocean. Moscow: Nauka, 271 pp. (in Russian).

Jorgensen, N.O., 1992. Methane-derived carbonate cementation of marine sediments from the Kattegat, Denmark: geochemical and geological evidence. Mar. Geol., 103, 1-13.

Kharakhinov, V.V., 1998. Tectonics of the Oil and Gas potential province of the Okhotsk Sea. Okha, 77 pp.

Korenbaum, S.A., Mishkin, M.A., Valuy, G.A., Gnibidenko, G.S. & Kurentsova, N.A., 1981. Petrology of bedrocks of the Sea of Okhotsk. In: The structure of the Okhotsk Sea bottom. Moscow: Nauka, 176 pp. (in Russian).

Kulm, L.D. & Suess, E., 1990. Relationship between carbonate deposits and fluid venting: Oregon accretionary prism. J. Geoph. Res., 95, 8899-8915.

Lueker, T.J., Dickson, A.G. & Keeling, C.D., 2000. Ocean pCO_2 calculated from dissolved inorganic carbon, alkalinity, and equations for K_1 and K_2: validation based on laboratory measurements of CO_2 in gas and sea water at equilibrium. Mar. Chem., 70, 105-119.

Luff, R. & Wallmann, K., submitted. Fluid flow, methane fluxes, carbonate precipitation and biogeochemical turnover in gas hydrate-bearing sediments at Hydrate Ridge, Cascadia Margin: Numerical modeling and mass balances. Geochim. Cosmochim. Acta.

Luff, R., Wallmann, K., Grandel, S. & Schlüter, M., 2000. Numerical modeling of benthic processes in the deep Arabian Sea. Deep-Sea Research II, 47, 3039-3072.

Millero, F., 1995. Thermodynamics of the carbon dioxide system in the oceans. Geochim. Cosmochim. Acta, 59, 661-677.

Nürnberg, D., Baranov, B.V. & Karp, B.Ya. (eds.), 1997. RV Akademik M. A. Lavrentyev cruise 27 - Cruise Report GREGORY. GEOMAR Report, 60, 69 pp.

Obzhirov, A.I., 1993. Gas and geochemical fields of the benthic layer of seas and oceans. Moscow: Nauka, 131 pp. (in Russian).

Obzhirov, A.I., 1992. Gas-geochemical manifestations of gas-hydrates in the Okhotsk Sea. Alaska Geology, 21 (7), 1-7.

Pitzer, K.S., 1991. Ionic interaction approach: Theory and data correlation. In: Pitzer, K.S. (ed.). 2nd Edition, Activity Coefficients in Electrolyte Solutions. Roca Raton, Ann Arbor, Boston, London: CRC Press, 75-153.

Sahling, H., Galkin, S.V., Foerstel, H., Greinert, J., Salyuk, A., Sosnin, V., Winckler, G. & Suess, E., submitted. Cold seep communities on the Sakhalin continental shelf and slope,

and in the Derugin Basin (Sea of Okhotsk); site description and depth related distribution patterns. Deep Sea Research.

Sakai, H., Gamo, T., Ogawa, Y. & Boulegue, J., 1992. Stable isotopic ratios and origins of the carbonates associated with cold seepage at the eastern Nankai Trough. Earth and Planet. Sci. Lett., 109 (3-4), 391-404.

Stakes, D.S., Orange, D. et al., 1999. Cold-seeps and authigenic carbonate formation in Monterey Bay, California. Marine Geology, 159, 93-109.

Suess, E., Bohrmann, G., Greinert, J., Derkachev, A.N., Kulinich, R.G. et al., 1999. Giant cold vents and barite mineralization in the Derugin Basin. 2nd Workshop on Russian-German Cooperation in the Sea of Okhotsk - Kurile Island Arc System. Kiel, January 26-29, p. 20.

Tishchenko, P.Ya., Chichkin, R.V., Il'ina, E.M. & Wong, C.S., 2002. pH Measurements in estuary by means of cell without Liquid Junction. Okeanologiya (Oceanology), 41 (1), 32-41 (in Russian).

Tishchenko, P.Ya., Pavlova, G.Yu., Salyuk, A.N. & Bychkov, A.S., 1998. Carbonate system and dissolved oxygen in the Japan Sea. Estimation of biological and thermal terms. Okeanologiya (Oceanology), 38 (5), 678-684 (in Russian).

Tishchenko, P.Ya., Wong, C.S., Pavlova, G.Yu., Johnson, W.K., Kang, D.-J. & Kim, K.-R., 2001. pH measurements of sea water by means of cell without liquid junction. Okeanologiya (Oceanology), 41 (6), 849-859 (in Russian).

Tsunogai, S., Niskimura, M. & Nakaya, S., 1968. Complexometric titration of calcium in the presence of larger amounts of magnesium. Talanta, 15, 385-390.

Wakatsuchi, M. & Martin, S., 1991. Water circulation of the Kurile Basin of the Okhotsk Sea and its relation to eddy formation, J. Oceanogr. Soc. Japan, 47, 152-168.

Werner, R., Tararin, I.A., Hoernle, K. & Lelikov, E.P., submitted. Petrology and geochemistry of submarine volcanism from the northeastern part of the Kurile Basin: Evidence for interaction of basic magma with continental crust. Gondwana Research (Special Issue).

Wong, H.K., 1999. TP7: Sedimentationsprozesse und strukturgeologische Entwicklung des Okhotskischen Meeres. In: Suess, E. (ed.). KOMEX-Zwischenbericht, Kiel, 114-143.

Worrall, D.M., Kruglyak, V., Kunst F. & Kuznetsov, V., 1996. Tertiary tectonics of the Sea of Okhotsk, Russia: Far-field effects of the India-Eurasia collision. Tectonics, 15 (4), 813-826.

Valentine, D.L., Blanton, D.C., Reebugh, W.S. & Kastner, M., 2001. Water column methane oxidation adjacent to an area of active hydrate dissociation, Eel River Basin, 65 (16), 2633-2640.

Zhuravlev, A.V., 1982. Geological structure and development of the South Okhotsk (Kurile) Basin. In: Tuezov, I.K. (ed.). Structure and Composition of the Sedimentary Cover of the Northwestern Pacific. Vladivostok: Far East Scientific Center, 23-33 (in Russian).